


AN ABSTRACT OF THE THESIS OF

BRUNO RICHARD PAGNANI for the DOCTOR OF PHILOSOPHY
(Name) (Degree)

in MECHANICAL ENGINEERING presented on May 1, 1968
(Major) (Date)

Title: AN EXPLICIT FINITE-DIFFERENCE SOLUTION FOR
NATURAL CONVECTION IN AIR IN RECTANGULAR
ENCLOSURES

Abstract approved: 

Dr. James R. Welty

An explicit finite-difference formulation of the general momentum and energy equations has been developed for a constant property, transient natural convective system. This technique has been successfully applied to the vertical rectangular enclosure problem. Computer solutions for this problem have been obtained for an aspect ratio (H/L) of five, over a Rayleigh number range of 3×10^3 to 2.5×10^5 . Additional solutions, for an aspect ratio of ten, are also included for comparison with existing experimental data. Computed steady state temperature profiles are in close agreement with the experimental data.

For an aspect ratio of five, transient and steady state temperature and velocity profiles are also shown for specific Rayleigh numbers. Overall heat transfer characteristics computed for the

enclosure were compared to previous correlations and favorable agreement was obtained. An equation in the form

$$\text{Nu}_L = .137(\text{Ra}_L)^{.28}$$

best describes the overall heat transfer characteristics for the Rayleigh number range of 3×10^3 to 2.5×10^5 for this study. The same data may also be expressed by two relationships

$$\text{Nu}_L = (.046)(\text{Ra}_L)^{.403}$$

and

$$\text{Nu}_L = (.153)(\text{Ra}_L)^{.272}$$

for the Rayleigh number ranges of 3×10^3 to 2×10^4 and 2×10^4 to 2.5×10^5 , respectively.

Flow diagrams and a complete computer listing, written in FORTRAN IV language are also included.

An Explicit Finite-Difference Solution for Natural
Convection in Air in Rectangular Enclosures

by

Bruno Richard Pagnani

A THESIS

submitted to

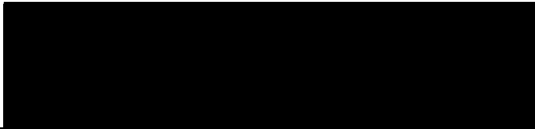
Oregon State University

in partial fulfillment of
the requirements for the
degree of

Doctor of Philosophy

June 1968


APPROVED:



Professor of Mechanical Engineering
in charge of major



Head of Department of Mechanical Engineering



Dean of Graduate School

Date thesis is presented

May 1, 1968

Typed by Clover Redfern for

Bruno Richard Pagnani

ACKNOWLEDGMENT

The author wishes to thank Dr. J. R. Welty for his personal guidance throughout my graduate study program and for his valuable suggestions in writing this thesis.

The author is grateful to the IBM Corporation Resident Study Program for their financial support during the past three years. Many fellow IBM employees have been helpful during this time and the author particularly wishes to cite: F. James Price for his assistance and recommendations which led to my participation in the Resident Program and for his general "encouragement" throughout the graduate study; Robert Sharp for his assistance in the programming aspects of this thesis and timely responses to the required program alterations.

Certainly the student-faculty friendships which develop during the graduate tenure are long remembered. The author's personal friendship with Hans Dahlke has been of particular importance to the author; and hopefully, this friendship will continue in the future.

A special form of gratitude is reserved for my wife, children and parents for helping in so many tangible and intangible ways.

NOMENCLATURE

English Symbols

- A - heat transfer area
- c_p - specific heat
- g - gravitational acceleration
- h - convective heat transfer coefficient
- H - total height of enclosure or plate
- k - conductivity of fluid
- L - distance between plates
- P - pressure
- q - heat transferred
- t - time
- T - temperature
- U - velocity component in x-direction
- V - velocity component in y-direction
- W - width of enclosure or plate
- x - direction normal to the heated plate
- y - direction tangent to the heated plate

Parameters

- Gr_L - Grashof number $\frac{gL^3\beta(T_H - T_C)}{\nu^2}$
- Nu_L - Nusselt number $\frac{hL}{k}$
- Pr - Prandtl number $\frac{c_p\mu}{k}$

Ra_L - Rayleigh number $\frac{gL^3\beta(T_H-T_C)}{\nu\alpha}$

Greek Symbols

α - thermal diffusivity

β - coefficient of volumetric expansion

δ - increment

θ - dimensionless temperature

μ - absolute (or dynamic viscosity)

ν - kinematic viscosity

ω - vorticity

Φ - pressure - density ratio

ψ - stream function

ρ - density

Subscripts

CL - centerline

R - REFERENCE conditions for enclosure

∞ - REFERENCE conditions for plate

Superscripts

n - n^{th} time increment

$'''$ - third derivative

h - h^{th} pressure iteration

$\hat{\Lambda}$ - unit vector

$'$ - first derivative

\rightarrow - vector

$''$ - second derivation

TABLE OF CONTENTS

Chapter	Page
I. INTRODUCTION	1
II. LITERATURE REVIEW	9
General	9
Vertical Rectangular Cells	9
Experimental	11
Analytical	18
Vertical Plates	27
III. DEVELOPMENT OF EQUATIONS	45
General	45
Governing Equations	46
Finite Difference Equations	53
Stability and Convergence Criteria	64
Boundary Conditions	66
Computational Method and Flow Diagrams	70
IV. RESULTS AND DISCUSSION	84
General	84
Computer Program Tests	89
Validity of Results	92
Velocity and Temperature Profiles for Specific Rayleigh Numbers	99
Rayleigh Number Variation	110
Aspect Ratio Variation	113
Transient Temperature of Velocity Profiles	113
Overall Heat Transfer Characteristics	121
V. CONCLUDING REMARKS AND SUGGESTIONS FOR FUTURE WORK	128
BIBLIOGRAPHY	130
APPENDIX	136
Appendix A Stability Criteria	136
Appendix B Reduced Computational Data for $Ra_L = 1.5 \times 10^5$ Case	144
Appendix C Computer Program Listing	151

LIST OF FIGURES

Figure	Page
1. Various flow regimes for rectangular enclosure.	2
2. Overall dimensions of the rectangular enclosure.	10
3. Various experimental correlations for heat transfer in rectangular enclosures.	12
4. Solution of differential equations (45) and (46) for $Pr = .733$ (from Schmidt and Beckmann [40]).	36
5. Cross section of rectangular enclosure with isothermal walls.	45
6. Cell (i, j) and neighboring points.	54
7. Orientation of cells for rectangular enclosure problem.	67
8. Typical velocity components for fluid and boundary cells.	67
9. Flow diagram for MAIN.	77
10. Flow diagram for subroutine INPUT.	79
11. Flow diagram for subroutine SET.	80
12. Flow diagrams for subroutines BOUND and POLATE.	81
13. Flow diagram for subroutine COMPUTE.	82
14. Computed and experimental temperature profiles for small y/H .	94
15. Computed and experimental temperature profiles for $y/H \approx .5$.	95
16. Computed and experimental temperature profiles for $y/H \approx 1.0$.	96
17. Computed and experimental data for temperature along the enclosure centerline ($\frac{x}{L} = .5$).	97

Figure	Page
18. Dimensionless temperature profiles for $Ra_L = 1.5 \times 10^4$.	100
19. Dimensionless vertical velocities for $Ra_L = 1.5 \times 10^4$.	101
20. Dimensionless horizontal velocities for $Ra_L = 1.5 \times 10^4$.	102
21. Fluid cell adjacent to heated wall.	103
22. Dimensionless temperature profiles for $Ra_L = 1.5 \times 10^5$.	106
23. Dimensionless vertical velocities for $Ra_L = 1.5 \times 10^5$.	107
24. Dimensionless horizontal velocities for $Ra_L = 1.5 \times 10^5$.	108
25. Temperature profiles for various Rayleigh numbers at $y/H = .5$.	111
26. Vertical velocity profiles for various Rayleigh numbers at $y/H = .5$.	112
27. Dimensionless temperature profiles for indicated aspect ratios for $Ra_L \approx 7 \times 10^3$.	114
28. Dimensionless vertical velocity profiles for indicated aspect ratios for $Ra_L \approx 7 \times 10^3$.	115
29. Transient temperature profiles at $y/H = .2$ for $Ra_L = 1.5 \times 10^4$.	116
30. Transient vertical velocity profiles at $y/H = .2$ for a $Ra_L = 1.5 \times 10^4$.	117
31. Transient temperature profiles at $y/H = .2$ for $Ra_L = 1.5 \times 10^5$.	119
32. Transient vertical velocity profiles at $y/H = .2$ for $Ra_L = 1.5 \times 10^5$.	120
33. Analytical comparisons of dimensionless heat transfer coefficients.	122
34. Comparison of this study with previous experimental correlations.	123

LIST OF TABLES

Table	Page
1. Boundary conditions for rectangular enclosure problem in finite difference form.	71
2. Summary of computer results for the vertical rectangular enclosure.	88
3. Heat transfer correlations for heat transfer in a rectangular enclosure.	125

AN EXPLICIT FINITE-DIFFERENCE SOLUTION FOR NATURAL CONVECTION IN AIR IN RECTANGULAR ENCLOSURES

I. INTRODUCTION

The first experimental heat transfer studies related to vertical rectangular enclosures were initiated in the late nineteenth century. Since then experimental studies have been expanded to include the use of various fluids under the influence of both constant flux and isothermal conditions.

Analytical studies of the vertical rectangular enclosure problem have lagged the experimental studies considerably. The first attempt to analyze this problem was reported 15 years ago and the analysis was very limited. Progress in the area of analysis has been somewhat retarded due to the complexity of the governing equations.

The objective of the present study is to formulate a computer program capable of achieving solutions using the governing equations of momentum and energy for a broad range of physical problems. The program so generated is applied to the specific case of natural convection in rectangular enclosures.

A basic description of the flow regimes which occur under the influence of natural convection within a closed vertical rectangular cell are shown in Figure 1. The ordinate and abscissa of this plot are the average Nusselt number (dimensionless heat transfer coefficient) and the Rayleigh number (product of Grashof and Prandtl number),

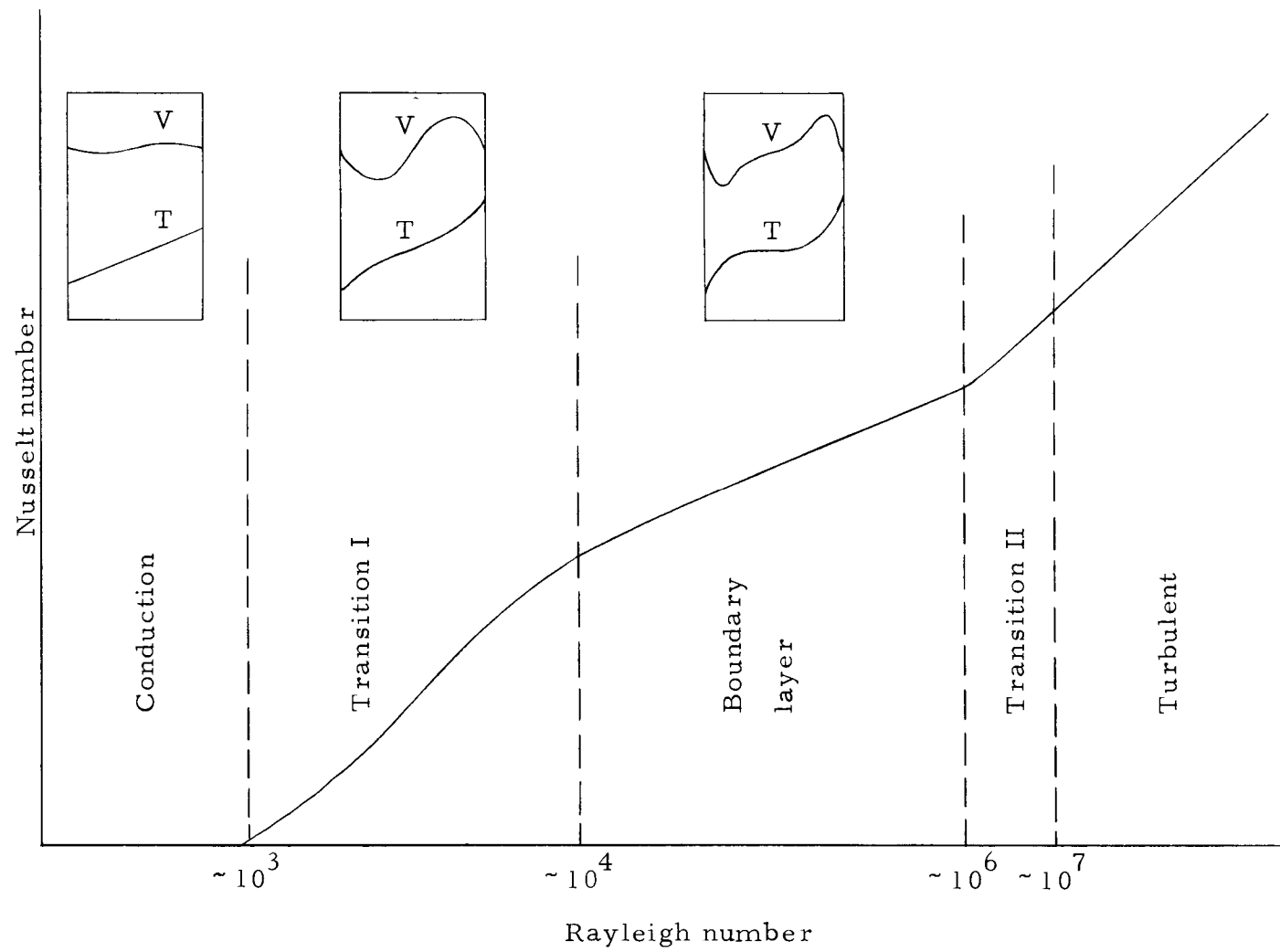


Figure 1. Various flow regimes for rectangular enclosure.

respectively. Recall that the Grashof number, a dimensionless parameter, is associated with free convection from a vertical element, whereas the Prandtl number represents the ratio of momentum diffusivity to thermal diffusivity.

In order to complete the description of flow, characteristic temperature and velocity profiles are shown in Figure 1 for those regions considered in this dissertation. A written description of the mechanisms which create the various flow regimes follows.

Consider a rectangular enclosure with two isothermal vertical walls, one at temperature, T_H , and the other at a lower temperature, T_C .

For small temperature differences, buoyancy effects are small or non-existent and, therefore, heat transfer is primarily by conduction. Temperature profiles are linear throughout most of the enclosing region except possibly for that portion of the fluid subjected to end effects. Velocity profiles are small in magnitude and are asymmetrical about any height, y .

As the temperature difference increases, the convective effects become more pronounced at the enclosure top and bottom resulting in higher Nusselt numbers, as portrayed in the transition regime, zone I. In this regime, the central core is still dominantly conduction and any increase in heat transfer coefficient is due to the convection prevalent at the bottom of the enclosure. The temperature and velocity

profiles show noticeable distortion at the top and bottom, while the enclosure center remains typical of the conduction regime.

With Rayleigh numbers on the order of 10^4 , convective effects completely dominate and the resulting patterns are similar to boundary layer velocity and temperature profiles.

With further increases in the temperature differential, a transition to turbulent flow occurs with completely turbulent flow occurring above a Rayleigh number of approximately 10^7 .

MacGregor [27] stated that it is in the region of moderate temperature differentials (i. e., transition zone I) that existing analyses and experimental correlations are least adequate. For situations involving Rayleigh numbers above the transition zone values, boundary layer integral techniques have been applied, resulting in adequate correlations with experimental data.

The partial differential equations governing a Newtonian two-dimensional, transient, laminar, incompressible, constant property system are as follows:

Conservation of Momentum (x-direction)

$$\rho \frac{\partial U}{\partial t} + \rho U \frac{\partial U}{\partial x} + \rho V \frac{\partial U}{\partial y} = \mu \left[\frac{\partial^2 U}{\partial x^2} + \frac{\partial^2 U}{\partial y^2} \right] + \rho g_x - \frac{\partial P}{\partial x} \quad (1)$$

Conservation of Momentum (y-direction)

$$\rho \frac{\partial V}{\partial t} + \rho U \frac{\partial V}{\partial x} + \rho V \frac{\partial V}{\partial y} = \mu \left[\frac{\partial^2 V}{\partial x^2} + \frac{\partial^2 V}{\partial y^2} \right] + \rho g_y - \frac{\partial P}{\partial y} \quad (2)$$

Conservation of Energy

$$\rho c_p \frac{\partial T}{\partial t} + \rho c_p U \frac{\partial T}{\partial x} + \rho c_p V \frac{\partial T}{\partial y} = k \left[\frac{\partial^2 T}{\partial x^2} + \frac{\partial^2 T}{\partial y^2} \right] \quad (3)$$

Continuity

$$\frac{\partial U}{\partial x} + \frac{\partial V}{\partial y} = 0 \quad (4)$$

No general analytical solution is known to exist for the above set of equations. Previous analyses have been performed on a simplified version of these equations and solutions have been achieved by either numerical or integral methods.

With the advent of large capacity digital computers, an additional method has become available in the form of finite-difference techniques. Using finite differences, the partial differential equations can be written in their most complete form allowing a more inclusive evaluation of the velocity and temperature fields at desired time increments.

Recent publications, by Welch, et al. [49], covering the use of finite-difference techniques has provided the impetus for further study of momentum equations at a more definitive level. The intent

of the present study is to extend this basic method and to incorporate the energy and momentum equations in a coupled system to provide transient and steady state solutions for natural convection. This basic method, to this writer's knowledge, has not been applied to a natural convective system or, specifically, to the rectangular enclosure problem.

This leads to the tri-fold intent of this dissertation, namely:

To establish the governing equations in finite-difference form and incorporate them into a computer program capable of solving velocity and temperature fields for transient and steady state condition.

To apply this mathematical technique to a basic engineering problem, preferably one in which solutions exist presently and/or specific test data have been made available.

To extend the existing technical data available, and to aid in a more thorough understanding of the basic flow and energy exchange mechanisms.

To accomplish these tasks, the problem of the vertical rectangular enclosure has been chosen as the mode of proof since analytical solutions exist which portray velocity and temperature profiles for both the transient and steady state conditions. Furthermore, temperature test data are also available for a few specialized cases.

Until very recently, solutions to the enclosure problem could

not be achieved using finite difference techniques for Rayleigh numbers greater than 7.5×10^4 . The recent solutions obtained for Rayleigh numbers on the order of 10^5 are based on a finite difference form of a modified set of equations. The present study offers a parallel method for the attainment of solutions pertinent to enclosure characteristics and possibly a more definitive mode for obtaining results with more complicated boundary conditions. The method used in this study also includes the effect of pressure, which has been neglected heretofore.

For air at low pressures, as considered in this study, the pressure field is not of paramount interest. However, in the expected follow-on studies, the pressure terms play a major role in determining the fluid flow characteristics, especially for more dense fluids.

In accordance with the survey of current literature in the general area of natural convection, it appears that some renewed interest has been generated in the consideration of transient heat transfer. This is especially true in the case of vertical elements (i. e., plates, cylinders, etc.) as well as vertical enclosures. Along these same lines are the problems of mixed natural and forced convection in which the computer program developed for this dissertation could be easily adapted.

This dissertation is organized in the following manner:

Chapter II contains a literature review of both vertical

enclosures and vertical plates with special attention given to the evaluation of various analytical techniques in both cases.

Chapter III contains the development of the finite difference equations, boundary conditions and computer technique utilized in this study.

Chapter IV delineates the obtained computed results and comparisons to available experimental and computed data.

Chapter V contains the concluding remarks of this study and offers suggestions for future endeavors.

The Appendices contain a discussion of the stability criteria, a FORTRAN IV listing of the program and a partial tabulation of the computed data.

II. LITERATURE REVIEW

General

The literature review contained in the following sections is best described in two major categories: The first category includes those endeavors directly related to the case of vertical rectangular enclosures under the influence of natural convection. The second category includes related work on vertical plates with special attention given to the governing equations, analytical techniques and, most recently, analysis pertaining to natural convection transients.

Throughout the literature review, reference will be made to distances along and/or normal to the heated plate and the velocity components in these directions. In order to avoid confusion in this matter, the point $x = 0, y = 0$ refers to the bottom of the heated plate. The positive y axis is parallel to the heated plate and the positive x axis is defined to be normal to the heated plate.

Vertical Rectangular Cells

Consider the enclosed vertical layer shown in Figure 2 with dimensions L, W and H .

By means of dimensional analysis, it can be shown that the heat transferred across such layers is a function of the Grashof number, the Prandtl number, the fluid layer length-to-height ratio and the

width-to-height ratio. The dimensionless heat transfer coefficient, the Nusselt number, can be written as a function of these quantities:

$$\text{Nu} = f(\text{Gr}, \text{Pr}, H/L, W/L)$$

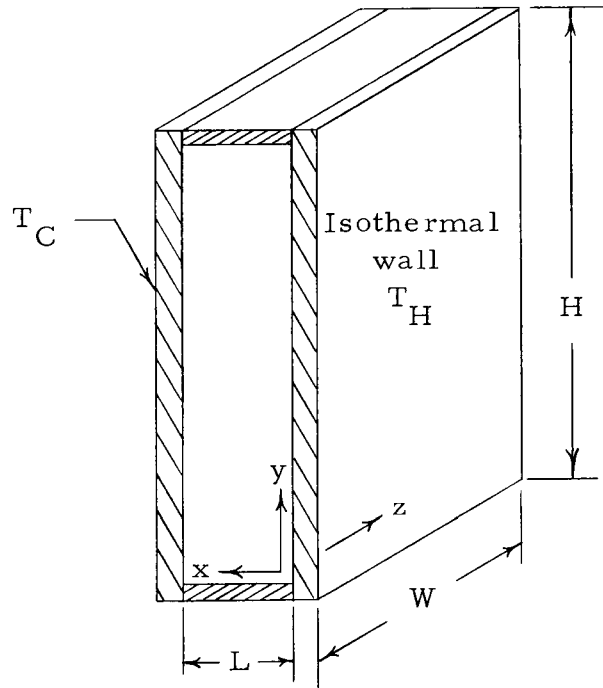


Figure 2. Overall dimensions of the rectangular enclosure.

For fluid layers that are sufficiently large in the z direction, the Nusselt number is independent of the W/L ratio and the layer can be considered as plane.

A multitude of literature exists pertaining to the heat transfer analysis and experimentation on vertical plates and close vertical and horizontal cells. In many cases, the data vary in accordance with the experimenter, such that a range of average dimensionless heat

transfer coefficients exist for a given Rayleigh number. An illustration of this is shown in Figure 3 (from reference [24]), which is a summary plot of the average Nusselt number as a function of Rayleigh number for vertical enclosures obtained by the referenced authors.

For engineering use, probably a mean value of the data shown in Figure 3 would suffice. However, in some instances, the correlations resulting from the experimental data have differed depending upon the discretion of the experimenter as to which of the controlling parameters best described the heat transfer condition. Therefore, throughout the literature a host of correlations exist, each being slightly different in principle, all being in numerical proximity.

In view of this, this writer has chosen to highlight, only briefly, the experimental data available in the literature. Special attention is given to the analytical aspects of certain publications, especially that of Wilkes [50] and MacGregor [27] where finite differences are utilized in the type of problem that is of interest in this dissertation.

Experimental

Experimental measurements on vertical enclosures were made by Nusselt [29] in 1909 supplementing his work regarding the thermal conductivities of insulating materials. In his work, Nusselt introduced an equivalent coefficient of thermal conductivity, k_c , such that:

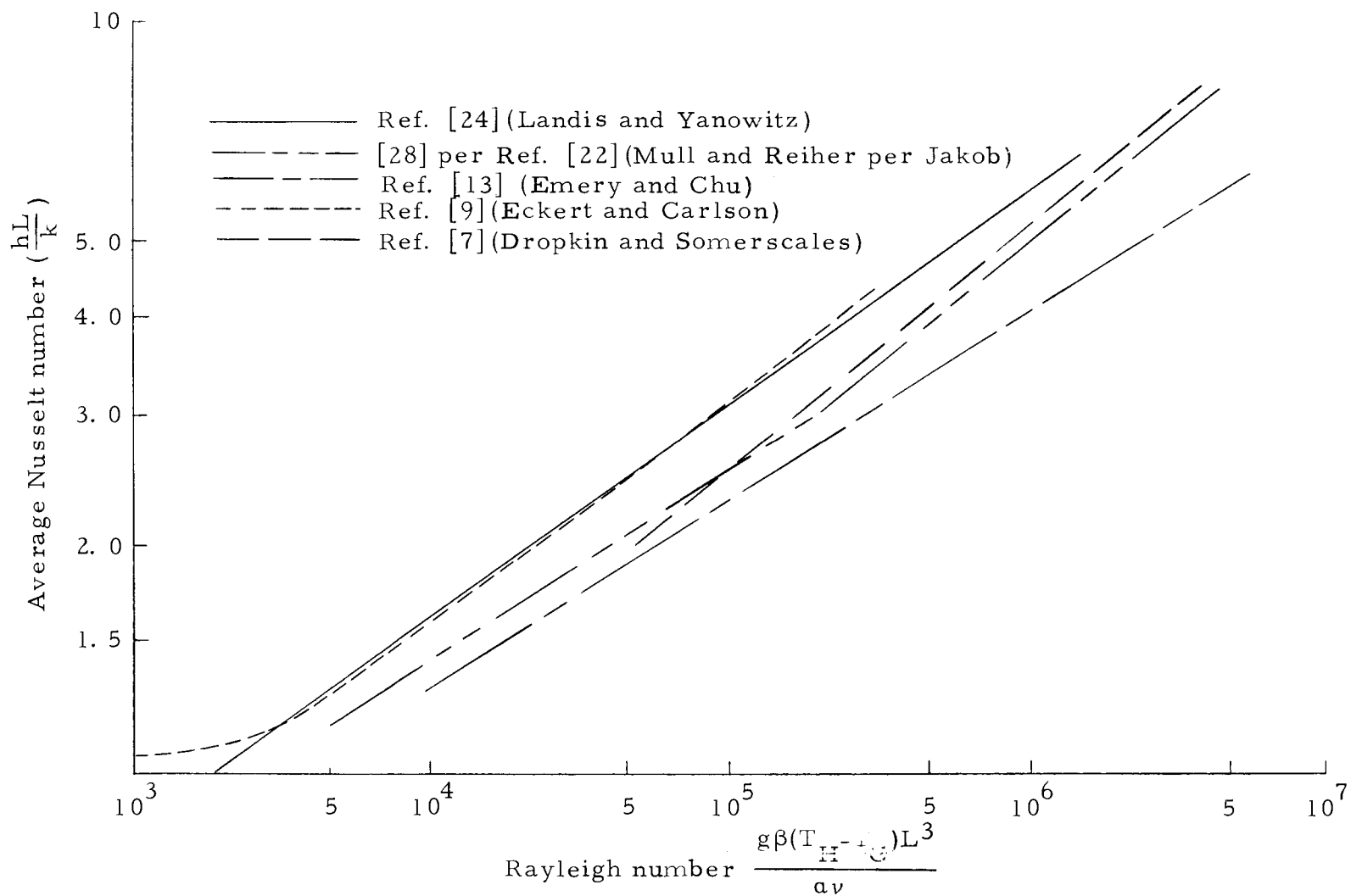


Figure 3. Various experimental correlations for heat transfer in rectangular enclosures.

$$q = \frac{k_c}{L} (T_H - T_C) \quad (5)$$

where

$$k_c = hL = kNu_L$$

Nusselt concluded that the heat transfer between the two walls depended upon the distance between them and, for wider spacings, convection effects increased the heat transferred beyond that which would normally be expected under the conditions of pure conduction. Nusselt's experimental data with air indicated that, for spacing between four and fourteen centimeters, the equivalent thermal conductivity had a value of .070 Cal/M-Hr-°C and for spacings of approximately one and a half centimeters, the equivalent thermal conductivity was essentially equal to 0.35 Cal/M-Hr. °C or approximately the conductivity of air. Nusselt's data still remain valid, however, observations made after Nusselt have indicated that spacing is not the only factor of significance when considering the total heat transfer across the layer.

Although supplementary experiments were performed paralleling the work of Nusselt, it wasn't until 1930 that an investigation by Mull and Reiher [28] set forth some important and useful relationships to determine the magnitude of heat transfer for enclosed vertical gas layers. For their experimental work, the authors built a channel composed of two flat plates 40 inches high and 24 inches wide. The

plates could then be adjusted to accomodate air layers one-half inch to seven and three-quarters of an inch thick. Mull and Reiher concluded that the effects of changing the width-to-thickness ratio were negligible by comparison to the other significant parameters.

Using their experimental results and also those data points obtained by Nusselt [29] and Schmidt [39], Mull and Reiher constructed curves in the form:

$$\text{Nu}_L = C \text{Gr}_L^m (\text{H}/\text{L})^n \quad (6)$$

These plots showed that the Nusselt number decreased with increased aspect ratio (H/L) for a given Grashof number. This phenomenon was explained by the fact that, as the air along the warm plate was heated and ascended, the temperature difference between the air and the plate became smaller. Thus, for a given spacing, L , a reduction in the heat transferred occurred for increases in enclosure height.

In 1931, van der Held [19] derived an expression for the Nusselt number for enclosed vertical air layers based on the experimental work of Mull and Reiher. His derived expressions were as follows:

$$\text{for } \text{Gr}_L > 10^5 \quad \text{Nu}_L = .0356(\text{Gr}_L)^{.36} \quad (7a)$$

$$\text{for } \text{Gr}_L < 10^4 \quad \text{Nu}_L = 1 \quad (7b)$$

Note that the above expressions are independent of the enclosure aspect ratio and that (7b) established the conduction regime at Grashof numbers less than 10,000.

Experimental work reported by Queer [34] (1932), Carpenter and Wassel [4] (1934), Wilkes and Peterson [51] (1937) further substantiated the basic data published by Mull and Reiher.

In 1946 Jakob [22] replotted the basic data bilogarithmically and suggested the following relationships:

$$\begin{aligned}
 &\text{for } Gr_L < 2 \times 10^3 & Nu_L &= 1 \\
 \text{and} & 2 \times 10^4 \leq Gr_L \leq 2 \times 10^5 & Nu_L &= .18 Gr^{1/4} (H/L)^{-1/9} \\
 \text{and} & 2 \times 10^5 \leq Gr_L \leq 10^7 & Nu_L &= .065 Gr^{1/3} (H/L)^{-1/9}
 \end{aligned} \tag{8}$$

Jakob defined the above three basic flow regimes as conduction, laminar flow, and turbulent flow region, respectively. Basically, Jakob used Grashof number exponents for air layers identical to those which describe laminar and turbulent heat convection for single vertical plates. The apparent differences between Equations (7) and (8) lie in (a) establishing where the conduction regime ends and (b) the inclusion of a geometrical parameter.

DeGraaf and van der Held [5] continued investigations on enclosed air layers in horizontal, vertical and oblique positions. As a result of their smoke studies, it was found that for a Rayleigh number

less than 4×10^4 , laminar circulation appeared. As the Rayleigh number exceeded 4×10^4 , a transition to turbulence was witnessed and the flow appeared to be fully turbulent at a Rayleigh number of 6×10^4 . Analytical expressions for the results obtained by the authors indicated that they were in close agreement with data published by Mull and Reiher. However, unlike Jakob's relationships, the expressions for average Nusselt numbers obtained by de Graaf and van der Held did not include any geometrical effect.

The correlations obtained by both parties agree well with experimental data available in the literature. Studies conducted since these have indicated a dependency to the enclosure aspect ratio. The strength of this dependency is accentuated as the magnitude of the Grashof number increases.

Investigations concerning rectangular enclosures by means of an optical interferometer were conducted and reported by Carlson [3] in his thesis of 1956. Carlson was specifically interested in the distribution of air temperatures in a rectangular enclosure with one vertical side heated, the other cooled and whose top and bottom sides were thermally insulated. Measurements were recorded for length-to-thickness ratios varying from 1 to approximately 50 for temperature differences between the hot and cold plates of 10 to 160°F. His findings indicated three distinct temperature regimes, namely the conduction regime for Grashof numbers less than 4000, a transition

region for Grashof numbers between 4000 and 60,000, and a boundary layer regime for Grashof numbers exceeding 60,000. The difference in these regimes can be best characterized by the appearance of the temperature profiles within the cavity. In the conduction regime, the temperature profiles exhibited a nearly linear variation between the hot and cold walls. However, in the boundary layer regime, a central portion of the cavity exhibited essentially a zero slope with most of the temperature variation occurring at either the hot or cold wall. Reference to these experimental data will be made, relative to computational results of this present study, in Chapter IV.

Further experimental investigations on the subject of vertical rectangular enclosure heat transfer were conducted in recent times by Dropkin and Somerscales [7], Emery and Chu [13] and Landis and Yanowitz [24] on various fluids under the influence of either an isothermal or constant heat flux condition. In addition, MacGregor [27], in a most recent publication, has provided experimental data for fluids (other than air) covering the spectrum of the conduction to turbulent regimes.

The preceding represents a very cursory review of experimental data presently available on vertical enclosures. Differences in values for specific data can probably be attributed to slight discrepancies in experimental apparatus, in the measuring techniques and specific interpretations of experimental error.

It should be noted that very little data exists for air velocity profiles within vertical enclosures. From an analytical point of view, the momentum and energy equations are coupled and therefore, the velocity profiles can easily be obtained from the equations of motion.

Analytical

The first attempt to examine analytically the problem of heat transfer for enclosed fluid layers was made by Batchelor [2] in 1954. He subdivided the problem into three cases:

- a) small Rayleigh number with H/L on the order of unity.
- b) large H/L with various values of Rayleigh number.
- and c) large Rayleigh number with various values of H/L .

Using the governing momentum and energy equations for steady state, Batchelor simplified the equations by taking cross partials of the momentum equations, thus eliminating the pressure terms. In addition, the stream and vorticity function were introduced providing the following set of equations:

$$\frac{\partial \theta}{\partial \bar{x}} \frac{\partial \psi}{\partial \bar{y}} - \frac{\partial \theta}{\partial \bar{y}} \frac{\partial \psi}{\partial \bar{x}} = \frac{\partial(\theta, \psi)}{\partial(\bar{x}, \bar{y})} = \nabla^2 \theta \quad (9)$$

and

$$\frac{1}{Pr} \frac{\partial(\omega, \psi)}{\partial(\bar{x}, \bar{y})} = Ra \frac{\partial \theta}{\partial \bar{y}} + \nabla^2 \omega \quad (10)$$

where \bar{x} and \bar{y} refer to dimensionless distances for a square

enclosure in which one side is of length L , then:

$$\bar{x} = \frac{x}{L} \quad \text{and} \quad \bar{y} = \frac{y}{L}$$

and θ , ψ and ω refer to the dimensionless temperature, stream function and vorticity, respectively.

The temperature boundary conditions were specified as isothermal for the vertical walls with a linear variation in temperature for the top and bottom border strips. In addition, both velocity components were specified to be zero at all enclosure walls.

The transformed boundary conditions became:

$$\begin{aligned} \text{at } \bar{x} = 0 \quad \frac{\partial \psi}{\partial \bar{x}} = \psi = 0 \quad \theta = 0 \quad \text{for } 0 \leq \bar{y} \leq 1 \\ \bar{x} = 1 \quad \frac{\partial \psi}{\partial \bar{x}} = \psi = 0 \quad \theta = 1 \quad \text{for } 0 \leq \bar{y} \leq 1 \\ \bar{y} = 0 \quad \frac{\partial \psi}{\partial \bar{y}} = \psi = 0 \quad \theta = \bar{x} \quad \text{for } 0 \leq \bar{x} \leq 1 \end{aligned} \quad (11)$$

Batchelor obtained an approximate solution by substituting power series expansion of ψ and θ into Equations (9) and (10) using only the first few terms in the expansions. The truncated series limited the validity of his results to the conduction region (Rayleigh numbers below 10,000).

The results of Batchelor's work, referring to each case mentioned previously, are summarized as follows:

For case (a), the restrictions placed on a low Rayleigh number virtually precluded any convection effects. The primary mode of heat transfer in this case was assumed to be conduction. Batchelor obtained an expression for the average Nusselt number in this regime to be:

$$\text{Nu} = \frac{H}{L} + C_1 (\text{Ra})^2 \quad \text{where} \quad C_1 \approx 10^{-8} \quad (12)$$

For case (b), a relationship was determined which depicted the onset of convection effects, at least in the regions in the vicinity of the enclosure ends. Roughly, Batchelor found this to occur at

$$\frac{H}{L} > \frac{\text{Ra}}{1000} \quad (13)$$

For case (c), it was assumed that the enclosure walls were lined with a single continuous boundary layer which surrounded a central core of fluid of uniform temperature and vorticity. The onset of this boundary layer regime, as predicted by Batchelor, was established at

$$\text{Ra} \left(\frac{H}{L} \right)^3 < 10^9 \quad \text{for} \quad \frac{H}{L} < 42$$

(14)

and

$$\text{Ra} < 13,700 \quad \text{for} \quad \frac{H}{L} > 42$$

Essentially, Batchelor's method could apply for $Ra < 10^3$ with reasonable accuracy. His correlation to Mull and Reiher's data in this range is very good.

The next significant analysis was presented by Poots [33] in 1958. He derived a set of equations identical to (9) and (10); but instead of expanding into a power series, Poots assumed that the dimensionless temperature and stream function could be represented by a double infinite series of orthogonal functions in the following manner:

$$\theta = \sum_{i=1}^{\infty} \sum_{j=1}^{\infty} A_{ij} \sin i\pi\xi \sin j\pi\eta \quad (15)$$

$$\psi = \sum_{i=1}^{\infty} \sum_{j=1}^{\infty} B_{ij} X_i(\xi) X_j(\eta) \quad (16)$$

In the above expressions, A_{ij} and B_{ij} are weighting coefficients which are functions of the aspect ratio, Prandtl number and Rayleigh number. The symbols ξ and η represent dimensionless distances in the form:

$$\xi = \frac{1}{C} \frac{y}{L} \quad \text{and} \quad \eta = \frac{x}{L}$$

where C is a constant and dependent upon the desired aspect ratio.

The assumed orthogonal functions satisfy the boundary

conditions (11) provided $X_j(\eta)$ satisfied the fourth order Sturm-Liouville equation:

$$\frac{d^4 X_j}{d\eta^4} = \mu_j^4 X_j$$

and

$$X_j(0) = X_j(1) = X_j'(0) = X_j'(1) = 0 \quad (17)$$

The eigenfunctions which satisfy (17) were given as:

$$X_j(\eta) = \cosh \mu_j \eta - \cos \mu_j \eta - \left(\frac{\cosh \mu_j - \cos \mu_j}{\sinh \mu_j - \sin \mu_j} \right) (\sinh \mu_j \eta - \sin \mu_j \eta) \quad (18)$$

where μ_j satisfy the equation:

$$\cosh \mu_j - \cos \mu_j - 1 = 0 \quad (19)$$

For the range of integration $\eta(0,1)$, $X_i(\eta)$ and $X_j(\eta)$ are orthogonal. In order to determine the weighting coefficients, the series were substituted into the modified momentum and energy equations, (9) and (10), and Fourier transforms of the equations were taken. This led to a series of algebraic equations which could then be solved by an iterative procedure.

Poots used only a few terms in the expansions in order to obtain a reasonable computational period. He presented results for a

square enclosure for Rayleigh numbers of 500, 2500 and 10,000.

Above a Rayleigh number of 10,000, Poots found that computational times were too lengthy and this was also verified by Leary [25] in his attempt to obtain solutions by Poots' method for Rayleigh numbers greater than 20,000.

In 1965, deVahl Davies and Kettleborough [6] solved a finite difference set of the steady state equations using matrix techniques. Solutions were obtained to provide a verification of those computations performed by Poots.

Emery [12] in 1963 analyzed the heat transfer phenomenon in a vertical enclosure by considering two boundary layers existing on the vertical plate and applied the von Kármán integral method to obtain a solution. This method was extended to include the constant heat flux hot wall and isothermal cold wall by Emery and Chu [13] in 1965. In both cases, a parabolic velocity profile was assumed and good correlation with experimental data was achieved, especially for high Rayleigh numbers.

The first paper which considered the transient flow in a vertical enclosure was provided by Wilkes [50] in 1963. In his doctoral thesis, Wilkes used a finite difference set of time dependent equations similar to those derived by Hellums and Churchill [20].

Following a procedure previously used by Batchelor and Poots, cross derivatives of the momentum equations were taken and the

resulting equations had the form:

$$\frac{\partial \bar{\omega}}{\partial \bar{t}} + \bar{u} \frac{\partial \bar{\omega}}{\partial \bar{x}} + \bar{v} \frac{\partial \bar{\omega}}{\partial \bar{y}} = Gr \frac{\partial \theta}{\partial \bar{x}} + \frac{\partial^2 \bar{\omega}}{\partial \bar{x}^2} + \frac{\partial^2 \bar{\omega}}{\partial \bar{y}^2} \quad (20)$$

$$\frac{\partial \theta}{\partial \bar{t}} + \bar{u} \frac{\partial \theta}{\partial \bar{x}} + \bar{v} \frac{\partial \theta}{\partial \bar{y}} = \frac{1}{Pr} \left[\frac{\partial^2 \theta}{\partial \bar{x}^2} + \frac{\partial^2 \theta}{\partial \bar{y}^2} \right] \quad (21)$$

where:

$$\bar{u} = \frac{uL}{\nu}, \quad \bar{v} = \frac{vL}{\nu}, \quad \bar{x} = \frac{x}{L}, \quad \bar{y} = \frac{y}{H}, \quad \bar{t} = \frac{t\nu}{L^2}, \quad \theta = \frac{T - T_R}{T_H - T_R} \quad (21a)$$

$$\bar{\omega} = \frac{\partial^2 \psi}{\partial \bar{x}^2} + \frac{\partial^2 \psi}{\partial \bar{y}^2} = \nabla^2 \psi \quad (\psi \text{ again being the stream function})$$

Wilkes solved an implicit form of Equations (20) and (21) using, primarily, a central difference approximation. Based on this set of equations he derived a relationship to establish a stability criterion dependent upon mesh size, the expected magnitude of the velocities and time increment.

Wilkes subdivided his dissertation into two cases: the case of natural convection between two infinite parallel plates, and an extension of previous work on vertical enclosures.

For the case of infinite vertical plates, solutions were obtained for Grashof numbers of 10,000 and 100,000 for a fluid with a Prandtl number of .733. Wilkes' computer solutions compared well with the analytical solution for this problem as presented in Rohsenow and Choi [37] and other references.

Wilkes extended the work of Poots on vertical enclosures to include transient and steady state data for a Grashof number range of 6850 to approximately 100,000. In addition, supplementary data were included for H/L ratios of 1.0, 2.0 and 3.0. The majority of his results were portrayed in dimensionless temperature and stream function plots.

Wilkes' results agree extremely well with those of Poots for the case of a square cavity with a Grashof number of 6850. In his concluding remarks, mention was made of the unsuccessful attempts to obtain solutions for Grashof numbers of 200,000 or higher. Wilkes did not feel that this was due to the onset of turbulence, but rather in the method of advancing the boundary vorticities across a time increment. In addition, he stated that an explicit form of the equations may be more applicable, especially in setting the boundary conditions for the advancing time step.

MacGregor [27], in his recent doctoral thesis, was successful in attaining solutions to Equations (20) and (21) by basically using an explicit form of the equations and calculating the boundary vorticities from the velocity field rather than extrapolating vorticity values. With these implementations, computer solutions were obtained for Rayleigh numbers greater than 10^5 for various aspect ratios, Grashof and Prandtl moduli. Also included in this publication are fairly complete descriptions of velocity and temperature profile

data for many of the transient and steady state cases.

As a result of his investigations MacGregor concluded that the Rayleigh number was more influential in the flow development than the Grashof number. In addition, he found that the enclosure heat transfer was strongly dependent upon the mode of heating (isothermal or a specified wall flux) and the aspect ratio.

The question of determining which moduli most clearly depict the flow situation was studied also by Landis and Yanowitz [24], who extended Poots' analytical method to include mixed boundary conditions and experimentally obtained transient results for water and silicone oil. The majority of their work was accomplished using an aspect ratio of 20. They also concluded that the Rayleigh number was the most important parameter in determining the flow characteristics. Their correlations do not include a geometrical variation factor.

Through the use of dye traces, Landis and Yanowitz were able to observe transient velocity profiles up to and including the steady state condition for constant flux heating. For water, the photographs taken clearly indicate that maximum velocity values occurred prior to steady state. In addition, they found the velocity profiles of the ascending fluid attained a higher absolute maximum value than the descending fluid; and they observed a slight off-center shift in the point of zero velocity at the mid-height of the enclosure.

Landis and Yanowitz also modified Wilkes' computational

technique to determine solutions for the rectangular enclosure for higher Rayleigh numbers. However, due to the large computational times required, sample calculations were not given in their publication.

Vertical Plates

The first analysis related to natural convection heat transfer phenomena associated with a vertical plate at a uniform temperature is attributed to Lorenz [26] in 1881. His analysis was based upon the assumption that the flow in the convection layers was primarily parallel to the surface and contributions to the convective streams occurred from horizontal layer to horizontal layer, similar to streamline flow adjacent to a vertical wall. Furthermore, he assumed that all fluid properties such as ρ , c_p , k and μ were constant and independent of temperature and that at some infinite distance from the plate an ambient temperature, T_∞ , was also constant. The following governing momentum and energy equations for steady state conditions were used in his analysis: (Recall that $x = y = 0$ refers to the leading edge of the heated plate)

$$\rho V \frac{\partial V}{\partial y} = \mu \left(\frac{\partial^2 V}{\partial x^2} + \frac{\partial^2 V}{\partial y^2} \right) + (\rho_\infty - \rho)g \quad (22)$$

$$\rho c_p V \frac{\partial T}{\partial y} = k \left(\frac{\partial^2 T}{\partial x^2} + \frac{\partial^2 T}{\partial y^2} \right) \quad (23)$$

Lorenz found it convenient to introduce the ideal gas relationship in order to relate ρ and T in the following form.

$$\rho = \frac{T_{\infty}}{T} \rho_{\infty} \quad (24)$$

Equations (22) and (23) were thus written as

$$V \frac{\partial V}{\partial y} = \frac{\mu}{\rho_{\infty}} \frac{T}{T_{\infty}} \left(\frac{\partial^2 V}{\partial x^2} + \frac{\partial^2 V}{\partial y^2} \right) + \left(\frac{T - T_{\infty}}{T_{\infty}} \right) g \quad (25)$$

$$V \frac{\partial T}{\partial y} = \frac{k}{\rho_{\infty} c_p} \frac{T}{T_{\infty}} \left(\frac{\partial^2 T}{\partial x^2} + \frac{\partial^2 T}{\partial y^2} \right) \quad (26)$$

A further simplification in the preceding equations was achieved by assuming the following:

the vertical velocity component V was constant for any arbitrary x , so

$$\frac{\partial V}{\partial y} = \frac{\partial^2 V}{\partial y^2} \approx 0$$

for small temperature differences, $\frac{T}{T_{\infty}}$ was considered to be unity,

at the upper edge of the vertical plate, $y = H$, V and T were considered to be constant, and

the temperature change along the wall was considered

small with respect to the change in the horizontal direction (i. e., normal to the wall) so that $\frac{\partial^2 T}{\partial y^2}$ could be neglected.

The introduction of the preceding assumption left Equation (26) with only one independent variable, y , so that the energy equation could now be transformed into an ordinary differential equation. Multiplying both sides of the equation by $\frac{dx}{H}$ and integrating yielded:

$$\frac{VT}{H} = \frac{k}{\rho c_p} \frac{d^2 T}{dx^2} \quad (27)$$

And similarly, using the above assumption, the momentum equation (25) became:

$$0 = \frac{\mu}{\rho_\infty} \frac{d^2 V}{dx^2} + \frac{T - T_\infty}{T_\infty} g \quad (28)$$

Using the boundary conditions

at $x = 0$ $T = T_s$ and $V = 0$

$x = \infty$ $T = T_\infty$ and $V = 0$,

the solution of these equations yielded expressions for both the steady state velocity and temperature profiles.

Since the heat transfer rate at the surface is related to the temperature distribution through the definition of the surface coefficient

by the following relationship:

$$h(T_s - T_\infty) = \frac{1}{A} \int_A k \left(\frac{\partial T}{\partial x} \right)_{x=0} dA = \frac{q}{H} \quad (29)$$

it then followed that the average convection coefficient for empirical solution of (27) and (28) could be evaluated using Equation (29).

Lorenz found this relationship to be:

$$h = N \left[\frac{g_c p_\infty^2 k^3 (T_s - T_\infty)}{\mu H T_\infty} \right]^{1/4} \quad (30)$$

where N is a numerical coefficient dependent upon the particular fluid. Lorenz determined experimentally that for air $N = .548$. An expression for the total heat flux, q'' , using (30) and the relationship between q and h was obtained:

$$\frac{q}{A} = q'' = h(T_s - T_\infty) = .548 \left[\frac{g_c p_\infty^2 k^3}{\mu H T_\infty} \right] (T_s - T_\infty)^{5/4} \quad (31)$$

The work of Lorenz represents, at best, an approximation to the vertical plate natural convection problem. His most notable achievement was, most probably, the attainment of the form of expression (31). In 1817, DuLong and Petit [8] hypothesized that the heat transfer rate for this type of process would be proportional to

$(\Delta T)^{1.23}$ comparable to Lorenz's expression (31) of $(\Delta T)^{1.25}$.

The close agreement between these two independent researchers provided a basis for much of the natural convection correlation efforts to be achieved by noted experimentalists in later years.

Additional experimentation with air relating to Lorenz's work was carried out by Nusselt [29] in 1909 and his results indicated that, in the range of excess temperature $(\theta = T_s - T_\infty)$ from 0 to 20°F, the Lorenz solution was not applicable, especially as the excess temperature approached zero.

Further experimentation on vertical plates was conducted by Griffiths and Davis [17] 1922, in which the authors verified Lorenz's theory that the heat transfer coefficient increases in direct proportion to the fourth root of the plate height for plates 3 to 4 feet high. In experiments conducted on plates 9 feet high, they found that neither the velocity nor the temperature increased for measurements taken beyond 3.6 feet from the lower edge and at a distance of 1/5 inches from the plate. This was hypothesized to be the effect of turbulence. Initial turbulence was observed to occur at a point approximately 1.5 feet from the lower edge. This point was clearly observed, since a minimum of heat transfer occurred there, indicating a mixing region similar to forced flows.

Experiments similar to Griffiths and Davis were conducted by Nusselt and Juerges [30] 1928, on vertical plates of approximately

two feet in length and their results substantiated those of Griffiths and Davis in the region below the start of turbulence.

Improvements in the analytical theory were attempted by Nusselt and Juerges, but it wasn't until 1930 that E. Schmidt and W. Beckmann [40] made improvements in the theory that provided a more substantial analytical solution to the vertical plate natural convection problem. Schmidt and Beckmann solved, with the aid of E. Pohlhausen, a modified set of the momentum and energy equations by introducing the stream function and two variables which allowed the resulting equations to be numerically integrated.

Starting with the basic equations involved for a steady state condition:

$$U \frac{\partial V}{\partial x} + V \frac{\partial V}{\partial y} = \nu \left(\frac{\partial^2 V}{\partial x^2} + \frac{\partial^2 V}{\partial y^2} \right) + g \left(\frac{\rho_\infty - \rho}{\rho} \right) \quad (32)$$

$$U \frac{\partial U}{\partial x} + V \frac{\partial U}{\partial y} = \nu \left(\frac{\partial^2 U}{\partial x^2} + \frac{\partial^2 U}{\partial y^2} \right) \quad (33)$$

$$\frac{\partial U}{\partial x} + \frac{\partial V}{\partial y} = 0 \quad (34)$$

$$U \frac{\partial T}{\partial x} + V \frac{\partial T}{\partial y} = \frac{k}{\rho c_p} \left(\frac{\partial^2 T}{\partial x^2} + \frac{\partial^2 T}{\partial y^2} \right) \quad (35)$$

Schmidt and Beckmann chose to consider an incompressible flow with the buoyant effect introduced in the last term of Equation (32). Considering a low-pressure isobaric field; the buoyancy term, with the

use of the ideal gas relationship, was approximated to be:

$$\frac{\rho_{\infty} - \rho}{\rho} \approx \frac{T - T_{\infty}}{T_{\infty}} \quad (36)$$

Schmidt and Beckmann conducted an order-of-magnitude study which led to the deletion of some of the terms in Equations (32) through (35). The deletion of these terms and the logic justifying their removal are shown here.

Since $U \ll V$ for nearly all y (the only deviation here is in the vicinity of the lower edge of the plate); the entire momentum equation in the "x" direction, Equation (33), was eliminated.

Since $\frac{\partial T}{\partial y} < \frac{\partial T}{\partial x}$, then $\frac{\partial^2 T}{\partial y^2}$ was eliminated on the basis that

$$\frac{\partial^2 T}{\partial y^2} \ll \frac{\partial^2 T}{\partial x^2}$$

Similarly, $\frac{\partial V}{\partial y} < \frac{\partial V}{\partial x}$, thus $\frac{\partial^2 V}{\partial y^2}$ was eliminated since

$$\frac{\partial^2 V}{\partial y^2} \ll \frac{\partial^2 V}{\partial x^2}$$

With these deletions, the system of Equations, (32) through (35), became

$$U \frac{\partial V}{\partial x} + V \frac{\partial V}{\partial y} = \nu \frac{\partial^2 V}{\partial x^2} + g \left(\frac{T_s - T_\infty}{T_\infty} \right) \theta \quad (37)$$

$$\frac{\partial U}{\partial x} + \frac{\partial V}{\partial y} = 0 \quad (38)$$

$$U \frac{\partial \theta}{\partial x} + V \frac{\partial \theta}{\partial y} = \alpha \frac{\partial^2 \theta}{\partial x^2} \quad (39)$$

where θ (excess temperature) was defined as $\left(\frac{T - T_\infty}{T_s - T_\infty} \right)$.

Introducing the stream function, ψ , where:

$$U = \frac{\partial \psi}{\partial y}$$

and

$$V = - \frac{\partial \psi}{\partial x}$$

Equations (37) and (39) were then written as a function of θ and ψ

$$- \frac{\partial \psi}{\partial y} \frac{\partial^2 \psi}{\partial x^2} + \frac{\partial \psi}{\partial x} \frac{\partial^2 \psi}{\partial x \partial y} = - \nu \frac{\partial^2 \psi}{\partial x^2} + g \left(\frac{T_s - T_\infty}{T_\infty} \right) \theta \quad (40)$$

$$\frac{\partial \psi}{\partial y} \frac{\partial \theta}{\partial x} - \frac{\partial \psi}{\partial x} \frac{\partial \theta}{\partial y} = \alpha \frac{\partial^2 \theta}{\partial x^2} \quad (41)$$

To solve this system of equations, Pohlhausen defined the similarity parameter:

$$\xi = \sqrt{\frac{4(T_s - T_\infty)g}{4\nu^2 T_\infty}} \frac{x}{4\sqrt{y}} = C \frac{x}{4\sqrt{y}} \quad (42)$$

and the functions θ and ψ were transferred to F and G where:

$$\psi(x, y) = 4\nu Cy^{3/4} F(\xi) \quad (43)$$

$$\theta(x, y) = G(x, y) \quad (44)$$

Since the components of velocity, U and V , were related through the stream function and also to the variable ξ ,

$$V = - \frac{\partial \psi}{\partial x} = - 4\nu Cy^{3/4} \frac{\partial F}{\partial x} = - 4\nu Cy^{3/4} \frac{\partial F}{\partial \xi} \frac{\partial \xi}{\partial x}$$

but

$$\frac{\partial \xi}{\partial x} = \frac{C}{4\sqrt{y}}$$

therefore:

$$V = - 4\nu C^2 y^{1/2} \frac{\partial F}{\partial \xi}$$

and similarly:

$$U = \nu C \left[\frac{3}{4\sqrt{y}} F - \frac{cx}{\sqrt{y}} \frac{\partial F}{\partial \xi} \right]$$

Accomplishing all necessary operations and substituting into Equations (40) and (41), the final equations became:

$$F''' + 3F F'' - 2(F')^2 + G = 0 \quad (45)$$

$$G'' + \frac{3\nu}{a} FG' = 0 \quad (46)$$

where the primed values are successive derivatives with respect to ξ .

The introduction of ξ as the only independent variable transformed the original partial differential equations to a simple system of two ordinary differential equations, in F and G , which were solvable by numerical integration.

The transformed boundary conditions were

$$\text{for } \xi = 0 \quad F = 0, \quad F' = 0 \quad G = 1$$

$$\text{and at } \xi = \infty \quad F' = 0, \quad F'' = 0 \quad G = 0$$

Pohlhausen performed a numerical integration using a series expansion for F and G and using values of F'' and G' which were determined experimentally. A plot of the G , G' , F , F' and F'' terms of differential equations (45) and (46) are shown in Figure 4.

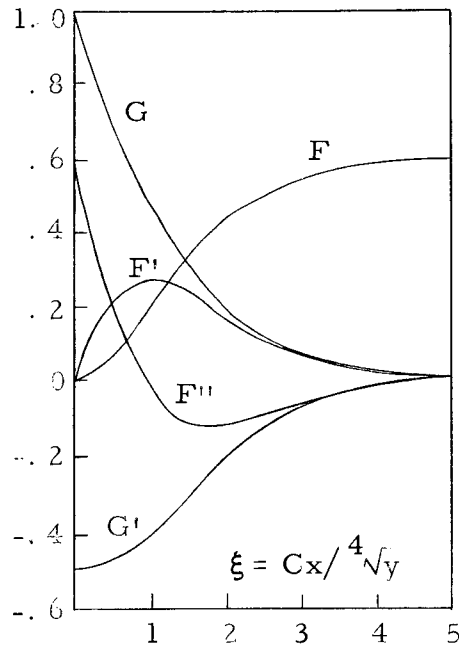


Figure 4. Solution of differential equations (45) and (46) for $Pr = 0.733$ [from Schmidt and Beckmann [40]].

The difference between the Schmidt-Beckmann analysis and those attempted previously (Lorenz, Nusselt-Juerges) lies primarily in the assumed form of the simplified momentum equation. Recall that in Equation (28), both the $U \frac{\partial V}{\partial x}$ and $V \frac{\partial V}{\partial y}$ terms were deleted. These terms were not eliminated from the Schmidt-Beckmann analysis and, in accordance with the test data obtained by Schmidt-Beckmann, this more inclusive analysis was verified.

Experimental data obtained with a plate five inches high indicated a F' deviation of approximately 5% whereas G was closely verified with the numerical calculations. The error in F' tended to increase with test plates larger than five inches (showing effects of turbulence), but the excess temperature remained within the realm of analytical prediction. An evaluation of the average film heat transfer coefficient in the form

$$h = N \frac{k}{H} \sqrt[4]{\frac{gH^3(T_s - T_\infty)}{\nu^2 T_\infty}} \quad (47)$$

yielded a value of $N = .479$ whereas Lorenz obtained a value of .507.

Experiments performed by R. Weise [48] 1935, produced results which were some 25% higher than the average heat transfer coefficient calculated by Schmidt and Beckmann. It is believed that the experimental set-up for both Lorenz and Weise was subject to

disturbances which may have caused a significant error in their readings. Schmidt and Beckmann [40] observed a considerable change in their results due to small air disturbances near the heated wall. Both these effects would cause their "apparent" heat transfer coefficient to be higher.

Further significant analysis paralleling the Schmidt-Beckmann solution was not attempted until 1953, when Ostrach [31, 32] performed an analytical study to determine the conditions under which the simplified Equations (37) and (39) were sufficiently accurate to describe a physical case. In his analysis, Ostrach started with the complete set of momentum and energy equations but introduced three variables in the form:

$$\begin{aligned} d\rho &= \rho(\kappa dP - \beta dT) \\ \mu &= \mu_{\infty} \left(\frac{T}{T_{\infty}} \right)^m \\ k &= k_{\infty} \left(\frac{T}{T_{\infty}} \right)^n \end{aligned} \tag{48}$$

He concluded that the modified equations represented the physical case adequately, provided that the temperature difference was small, thus resulting in relatively low Grashof numbers. For high Grashof numbers, Ostrach concluded that Nusselt numbers comparable to those in forced convection could be obtained. Velocity and temperature profiles for Prandtl numbers of .01, .72, .733, 1, 2, 10, 100

and 1000 were computed with the aid of L. U. Albers [1], on the basis of a constant body force and plate temperature. Ostrach's analysis agreed very well with Schmidt-Beckmann velocity experimental data for $\xi < 1$ and for all Schmidt and Beckmann temperature data taken on small plates. A comparison of the average heat transfer coefficient obtained by Ostrach in the form of Equation (47) gave a $N = .505$, a value nearly identical to that obtained by Lorenz.

The work of Sparrow and Gregg [45] in 1956, provided a solution of the modified equations for conditions other than an isothermal vertical plate. Specifically, their analysis considered a plate which dissipated heat at a uniform rate q'' over its entire surface. For their case, the following boundary conditions applied:

$$\begin{array}{llll}
 \text{at} & x = 0 & U = V = 0 & \frac{\partial T}{\partial y} = \text{constant} \\
 & x = \infty & U = 0 & T = T_{\infty}
 \end{array} \quad (49)$$

To satisfy the preceding boundary conditions, the temperature variable, generalized stream function and similarity variable were required to be slightly different than those utilized by Schmidt and Beckmann. The newer forms were

$$\xi = C_1 \frac{x}{\sqrt[4]{y}}$$

$$F(\xi) = \frac{\psi}{C_2 y^{4/5}}$$

$$G = \frac{C_1 (T_\infty - T)}{\frac{y^{1/5} q}{k}}$$

where

$$C_1 = \left(\frac{gq}{5kv^2 T_\infty} \right)$$

and

$$C_2 = 5 \left[\frac{gqv^3}{T_\infty k} \right]^{1/5}$$

The resulting differential equations then became:

$$F''' - 3(F')^2 + 4FF'' - G = 0 \quad (50)$$

$$G'' + \text{Pr } 4G'F - G F' = 0 \quad (51)$$

Equations (50) and (51) were comparable to the Schmidt-Beckmann equations (45 and 46). Sparrow and Gregg calculated heat transfer parameters resulting from the solution of Equations (50) and (51) for Prandtl numbers of .1, 1, 10 and 100. The uniform flux case was found to compare well with Ostrach's solution for the isothermal case suggesting that a single heat transfer relation may apply accurately for a number of different physical situations.

Sparrow and Gregg [46] also studied the problem of using variant

and non-variant fluid properties and concluded that, for the property variations typical for gases, the properties other than β should be evaluated at the following reference temperature for vertical isothermal plates with laminar boundary layers:

$$T_R = T_S - .38(T_S - T_\infty) \quad (52)$$

They stated that expression (52) was valid over the range of

$$.5 < \frac{T_S}{T_\infty} < 3.0$$

where temperatures are expressed in absolute units.

It is worth noting that, in the discussion section of the Sparrow and Gregg paper, some basic questions were put forth regarding the authors' use of the word "exact" rather than "mathematically rigorous" by D. P. Timo [47]. The question here was in relation to the modified Equations (37) and (39) first used by Schmidt and Beckmann in their classical solution of the vertical plate problem. Timo pointed out that the "exact" solution of their type of problem required the simultaneous solution of the Navier-Stokes equations and energy equation, rather than a set of equations with some "irrelevant" terms having been discarded.

In more recent times, a publication by Yang [53] in 1960 generated some renewed enthusiasm in the vertical plate natural convection

heat transfer problem by considering similarity solutions which were possible in laminar free convection. In his paper, Yang made a study of the modified unsteady boundary layer equations establishing the necessary and sufficient conditions required for solution to the following vertical plate problems:

Steady state free convection with prescribed constant surface temperature (Schmidt-Beckmann problem).

Steady state free convection with surface temperature varying with any power of a linear function of x (Sparrow and Gregg problem [45]).

Steady state free convection with surface temperature varying both linearly with and exponentially with x . (Again, the Sparrow and Gregg problem).

Unsteady free convection with surface temperature varying inversely as a linear combination of y and t .

Unsteady free convection with surface temperature varying directly with a linear function of y and inversely with the square of a linear function of t .

Unsteady free convection with unsteady heat flux at the surface.

Yang concluded that many of the solutions possible for the steady state problem had been analyzed and reported in the past; however, there remained many cases for which a solution had not been achieved which

were both significant and useful.

Further examples of endeavors with respect to transient natural convection have appeared in publications by Gebhart [15, 16] in 1961 and 1963. In his papers, Gebhart considered the natural convection heating or cooling effects of plates and cylinders immersed in a fluid and subjected to a dissipation or absorption process within the solid material. Using the integral method, the energy equations for the fluid and element and the fluid momentum equation were solved for a Prandtl number range of .01 to 1000. In his earlier paper [15], Gebhart assumed that the thermal capacity of the vertical element was non-zero, but finite. He found that for a time dependent internal generation within the element, transient response is affected by two parameters, namely, the fluid Prandtl number and the element heat capacity. In view of this, Gebhart extended his analysis [16] to include elements of appreciable thermal capacity. Again using the integral method Gebhart found that for increases in element thermal capacity, the resulting temperature profiles approached the one-dimensional steady state case.

Landis and Yanowitz [24] used Gebhart's predicted values in their measurements of the time-temperature change of the heated plate in studying the responses of a vertical enclosure. They found that for measurements taken on the plate there existed a strong correlation to the predicted one-dimensional transient case, during the

application of energy to the plate.

In summary, the writer should re-emphasize that until recently (within the last seven years) very few solutions to transient problems, either on vertical plates or enclosures, have been reported. Until most recently, solutions for the rectangular enclosure could not be attained for Rayleigh numbers greater than 7.5×10^4 . Certainly there still exist a multitude of problems in this general area yet to be solved, provided that mathematical tools are established which are flexible enough to accomodate various boundary conditions.

As a qualitative proof of the method used in this study, the past works of Carlson and MacGregor will be extremely useful in comparing computed results to their experimental and calculated results.

III. DEVELOPMENT OF EQUATIONS

General

The problem studied in this dissertation is formulated in the following statement. Referring to Figure 5, consider a two-dimensional rectangular closure (H by L) initially at thermal equilibrium at some reference temperature T_R .

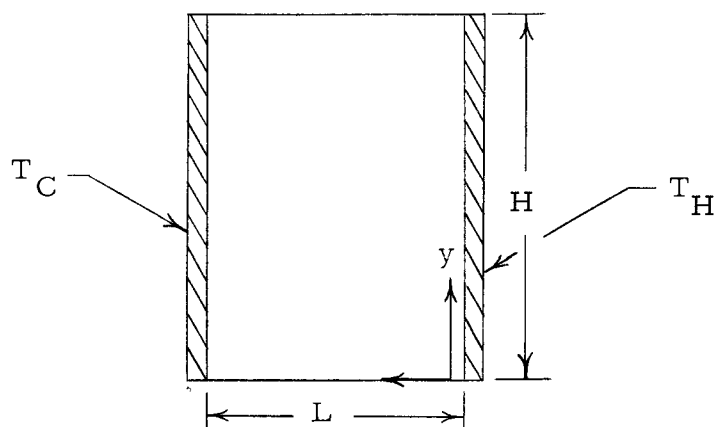


Figure 5. Cross section of rectangular enclosure with isothermal walls.

At some time, $t > 0$, the right hand wall temperature is elevated by some arbitrary amount ΔT such that $T_R + \Delta T = T_H$ and similarly, the left hand wall is lowered by an identical amount ΔT such that $T_R - \Delta T = T_C$. This establishes the isothermal boundaries for one set of calculations.

The top and bottom of the enclosure are considered to be

thermally insulated.

The remaining boundary conditions pertain to the velocity components. For the calculations in this dissertation, velocity components at all enclosure walls are set to zero for all computational time.

Using the stated isothermal boundary conditions, the problem consists of finding velocity and temperature distributions, within the enclosure, as a function of time up to and including the steady state condition. Subsequently, from the temperature distributions attained, the heat transfer characteristics of the enclosure that are usable from an engineering design standpoint, are to be evaluated.

Governing Equations

The general momentum equations which govern a two-dimensional, transient, Newtonian and incompressible fluid flow system are:

$$\rho \frac{\partial U}{\partial t} + \rho \left[U \frac{\partial U}{\partial x} + V \frac{\partial U}{\partial y} \right] = \rho \nu \left[\frac{\partial^2 U}{\partial x^2} + \frac{\partial^2 U}{\partial y^2} \right] - \frac{\partial P}{\partial x} \quad (53)$$

$$\rho \frac{\partial V}{\partial t} + \rho \left[U \frac{\partial V}{\partial x} + V \frac{\partial V}{\partial y} \right] = \rho \nu \left[\frac{\partial^2 V}{\partial x^2} + \frac{\partial^2 V}{\partial y^2} \right] - \rho g - \frac{\partial P}{\partial y} \quad (54)$$

In addition, the conservation of mass or continuity equation for incompressible flow is:

$$\frac{\partial U}{\partial x} + \frac{\partial V}{\partial y} = 0 \quad (55)$$

The energy equation, with negligible viscous dissipation is written as:

$$\rho c_p \left[\frac{\partial T}{\partial t} + U \frac{\partial T}{\partial x} + V \frac{\partial T}{\partial y} \right] = k \left[\frac{\partial^2 T}{\partial x^2} + \frac{\partial^2 T}{\partial y^2} \right] \quad (56)$$

In Equation (54), let P be the total pressure, composed of two elements P_R and P_D in the relationship.

$$P = P_D + P_R \quad (57)$$

where

P_R = static pressure at some reference time, say, $t = 0$

P_D = deviatoric pressure $P - P_R$

When the system shown in Figure 5 is at rest, no deviatoric pressure exists and Equation (54) reduces to:

$$\frac{\partial P_R}{\partial y} = - \rho_R g \quad (58)$$

Taking the partial derivative of Equation (57) results in

$$\frac{\partial P}{\partial y} = \frac{\partial P_D}{\partial y} + \frac{\partial P_R}{\partial y} = + \frac{\partial P_D}{\partial y} - \rho_R g \quad (59)$$

and similarly in Equation (53),

$$\frac{\partial P}{\partial x} = \frac{\partial P_D}{\partial x} \quad (60)$$

Substituting (59) and (60) into the original Equations (53) and (54)

yields:

$$\rho \frac{\partial U}{\partial t} + \rho \left[U \frac{\partial U}{\partial x} + V \frac{\partial U}{\partial y} \right] = \rho \nu \left[\frac{\partial^2 U}{\partial x^2} + \frac{\partial^2 U}{\partial y^2} \right] - \frac{\partial P_D}{\partial x} \quad (61)$$

and

$$\rho \frac{\partial V}{\partial t} + \rho \left[U \frac{\partial V}{\partial x} + V \frac{\partial V}{\partial y} \right] = \rho \nu \left[\frac{\partial^2 V}{\partial x^2} + \frac{\partial^2 V}{\partial y^2} \right] + g(\rho_R - \rho) - \frac{\partial P_D}{\partial y} \quad (62)$$

The transport terms as they appear in Equations (61) and (62) may be written collectively in vector form as:

$$\left(U \frac{\partial U}{\partial x} + V \frac{\partial U}{\partial y} \right) \hat{i} + \left(U \frac{\partial V}{\partial x} + V \frac{\partial V}{\partial y} \right) \hat{j} \equiv (\vec{A} \cdot \nabla) \vec{A} \quad (63)$$

where \vec{A} , in this case, represented the two-dimensional vector

$$\vec{A} = U \hat{i} + V \hat{j}$$

and \hat{i} and \hat{j} are unit vectors along the x and y coordinates.

In keeping with the conservation of momentum principle, a slightly different form of Equation (63) is more appropos. It is desirable to express a vector quantity which would represent momentum flux in form of $\nabla \cdot \vec{A} \vec{A}$.

Consider two arbitrary vectors, \vec{B} and \vec{C} , in the form

$$\vec{B} = U_1 \hat{i} + V_1 \hat{j}$$

$$\vec{C} = U_2 \hat{i} + V_2 \hat{j}$$

It can be shown that for the above set, the following identity:

$$\nabla \cdot \vec{B} \vec{C} = (\vec{B} \cdot \nabla \vec{C}) + \vec{C}(\nabla \cdot \vec{B}) \quad (64)$$

is valid.

First, forming the quantity on the left-hand side of the equation results in

$$\begin{aligned} \nabla \cdot \vec{B} \vec{C} &= \left(\frac{\partial}{\partial x} \hat{i}, \frac{\partial}{\partial y} \hat{j} \right) \cdot (U_1 \hat{i}, V_1 \hat{j}) \begin{pmatrix} U_2 \hat{i} \\ V_2 \hat{j} \end{pmatrix} \\ &= \left(\frac{\partial}{\partial x} \hat{i}, \frac{\partial}{\partial y} \hat{j} \right) \cdot \begin{pmatrix} U_1 U_2 \hat{i} \hat{i} & U_1 V_2 \hat{i} \hat{j} \\ V_1 U_2 \hat{j} \hat{i} & V_1 V_2 \hat{j} \hat{j} \end{pmatrix} \\ &= \left(\frac{\partial}{\partial x} (U_1 U_2) + \frac{\partial}{\partial y} (V_1 U_2) \right) \hat{i} + \left(\frac{\partial}{\partial x} (U_1 V_2) + \frac{\partial}{\partial y} (V_1 V_2) \right) \hat{j} \end{aligned} \quad (65a)$$

$$\begin{aligned} &= \left(U_1 \frac{\partial U_2}{\partial x} + U_2 \frac{\partial U_1}{\partial x} + V_1 \frac{\partial U_2}{\partial y} + U_2 \frac{\partial V_1}{\partial y} \right) \hat{i} + \left(U_1 \frac{\partial V_2}{\partial x} + V_2 \frac{\partial U_1}{\partial x} + V_1 \frac{\partial V_2}{\partial y} + V_2 \frac{\partial V_1}{\partial y} \right) \hat{j} \\ &\quad (65b) \end{aligned}$$

Expanding the left-hand side of Equation (64) results in

$$\begin{aligned} (\vec{B} \cdot \nabla \vec{C}) &= (U_1 \hat{i}, V_1 \hat{j}) \cdot \left(\frac{\partial}{\partial x} \hat{i}, \frac{\partial}{\partial y} \hat{j} \right) \begin{pmatrix} U_2 \hat{i} \\ V_2 \hat{j} \end{pmatrix} = (U_1 \hat{i}, V_1 \hat{j}) \cdot \begin{pmatrix} \frac{\partial U_2}{\partial x} \hat{i} \hat{i} & \frac{\partial V_2}{\partial x} \hat{i} \hat{j} \\ \frac{\partial U_2}{\partial y} \hat{j} \hat{i} & \frac{\partial V_2}{\partial y} \hat{j} \hat{j} \end{pmatrix} \\ &= \left(U_1 \frac{\partial U_2}{\partial x} + V_1 \frac{\partial U_2}{\partial y} \right) \hat{i} + \left(U_1 \frac{\partial V_2}{\partial x} + V_1 \frac{\partial V_2}{\partial y} \right) \hat{j} \end{aligned} \quad (65c)$$

and for

$$\begin{aligned}
 \vec{C}(\nabla \cdot \vec{B}) &= (U_2 \hat{i}, V_2 \hat{j}) \left(\frac{\partial}{\partial x} \hat{i}, \frac{\partial}{\partial y} \hat{j} \right) \cdot \begin{pmatrix} U_1 \hat{i} \\ V_1 \hat{j} \end{pmatrix} \\
 &= (U_2 \hat{i}, V_2 \hat{j}) \cdot \begin{pmatrix} \frac{\partial U_1}{\partial x} \hat{i} \hat{i} & \frac{\partial V_1}{\partial x} \hat{i} \hat{j} \\ \frac{\partial U_1}{\partial y} \hat{j} \hat{i} & \frac{\partial V_1}{\partial y} \hat{j} \hat{j} \end{pmatrix} \\
 &= (U_2 \frac{\partial U_1}{\partial x} + V_2 \frac{\partial U_1}{\partial y}) \hat{i} + (U_2 \frac{\partial V_1}{\partial x} + V_2 \frac{\partial V_1}{\partial y}) \hat{j} \quad (65d)
 \end{aligned}$$

Note here that the sum of the components in Equations (65c) and (65d) is equal to Equation (65b). For a special case of the identity,

let $\vec{B} = \vec{C} = \vec{A}$, then

$$\nabla \cdot \vec{A} \vec{A} = \vec{A} \cdot \nabla \vec{A} + \vec{A}(\nabla \cdot \vec{A}) \quad (66)$$

However, for incompressible flow, $\nabla \cdot \vec{A}$ is zero and Equation (66) is reduced to

$$\nabla \cdot \vec{A} \vec{A} = \vec{A} \cdot \nabla \vec{A}$$

Furthermore, substituting $U_1 = U_2 = U$ and $V_1 = V_2 = V$ into Equations (65b) and (65c) yields:

$$\begin{aligned}
 \left(\frac{\partial}{\partial x} (U^2) + \frac{\partial}{\partial y} (UV) \right) \hat{i} + \left(\frac{\partial}{\partial x} (UV) + \frac{\partial}{\partial y} (V^2) \right) \hat{j} &= \left(U \frac{\partial U}{\partial x} + V \frac{\partial U}{\partial y} \right) \hat{i} + \left(U \frac{\partial V}{\partial x} + V \frac{\partial V}{\partial y} \right) \hat{j} \\
 &\quad (67)
 \end{aligned}$$

Note that the right-hand side of Equation (67) contains those terms in the original equations shown in (63).

Replacing terms from Equation (67) into the appropriate Equations (61) and (62) results in:

$$\rho \frac{\partial U}{\partial t} + \rho \left[\frac{\partial(U^2)}{\partial x} + \frac{\partial(UV)}{\partial y} \right] = \rho \nu \left[\frac{\partial^2 U}{\partial x^2} + \frac{\partial^2 U}{\partial y^2} \right] - \frac{\partial P_D}{\partial x} \quad (68)$$

$$\rho \frac{\partial V}{\partial t} + \rho \left[\frac{\partial(V^2)}{\partial y} + \frac{\partial(UV)}{\partial x} \right] = \rho \nu \left[\frac{\partial^2 V}{\partial x^2} + \frac{\partial^2 V}{\partial y^2} \right] + g(\rho_R - \rho) - \frac{\partial P_D}{\partial y} \quad (69)$$

Dividing through by ρ , and using the ideal gas relationship, the buoyancy term in Equation (69) becomes:

$$g\left(\frac{\rho_R - \rho}{\rho}\right) = g\left(\frac{T - T_R}{T_R}\right)$$

Now the momentum partial differential equations, in final form, become:

$$\frac{\partial U}{\partial t} + \frac{\partial(U^2)}{\partial x} + \frac{\partial(UV)}{\partial y} = \nu \left(\frac{\partial^2 U}{\partial x^2} + \frac{\partial^2 U}{\partial y^2} \right) - \frac{1}{\rho} \frac{\partial P_D}{\partial x} \quad (70)$$

and

$$\frac{\partial V}{\partial t} + \frac{\partial(V^2)}{\partial y} + \frac{\partial(UV)}{\partial x} = \nu \left(\frac{\partial^2 V}{\partial x^2} + \frac{\partial^2 V}{\partial y^2} \right) + g\left(\frac{T - T_R}{T_R}\right) - \frac{1}{\rho} \frac{\partial P_D}{\partial y} \quad (71)$$

This results in a set of equations which consider the flow to be incompressible except for the one term in Equation (71) which allows a

variation in density which is essential in creating the buoyancy effect.

Equation (56) may also be modified through the use of the vector identity:

$$\vec{A} \cdot \nabla \phi = \nabla \cdot (\phi \vec{A}) - \phi \nabla \cdot \vec{A} \quad (72)$$

In Equation (72) ϕ is a scalar quantity or temperature in this case, and \vec{A} is the two-dimensional velocity vector defined in Equation (63). Substituting appropriate quantities into Equation (72), then:

$$\vec{A} \cdot \nabla T = \nabla \cdot T \vec{A} - T(\nabla \cdot \vec{A})$$

but

$$\nabla \cdot \vec{A} = 0$$

and therefore

$$\vec{A} \cdot \nabla T = \nabla \cdot \vec{A} T \quad (73)$$

Substituting (73) into Equation (56) and dividing both sides of the equation by ρc_p gives

$$\frac{\partial T}{\partial t} + \frac{\partial(UT)}{\partial x} + \frac{\partial(VT)}{\partial y} = \alpha \left(\frac{\partial^2 T}{\partial x^2} + \frac{\partial^2 T}{\partial y^2} \right) \quad (74)$$

where α is the thermal diffusivity and is equal to $k/\rho c_p$.

The resulting governing Equations now appear in the form of Equations (56, 70, 71 and 74).

The initial and boundary conditions for the problem of interest

can be listed as:

$$\text{at } t = 0 \quad U = V = 0 \quad T = T_R \quad \text{for } 0 \leq x \leq L \quad \text{and} \quad 0 \leq y \leq H \quad (75)$$

$$\text{at } t > 0 \quad U = V = 0 \quad \text{for } \begin{cases} 0 \leq y \leq H & \text{at } x = 0 \quad \text{and} \quad x = L \\ 0 \leq x \leq L & \text{at } y = 0 \quad \text{and} \quad y = H \end{cases} \quad (76)$$

$$\left. \begin{aligned} T &= T_H \quad \text{for } 0 \leq y \leq H \quad \text{at } x = 0 \\ T &= T_C \quad \text{for } 0 \leq y \leq H \quad \text{at } x = L \\ \frac{dT}{dy} &= 0 \quad \text{for } 0 \leq x \leq L \quad \text{at } y = 0 \quad \text{and} \quad y = H \end{aligned} \right\} \quad (77)$$

Finite Difference Equations

Finite difference approximations are basically established by considering a Taylor series expansion of a dependent variable about an arbitrary point. In this manner, the values of surrounding points and the derivatives (assuming they exist) in the vicinity of the point of interest can be expanded in two-dimensional form as:

$$\begin{aligned} f(x+a, y+b) &= f(a, b) + \left(a \frac{\partial}{\partial x} + b \frac{\partial}{\partial y} \right) f(x, y) \Big|_{a,b} + \frac{1}{2!} \left(a \frac{\partial}{\partial x} + b \frac{\partial}{\partial y} \right)^2 f(x, y) \Big|_{a,b} \\ &+ \dots + \frac{1}{(n-1)!} \left(a \frac{\partial}{\partial x} + b \frac{\partial}{\partial y} \right)^{n-1} f(x, y) \Big|_{a,b} + R_n \end{aligned}$$

where R_n is the remainder term. Considering a and b in the

interval $(0, 1)$ the remainder term has an associated round-off error of an order of magnitude (denoted as θ) in the range of

$$R_n \sim \theta(a+b)^n$$

A system of grids, as shown in Figure 6, is now defined to facilitate the incorporation of first and second order space derivatives. Note that in the accompanying figure, a "cell" which is centered at i, j is surrounded by boundary points $(i \pm \frac{1}{2}, j)$ and $(i, j \pm \frac{1}{2})$,

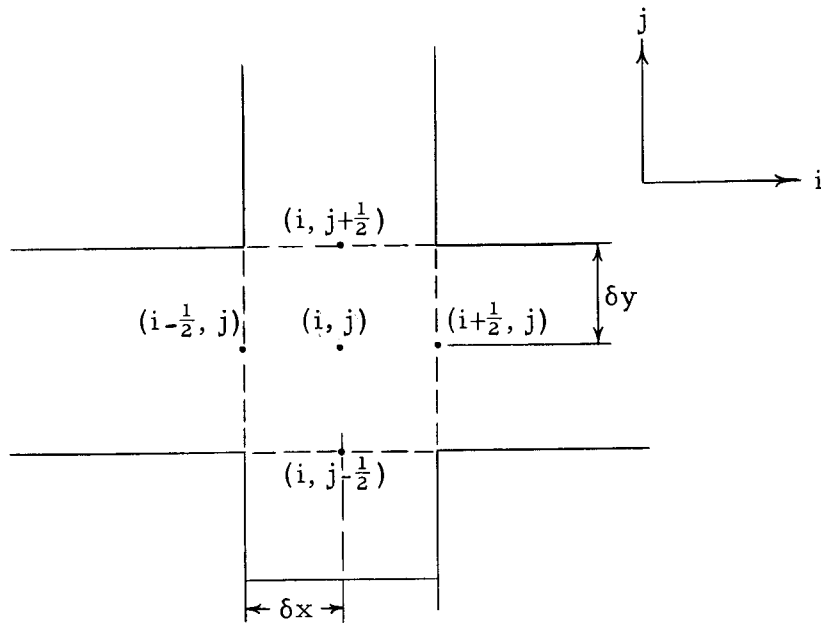


Figure 6. Cell (i, j) and neighboring points.

Expansions of the velocity component, U , as an example, can now be written as:

$$U_{i+\frac{1}{2},j} = U_{ij} + \delta x \frac{\partial U}{\partial x} + \frac{\delta x^2}{2!} \frac{\partial^2 U}{\partial x^2} + \frac{\delta x^3}{3!} \frac{\partial^3 U}{\partial x^3} + \dots \quad (78)$$

and

$$U_{i-\frac{1}{2},j} = U_{ij} - \delta x \frac{\partial U}{\partial x} + \frac{\delta x^2}{2!} \frac{\partial^2 U}{\partial x^2} - \frac{\delta x^3}{3!} \frac{\partial^3 U}{\partial x^3} + \dots \quad (79)$$

assuming $\frac{\partial U}{\partial x}$, $\frac{\partial^2 U}{\partial x^2}$ etc., do exist and can be evaluated at i, j .

From Equations (78) and (79), backward, forward and central differences can be easily formed. By subtracting the two equations, the central difference--first order approximation is established as:

$$\frac{\partial U}{\partial x} \approx \frac{U_{i+\frac{1}{2},j} - U_{i-\frac{1}{2},j}}{\delta x} + \theta(\delta x)^2 \quad (80)$$

where $\theta(\delta x)^2$ represents the truncation error associated with this finite difference approximation.

A similar expression of V can be written and substituting the U and V expressions into Equation (55) establishes the continuity equation in finite difference form as:

$$\frac{U_{i+\frac{1}{2},j} - U_{i-\frac{1}{2},j}}{\delta x} + \frac{V_{i,j+\frac{1}{2}} - V_{i,j-\frac{1}{2}}}{\delta y} = 0 \quad (81)$$

Unfortunately, the first few terms of Equations (70) and (71) cannot be as easily defined in finite difference form since they involve

squares and cross products of velocity components. These terms are defined to be approximated in the following manner,

$$\frac{\partial(U^2)}{\partial x} = \frac{U_{i+\frac{1}{2},j}^2 - U_{i-\frac{1}{2},j}^2}{\delta x} \quad (82)$$

and

$$\frac{\partial(UV)}{\partial y} = \frac{UV_{i,j+\frac{1}{2}} - UV_{i,j-\frac{1}{2}}}{\delta y} \quad (83)$$

The second order approximations are established by considering Taylor expansions about the point $(i-1, j)$ and $(i+1, j)$ and this, for example, leads to terms such as:

$$\frac{\partial^2 U}{\partial x^2} = \frac{U_{i+1,j} + U_{i-1,j} - 2U_{ij}}{\delta x^2} \quad (84)$$

and

$$\frac{\partial^2 U}{\partial y^2} = \frac{U_{i,j+1} + U_{i,j-1} - 2U_{ij}}{\delta y^2} \quad (85)$$

First- and second-order approximations of all the terms in Equations (70, 71 and 74) can be written in accordance with Equations (82) through (85). By substitution, now the governing equations become:

Momentum in the x Direction

$$\begin{aligned}
 & \frac{U_{i,j}^{n+1} - U_{i,j}^n}{\delta t} + \frac{U_{i+\frac{1}{2},j}^2 - U_{i-\frac{1}{2},j}^2}{\delta x} + \frac{(UV)_{i,j+\frac{1}{2}} - (UV)_{i,j-\frac{1}{2}}}{\delta y} \\
 &= \frac{\bar{\Phi}_{i-\frac{1}{2},j} - \bar{\Phi}_{i+\frac{1}{2},j}}{\delta x} + \nu \left[\frac{U_{i+1,j} + U_{i-1,j} - 2U_{ij}}{\delta x^2} + \frac{U_{i,j+1} + U_{i,j-1} - 2U_{ij}}{\delta y^2} \right] \quad (86)
 \end{aligned}$$

Momentum in the y Direction

$$\begin{aligned}
 & \frac{V_{i,j}^{n+1} - V_{i,j}^n}{\delta t} + \frac{V_{i,j+\frac{1}{2}}^2 - V_{i,j-\frac{1}{2}}^2}{\delta y} + \frac{(UV)_{i+\frac{1}{2},j} - (UV)_{i-\frac{1}{2},j}}{\delta x} \\
 &= \frac{\bar{\Phi}_{i,j-\frac{1}{2}} - \bar{\Phi}_{i,j+\frac{1}{2}}}{\delta y} + \nu \left[\frac{V_{i+1,j} + V_{i-1,j} - 2V_{ij}}{\delta x^2} + \frac{V_{i,j+1} + V_{i,j-1} - 2V_{ij}}{\delta y^2} \right] \\
 & \quad + g \left[\frac{T_{i,j+\frac{1}{2}} - T_R}{T_R} \right] \quad (87)
 \end{aligned}$$

Conservation of Energy

$$\begin{aligned}
 & \frac{T_{ij}^{n+1} - T_{ij}^n}{\delta t} + \frac{(UT)_{i+\frac{1}{2},j} - (UT)_{i-\frac{1}{2},j}}{\delta x} + \frac{(VT)_{i,j+\frac{1}{2}} - (VT)_{i,j-\frac{1}{2}}}{\delta y} \\
 &= \alpha \left[\frac{T_{i+1,j} + T_{i-1,j} - 2T_{ij}}{\delta x^2} + \frac{T_{i,j+1} + T_{i,j-1} - 2T_{ij}}{\delta y^2} \right] \quad (88)
 \end{aligned}$$

where the symbol, $\bar{\Phi}$, shown in Equations (86) and (87), represents the pressure head $\left(\frac{P_D}{\rho}\right)$. The superscripts n and $n+1$ represent advancements in the time frame. The four unknowns in

Equations (86, 87 and 88) are U , V , T and Φ . Substitution of the continuity equation into the above set is of little value since the momentum equations would revert to a form shown in Equations (61) and (62). Therefore, in order to obtain a fourth equation, the time rate of change of the continuity equation is considered. This appears to be contradictory to Equation (55) which established the continuity equation for incompressible flow. Theoretically, this is true; but for any real fluid analysis, it is finite. Finite values in this case are considerably less than 1, on the order of 10^{-3} .

Rewriting the continuity equation to be

$$\frac{U_{i+\frac{1}{2},j} - U_{i-\frac{1}{2},j}}{\delta x} + \frac{V_{i,j+\frac{1}{2}} - V_{i,j-\frac{1}{2}}}{\delta y} = D_{ij} \quad (81a)$$

Now the time rate of change of D_{ij} is written as:

$$\begin{aligned} \frac{D_{ij}^{n+1} - D_{ij}^n}{\delta t} = & \frac{1}{\delta t} \left[\left(\frac{U_{i+\frac{1}{2},j}^{n+1} - U_{i+\frac{1}{2},j}^n}{\delta x} \right) - \left(\frac{U_{i-\frac{1}{2},j}^{n+1} - U_{i-\frac{1}{2},j}^n}{\delta x} \right) \right] \\ & + \frac{1}{\delta t} \left[\left(\frac{V_{i,j+\frac{1}{2}}^{n+1} - V_{i,j+\frac{1}{2}}^n}{\delta y} \right) - \left(\frac{V_{i,j-\frac{1}{2}}^{n+1} - V_{i,j-\frac{1}{2}}^n}{\delta y} \right) \right] \quad (89) \end{aligned}$$

Note here that each of the elements of Equation (89) represent either a forward- or backward-difference of the derived Equations (86) and (87). In reference to Equations (82 and 84), examples of the spatial advancement of a few terms contained in that equations are as follows:

$$\frac{1}{\delta x} \left[\frac{U_{i+\frac{1}{2},j}^2 - U_{i-\frac{1}{2},j}^2}{\delta x} \right] \approx \frac{U_{i+1,j}^2 - U_{ij}^2}{\delta x^2} \quad (90)$$

$$\frac{1}{\delta x} \left[\frac{U_{i+1,j} + U_{i-1,j} - 2U_{ij}}{\delta x^2} \right] \approx \frac{U_{i+\frac{3}{2},j} + U_{i-\frac{1}{2},j} - 2U_{i+\frac{1}{2},j}}{\delta x^3} \quad (91)$$

The reason for applying the forward difference in the manner shown in Equations (90) and (91) is not readily apparent. It should suffice to mention here, that the use of the above method allows certain advantages in the latter part of this derivation. This will be called to the attention of the reader at the appropriate time.

By using terms similar to those shown in the above expressions, terms applicable to Equation (89) may be written as:

$$\begin{aligned} & \frac{1}{\delta t} \left[\frac{U_{i+\frac{1}{2},j}^{n+1} - U_{i+\frac{1}{2},j}^n}{\delta x} \right] + \frac{1}{\delta x^2} [U_{i+1,j}^2 - U_{ij}^2] + \frac{1}{\delta x \delta y} [(UV)_{i+\frac{1}{2},j+\frac{1}{2}} - (UV)_{i+\frac{1}{2},j-\frac{1}{2}}] \\ &= \frac{1}{\delta x^2} [\Phi_{ij} - \Phi_{i+1,j}] + v \left[\frac{1}{\delta x^2} \left(\frac{U_{i+\frac{3}{2},j} + U_{i-\frac{1}{2},j} - 2U_{i+\frac{1}{2},j}}{\delta x} \right) \right. \\ & \quad \left. + \frac{1}{\delta y^2} \left(\frac{U_{i+\frac{1}{2},j+1} + U_{i+\frac{1}{2},j-1} - 2U_{i+\frac{1}{2},j}}{\delta x} \right) \right] \end{aligned}$$

or by rearrangement the above becomes;

$$\begin{aligned}
& \frac{1}{\delta t} \left[\frac{U_{i+\frac{1}{2},j}^{n+1} - U_{i+\frac{1}{2},j}^n}{\delta x} \right] \\
&= \frac{1}{\delta x} [U_{ij}^2 - U_{i+1,j}^2] + \frac{1}{\delta x \delta y} [(UV)_{i+\frac{1}{2},j-\frac{1}{2}} - (UV)_{i+\frac{1}{2},j+\frac{1}{2}}] + \frac{1}{\delta x} (\Phi_{ij} - \Phi_{i+1,j}) \\
&+ \nu \left[\frac{1}{\delta x} \left(\frac{U_{i+\frac{3}{2},j} + U_{i-\frac{1}{2},j} - 2U_{i+\frac{1}{2},j}}{\delta x} \right) + \frac{1}{\delta y} \left(\frac{U_{i+\frac{1}{2},j+1} + U_{i+\frac{1}{2},j-1} - 2U_{i+\frac{1}{2},j}}{\delta x} \right) \right] \quad (92)
\end{aligned}$$

Similarly, the "backward" difference for the velocity component in the x direction $(U_{i-\frac{1}{2},j})$ can be written as:

$$\begin{aligned}
& \frac{1}{\delta t} \left[\frac{U_{i-\frac{1}{2},j}^{n+1} - U_{i-\frac{1}{2},j}^n}{\delta x} \right] \\
&= \frac{1}{\delta x} [U_{i-1,j}^2 - U_{ij}^2] + \frac{1}{\delta x \delta y} [(UV)_{i-\frac{1}{2},j-\frac{1}{2}} - (UV)_{i-\frac{1}{2},j+\frac{1}{2}}] + \frac{1}{\delta x} [\Phi_{i-1,j} - \Phi_{ij}] \\
&+ \nu \left[\frac{1}{\delta x} \left(\frac{U_{i-\frac{3}{2},j} + U_{i+\frac{1}{2},j} - 2U_{i-\frac{1}{2},j}}{\delta x} \right) + \frac{1}{\delta y} \left(\frac{U_{i-\frac{1}{2},j+1} + U_{i-\frac{1}{2},j-1} - 2U_{i-\frac{1}{2},j}}{\delta x} \right) \right] \quad (93)
\end{aligned}$$

Similar equations for the velocity components in the "y" direction can be expressed as:

$$\begin{aligned}
& \frac{1}{\delta t} \left[\frac{V_{i,j+\frac{1}{2}}^{n+1} - V_{i,j+\frac{1}{2}}^n}{\delta y} \right] = \frac{1}{\delta y} [V_{ij}^2 - V_{i,j+1}^2] + \frac{1}{\delta x \delta y} [(UV)_{i-\frac{1}{2},j+\frac{1}{2}} - (UV)_{i+\frac{1}{2},j+\frac{1}{2}}] \\
&+ \frac{1}{\delta y} [\Phi_{i,j+1} - \Phi_{ij}] + \nu \left[\frac{1}{\delta x} \left(\frac{V_{i+1,j+\frac{1}{2}} + V_{i-1,j+\frac{1}{2}} - 2V_{i,j+\frac{1}{2}}}{\delta y} \right) \right. \\
&\quad \left. + \frac{1}{\delta y} \left(\frac{V_{i,j+\frac{3}{2}} + V_{i,j-\frac{1}{2}} - 2V_{i,j+\frac{1}{2}}}{\delta y} \right) \right] + \frac{g}{\delta y} \left[\frac{T_{i,j+1} - T_R}{T_R} \right]
\end{aligned}$$

And:

$$\begin{aligned}
 & \frac{1}{\delta t} \left[\frac{V_{i,j-\frac{1}{2}}^{n+1} - V_{i,j-\frac{1}{2}}^n}{\delta y} \right] \\
 = & \frac{1}{\delta y} \left[V_{i,j-1}^2 - V_{ij}^2 \right] + \frac{1}{\delta x \delta y} \left[(UV)_{i-\frac{1}{2},j-\frac{1}{2}} - (UV)_{i+\frac{1}{2},j-\frac{1}{2}} \right] \\
 & + v \left[\frac{1}{\delta x} \left(\frac{V_{i+1,j-\frac{1}{2}} + V_{i-1,j-\frac{1}{2}} - 2V_{i,j-\frac{1}{2}}}{\delta y} \right) + \frac{1}{\delta y} \left(\frac{V_{i,j-2} + V_{i,j+\frac{1}{2}} - 2V_{i,j-\frac{1}{2}}}{\delta y} \right) \right] \\
 & + \frac{1}{\delta y} \left[\Phi_{ij} - \Phi_{i,j-1} \right] + \frac{g}{\delta y} \left[\frac{T_{i,j-1} - T_R}{T_R} \right] \quad (95)
 \end{aligned}$$

Substituting Equations (92) through (95) into Equation (89) and arranging terms results in:

$$\begin{aligned}
 & \frac{D_{ij}^{n+1} - D_{ij}^n}{\delta t} \\
 = & \frac{1}{\delta x} \left[2U_{ij}^2 - U_{i+1,j}^2 - U_{i-1,j}^2 \right] + \frac{1}{\delta y} \left[2V_{ij}^2 - V_{i,j+1}^2 - V_{i,j-1}^2 \right] \\
 & - \frac{2}{\delta x \delta y} \left[(UV)_{i+\frac{1}{2},j+\frac{1}{2}} + (UV)_{i-\frac{1}{2},j-\frac{1}{2}} - (UV)_{i+\frac{1}{2},j-\frac{1}{2}} - (UV)_{i-\frac{1}{2},j+\frac{1}{2}} \right] \\
 & + \frac{g}{\delta y} \left[\frac{T_{i,j+1} - T_{i,j-1}}{T_R} \right] - \frac{1}{\delta x} \left(2\Phi_{ij} - \Phi_{i+1,j} - \Phi_{i-1,j} \right) - \frac{1}{\delta y} \left(2\Phi_{ij} - \Phi_{i,j+1} - \Phi_{i,j-1} \right) \\
 & + v \left[\frac{1}{\delta x} \left(\frac{U_{i+\frac{1}{2},j} + U_{i-\frac{1}{2},j} - 2U_{i+\frac{1}{2},j} - U_{i-\frac{1}{2},j} - U_{i+\frac{1}{2},j} + 2U_{i-\frac{1}{2},j}}{\delta x} \right) \right. \\
 & \left. + \frac{1}{\delta y} \left(\frac{U_{i+\frac{1}{2},j+1} + U_{i+\frac{1}{2},j-1} - 2U_{i+\frac{1}{2},j} - U_{i-\frac{1}{2},j-1} - U_{i-\frac{1}{2},j+1} + 2U_{i-\frac{1}{2},j}}{\delta x} \right) + \right.
 \end{aligned}$$

$$\begin{aligned}
& + \frac{1}{\delta x^2} \left(\frac{V_{i+1, j+\frac{1}{2}} + V_{i-1, j+\frac{1}{2}} - 2V_{i, j+\frac{1}{2}} - V_{i+1, j-\frac{1}{2}} - V_{i-1, j-\frac{1}{2}} + 2V_{i, j-\frac{1}{2}}}{\delta y} \right) \\
& + \frac{1}{\delta y^2} \left(\frac{V_{i, j+\frac{3}{2}} + V_{i, j-\frac{1}{2}} - 2V_{i, j+\frac{1}{2}} - V_{i, j-\frac{3}{2}} - V_{i, j+\frac{1}{2}} + 2V_{i, j-\frac{1}{2}}}{\delta y} \right) \Bigg] \quad (96)
\end{aligned}$$

The advantage of allowing a modified difference advancement (Equations (90) and (91)) is readily discernible in the next step. Note that the transport terms of Equation (96) contain terms which are referenced beyond the $i \pm \frac{1}{2}, j$ and $i, j \pm \frac{1}{2}$ cell boundaries established in Figure 6. The remaining velocity terms in Equation (96) are either cross-product velocities surrounding the cell or square velocity terms at points one full increment away from the cell. This allows the matrix which stores the square velocity terms to be cell centered and, therefore, affords a saving in computer memory allocation. This could not have been accomplished by using standardized finite difference advancement techniques.

Moreover, it allows the resulting equations to be expressed in a more systematic and tractable form.

Additional continuity terms can be written, as follows,

$$\begin{aligned}
D_{i+1, j} &= \frac{U_{i+\frac{3}{2}, j} - U_{i+\frac{1}{2}, j}}{\delta x} + \frac{V_{i+1, j+\frac{1}{2}} - V_{i+1, j-\frac{1}{2}}}{\delta y} \\
D_{i-1, j} &= \frac{U_{i-\frac{1}{2}, j} - U_{i-\frac{3}{2}, j}}{\delta x} + \frac{V_{i-1, j+\frac{1}{2}} - V_{i-1, j-\frac{1}{2}}}{\delta y}
\end{aligned}$$

$$D_{i,j+1} = \frac{U_{i+\frac{1}{2},j+1} - U_{i-\frac{1}{2},j+1}}{\delta x} + \frac{V_{i,j+\frac{3}{2}} - V_{i,j+\frac{1}{2}}}{\delta y}$$

$$D_{i,j-1} = \frac{U_{i+\frac{1}{2},j-1} - U_{i-\frac{1}{2},j-1}}{\delta x} + \frac{V_{i,j-\frac{1}{2}} - V_{i,j-\frac{3}{2}}}{\delta y}$$

and substituted into Equation (96) results in

$$\begin{aligned} \frac{D_{ij}^{n+1} - D_{ij}^n}{\delta t} = & -Q_{ij} - \frac{1}{\delta x^2} (\Phi_{i+1,j} + \Phi_{i-1,j} - 2\Phi_{ij}) - \frac{1}{\delta y^2} (\Phi_{i,j+1} + \Phi_{i,j-1} - 2\Phi_{ij}) \\ & + \nu \left[\frac{1}{\delta x^2} (D_{i+1,j} + D_{i-1,j} - 2D_{ij}) + \frac{1}{\delta y^2} (D_{i,j+1} + D_{i,j-1} - 2D_{ij}) \right] \end{aligned} \quad (97)$$

where

$$\begin{aligned} -Q_{ij} = & \frac{U_{i+1,j}^2 + U_{i-1,j}^2 - 2U_{ij}^2}{\delta x^2} + \frac{V_{i,j+1}^2 + V_{i,j-1}^2 - 2V_{ij}^2}{\delta y^2} \\ & + \frac{2}{\delta x \delta y} [(UV)_{i+\frac{1}{2},j+\frac{1}{2}} + (UV)_{i-\frac{1}{2},j-\frac{1}{2}} - (UV)_{i+\frac{1}{2},j-\frac{1}{2}} - (UV)_{i-\frac{1}{2},j+\frac{1}{2}}] \\ & - \frac{g}{\delta y} \left[\frac{T_{i,j+1} - T_{i,j-1}}{T_R} \right] \end{aligned}$$

Another form of Equation (97) can be obtained by setting

$$-R_{ij} = Q_{ij} + \frac{D_{ij}^{n+1} - D_{ij}^n}{\delta t} + \nu \left[\frac{D_{i+1,j} + D_{i-1,j} - 2D_{ij}}{\delta x^2} + \frac{D_{i,j+1} + D_{i,j-1} - 2D_{ij}}{\delta y^2} \right] \quad (97a)$$

and also

$$-R_{ij} = \frac{1}{\delta x^2} (\bar{\Phi}_{i+1,j} + \bar{\Phi}_{i-1,j} - 2\bar{\Phi}_{ij}) + \frac{1}{\delta y^2} (\bar{\Phi}_{i,j+1} + \bar{\Phi}_{i,j-1} - 2\bar{\Phi}_{ij}) \quad (98)$$

Now, solving for $\bar{\Phi}_{ij}$ in Equation (98) results in

$$\bar{\Phi}_{ij} = 2 \left(\frac{\delta x^2 \delta y^2}{\delta x^2 + \delta y^2} \right) \left[\frac{\bar{\Phi}_{i+1,j} + \bar{\Phi}_{i-1,j}}{\delta x^2} + \frac{\bar{\Phi}_{i,j+1} + \bar{\Phi}_{i,j-1}}{\delta y^2} + R_{ij} \right] \quad (99)$$

This completes the derivation and formulation of the difference equations which are used in this study. Special attention is directed to Equations (88, 92, 94 and 99) which are used in the computational sequence to calculate T_{ij} , $U_{i+\frac{1}{2},j}$, $V_{i,j+\frac{1}{2}}$ and $\bar{\Phi}_{ij}$, respectively.

Stability and Convergence Criteria

In applying finite-difference approximations to the solution of partial differential equations, it is imperative that reasonable steps be taken to insure stability and convergence.

Convergence, by definition, implies that solutions attained through the use of an approximation technique approaches the exact solution of the partial differential equations if the increments in spacing and time are made infinitesimally small. For the computational results of the present study, an exact solution of the partial differential equations does not exist. The alternative then, is to compare the computed results to existing experimental data or with known analytical solutions of simplified problems. The results of such comparisons

are noted in Chapter IV.

By comparison to convergence, stability requirements are established to minimize the errors introduced through the use of the finite-difference approximations. Satisfying the stability requirement by itself does not guarantee convergence. A stability criterion for the set of equations used in this study is difficult to establish due to the non-linear nature of the equations. Requirements based on modified sets of governing equations are derived in Appendix A.

The stability requirement used as a guide for this analysis is:

$$\frac{|U|_{\max} \delta t}{\delta x} + \frac{|V|_{\max} \delta t}{\delta y} + \frac{2\nu \delta t}{Pr \delta x^2} + \frac{2\nu \delta t}{Pr \delta y^2} \leq .3 \quad (100)$$

Theoretically, the right-hand side of Equation (100) can be shown to be one. However, for computations in this study, a value of .3 was chosen.

When using approximation techniques of any sort, the selection of a suitable time increment becomes a matter of compromise. Ideally, it is advantageous to maintain a small mesh size ($2\delta x$ by $2\delta y$) in order to minimize truncation errors. This can be accomplished at the expense of a considerable increase in required computational time to obtain steady state solutions. For this study, a cell size of $2\delta x = .1$ and $2\delta y = .5$ is used which is not extremely prohibitive with respect to the allowable time increment. The cell size chosen is

comparable to those used by Wilkes [50] and MacGregor [27] in preceding analyses.

Boundary Conditions

Having completed the derivation of the finite difference equations to be used in the solution of the rectangular enclosure problem, consideration is now given to the boundary conditions stated in Equations (75) through (77). For the rectangular enclosure problem, it is assumed that both the normal and tangential velocity components vanish at the vertical and horizontal walls (i. e., no-slip condition). Furthermore, the horizontal walls are considered to be insulating surfaces and the vertical walls are taken as isothermal.

The cell orientation for the rectangular cavity problem is shown in Figure 7.

Cells at typical locations $(i-1, j)$ and $(i+m+1, j)$ are segments within isothermal cold and hot walls respectively. Cells at typical locations $(i, j-1)$ and $(i, j+n+1)$ represent segments of the horizontal insulated walls.

The boundary conditions required for the solution of the rectangular enclosure are now derived for a typical boundary cell location $(p-1, q)$ adjacent to a fluid cell (p, q) as shown in Figure 8.

In the accompanying figure, note that only the velocity terms, U and V , are shown along the cell boundaries and centers.

Temperature values with identical subscripts also exist at these locations.

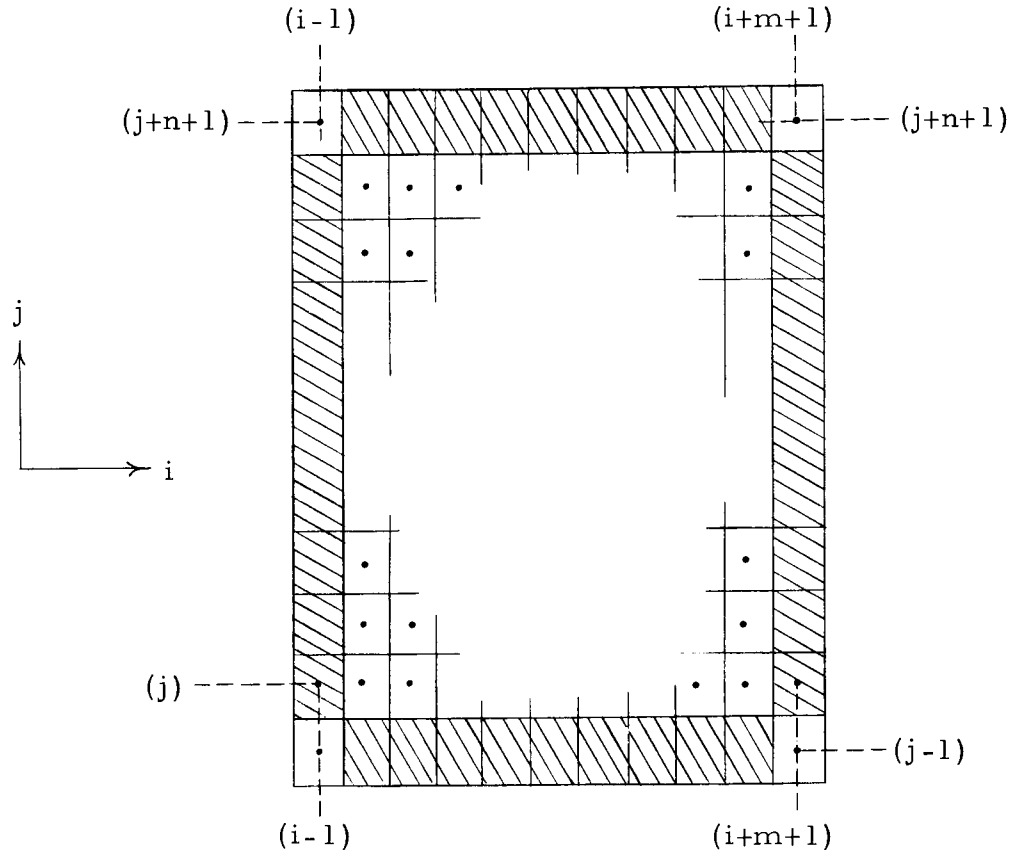


Figure 7. Orientation of cells for rectangular enclosure problem.

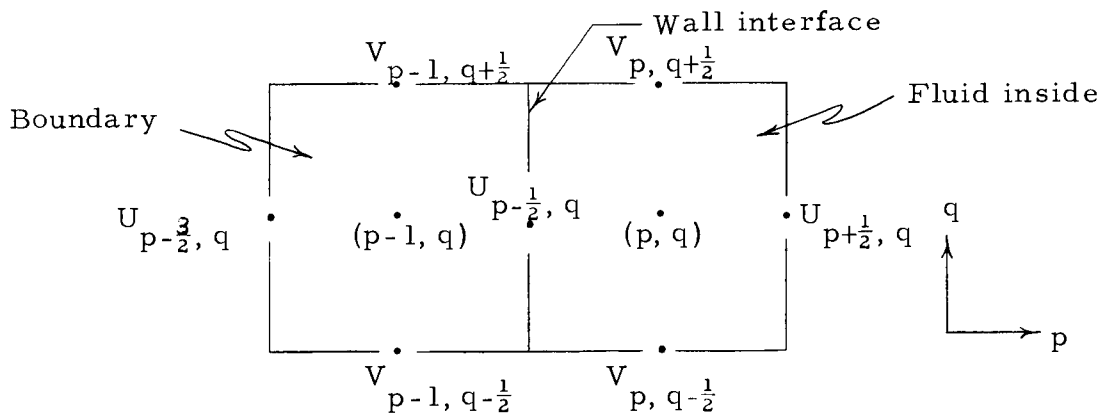


Figure 8. Typical velocity components for fluid and boundary cells.

Considering the temperature boundaries, the isothermal condition is easily established by letting:

$$\begin{aligned} T_{p-1, q} &= T_{p-\frac{1}{2}, q} = \text{constant} \\ T_{p-1, q \pm \frac{1}{2}} &= T_{p-\frac{1}{2}, q \pm \frac{1}{2}} = \text{constant} \end{aligned} \quad (101)$$

The insulated or adiabatic boundary condition is appropriately established by the relationship

$$\begin{aligned} T_{p-1, q} &= T_{p, q} \\ T_{p-1, q \pm \frac{1}{2}} &= T_{p, q \pm \frac{1}{2}} \end{aligned} \quad (102)$$

and by interpolating between the values in (102), also implies that

$$T_{p-\frac{1}{2}, q} = T_{p-\frac{1}{2}, q \pm \frac{1}{2}} = T_{p, q} \quad (103)$$

In order to establish the no-slip boundary condition for cells between cells $(p-1, q)$ and (p, q) the following conditions are specified.

Let

$$V_{p-1, q \pm \frac{1}{2}} = -V_{p, q \pm \frac{1}{2}} \quad (104)$$

and

$$V_{p-1, q} = -V_{p, q}$$

then interpolating between the values of (104), the tangential component

at the wall-fluid interface vanishes, or

$$V_{p-\frac{1}{2}, q \pm \frac{1}{2}} = V_{p-\frac{1}{2}, q} = 0 \quad (105)$$

For the normal velocity component, let

$$U_{p-\frac{1}{2}, q} = U_{p-\frac{1}{2}, q \pm \frac{1}{2}} = 0 \quad (106)$$

Also continuity is satisfied for both cells if $U_{p-\frac{3}{2}, q} = U_{p+\frac{1}{2}, q}$ thus requiring that $D_{p-1, q} = D_{pq}$. One additional requirement is necessary for the no-slip boundary condition in that a boundary " Φ " must be specified for cell $(p-1, q)$. Reference is made to Equation (93) which represents the "backward" difference equation of $U_{p-\frac{1}{2}, q}$. Solving this equation for $\Phi_{p-1, q}$ results in the following:

$$\begin{aligned} & \Phi_{p-1, q} - \Phi_{pq} \\ &= (U_{p, q}^2 - U_{p-1, q}^2) - \frac{\delta x}{\delta t} (U_{p-\frac{1}{2}, q}^{n+1} - U_{p-\frac{1}{2}, q}^n) + \frac{\delta x}{\delta y} [(UV)_{p-\frac{1}{2}, q+\frac{1}{2}} - (UV)_{p-\frac{1}{2}, q-\frac{1}{2}}] \\ & - \nu \left[\frac{U_{p-\frac{3}{2}, q} + U_{p+\frac{1}{2}, q} - 2U_{p-\frac{1}{2}, q}}{\delta x} + \frac{\delta x^2}{\delta y^2} \left(\frac{U_{p-\frac{1}{2}, q+1} + U_{p-\frac{1}{2}, q-1} - 2U_{p-\frac{1}{2}, q}}{\delta x} \right) \right] \end{aligned} \quad (107)$$

Now substituting the boundary conditions derived in Equations (104, 105 and 106), Equation (107) becomes

$$\Phi_{p-1, q} = \Phi_{p, q} - \frac{2\nu}{\delta x} (U_{p+\frac{1}{2}, q} - U_{p-\frac{1}{2}, q}) \quad (108)$$

where $\Phi_{p-1,q}$ represents a hypothetical boundary pressure term which is dependent upon values of the adjacent cell (p,q) .

Table 1 is a listing of the pertinent boundary conditions for the rectangular enclosure with reference to Figure 7.

The general equations are capable of handling "in" flow and "out" flow boundaries with relative ease. Welch et al. [49], have derived the necessary velocity and pressure boundary conditions for a one-dimensional, flat velocity profile (i. e. $V_{p-1,q \pm \frac{1}{2}} = V_{p-1,q} = \text{constant}$ in Figure 8) "in" flow condition. This can easily be extended to include the general use of any "in" flow velocity profile, through some simple manipulations of Equation (93).

Computational Method and Flow Diagrams

To provide solutions for the rectangular enclosure problem, a computer program was formed for use on the IBM 7094 Data Processing System, using equations derived earlier in this Chapter. A listing of this program, written in FORTRAN IV language, is contained in Appendix A.

This particular program can handle approximately 800 boundary and fluid cells of the type described earlier.

The intent of this section is to provide a step-by-step description of the computer program for one complete time increment.

Complementing this written description are flow diagrams shown in

Table 1. Boundary conditions for rectangular enclosure problem in finite difference form.

Condition	Location			
	$i-1, j$	$i+m+1, j$	$i, j-1$	$i, j+n+1$
Isothermal	$T_{i-1, j} = T_{i-\frac{1}{2}, j}$	$T_{i+m+1, j} = T_{i+m+\frac{1}{2}, j}$		
	$T_{i-1, j\pm\frac{1}{2}} = T_{i-\frac{1}{2}, j\pm\frac{1}{2}}$	$T_{i+m+1, j\pm\frac{1}{2}} = T_{i+m+\frac{1}{2}, j\pm\frac{1}{2}}$		
Adiabatic			$T_{ij} = T_{i, j-1}$ $T_{i\pm\frac{1}{2}, j} = T_{i\pm\frac{1}{2}, j-1}$	$T_{i, j+n+1} = T_{i, j+n}$ $T_{i\pm\frac{1}{2}, j+n+1} = T_{i\pm\frac{1}{2}, j+n}$
No-slip	$V_{i-1, j\pm\frac{1}{2}} = -V_{i, j\pm\frac{1}{2}}$ $V_{i-1, j} = -V_{ij}$ $U_{i-\frac{1}{2}, j} = U_{i-\frac{1}{2}, j\pm\frac{1}{2}} = 0$ $\Phi_{i-1, j} = \Phi_{ij}$ $-\frac{2\nu}{\delta x}(U_{i+\frac{1}{2}, j} - U_{i-\frac{1}{2}, j})$	$V_{i+m+1, j\pm\frac{1}{2}} = -V_{i+m, j\pm\frac{1}{2}}$ $V_{i+m+1, j} = -V_{i+m, j}$ $U_{i+m+\frac{1}{2}, j} + U_{i+m+\frac{1}{2}, j\pm\frac{1}{2}} = 0$ $\Phi_{i+m+1, j} = \Phi_{i+m, j}$ $+\frac{2\nu}{\delta x}(U_{i+m-\frac{1}{2}, j} - U_{i+m+\frac{1}{2}, j})$	$U_{i\pm\frac{1}{2}, j-1} = -U_{i\pm\frac{1}{2}, j}$ $U_{i, j-1} = -U_{ij}$ $V_{i, j-\frac{1}{2}} = V_{i\pm\frac{1}{2}, j-\frac{1}{2}} = 0$ $\Phi_{i, j-1} = \Phi_{ij}$ $-\frac{2\nu}{\delta y}(V_{i, j+\frac{1}{2}} - V_{i, j-\frac{1}{2}})$	$U_{i\pm\frac{1}{2}, j+n+1} = -U_{i\pm\frac{1}{2}, j+n}$ $U_{i, j+n+1} = -U_{i, j+n}$ $V_{i, j+n+\frac{1}{2}} = V_{i\pm\frac{1}{2}, j+n+\frac{1}{2}} = 0$ $\Phi_{i, j+n+1} = \Phi_{i, j+n}$ $+\frac{2\nu}{\delta y}(V_{i, j+n-\frac{1}{2}} - V_{i, j+n+\frac{1}{2}})$

Figures 9 through 13.

All the general features of the program stem from a format called MAIN (Figure 9). The basis of this portion of the program is to provide access to all subroutines in an orderly fashion, and initiate the necessary read, write and rewind of tapes. The subroutines called up in order of use are INPUT, SET, BOUND, POLATE and COMPUTE. Access to the output, per time increment, is provided through MAIN along with dump safety features and tape rewinds.

The abbreviated nomenclature used in Figure 9 is explained as follows:

ITNO - time step iteration number
 ITM - maximum number of time iterations per run
 ISTOP - termination flag
 NOIT - maximum number of iterations taken in previous computations
 TIMAX - upper bound on simulation time
 NOPRT - iteration number for printing

The first subroutine called upon by MAIN is INPUT (Figure 10) which reads and writes two kinds of input data. The first category consists of reading the following:

DELX (δx) - cell increment in the x direction
 DELY (δy) - cell increment in the y direction
 XNU (ν) - viscosity

GY (g) - gravitational constant

DELTA (δt) - time increment

TIMAX - total length of run time

TREF (T_R) - reference temperature for buoyancy term

For the second data category, a test is made on the value of INMODE to determine the type of input data to be used. Therefore:

If INMODE = 0 read velocity and temperature from provided
punched cards

```
or INMODE < 0    read tape from previous run
```

or INMODE > 0 choices on having velocity and/or temperature

INMODE = 2 read from cards or tape.

One additional function of this subroutine is to call output if a printout of the initial data is requested.

The next subroutine is SET, also shown in Figure 11, which computes some basic values dependent upon the input. Some of these values are:

$$\text{DEL X2} = (\delta \mathbf{x})^2$$

TREF (T_R).

The BOUND subroutine (Figure 12) sets the required boundary conditions for the adiabatic and no-slip walls.

The POLATE subroutine interpolates data along the rows and columns to provide a value for U , V and T between either the input values or the newly computed values. Examples of the types of equations stored in POLATE are as follows:

$$U_{ij} = \frac{U_{i+\frac{1}{2},j} + U_{i-\frac{1}{2},j}}{2}$$

$$V_{ij} = \frac{V_{i,j+\frac{1}{2}} + V_{i,j-\frac{1}{2}}}{2}$$

$$T_{i,j+\frac{1}{2}} = \frac{T_{ij} + T_{i+1,j}}{2}$$

Values for the quantities U^2 , V^2 , UV , UT and VT are also computed in this subroutine.

The COMPUTE subroutine (Figure 13) provides the update values for U , V and T based on the values of the previous iteration. To insure that only the last computed values are utilized in the update, temporary matrices in the forms of UOLD, VOLD and TOLD are established. In this manner, the explicit form of the partial differential equations is maintained throughout the entire computational sequence.

The major computations in this subroutine are accomplished in the following manner:

- a) Compute $U_{i+\frac{1}{2}, j}$ by Equation (92), starting with the first row of the fluid region and proceeding from left to right up the columns.
- b) Compute $V_{i+\frac{1}{2}, j}$ and T_{ij} from Equations (94) and (88), respectively, in a similar manner.
- c) Test U , V , and T , separately, at the $(n+1)^{\text{th}}$ time increment compared to steady state criteria.
- d) Call BOUND to perform the necessary manipulations required by Equations (101) through (108).
- e) Call POLATE to interpolate values between the computed or boundary set values.
- f) A test is performed on all three steady state criteria (U , V and T) and if all three are not met, the program continues to calculate.
- g) Continuity (D_{ij}) and (R_{ij}) at every cell center using Equations (81a) and (97a), respectively.
- h) Note here that the form of Equation (99) is easily adaptable to an iterative procedure for calculating Φ_{ij} . In calculating Φ_{ij} , values of $\Phi_{i\pm 1, j}$ and $\Phi_{i, j\pm 1}$ must be known. Assume that an initial guess for the field exists either in the form of data input or from a previously calculated time increment. In a systematic manner, new values for Φ_{ij} (for all i, j) can be obtained within a given time increment by the

equation:

$$\Phi_{ij}^{h+1} = 2 \left(\frac{\delta x^2 \delta y^2}{\delta x^2 + \delta y^2} \right) \left(\frac{\Phi_{i+1,j}^h + \Phi_{i-1,j}^h}{\delta x^2} + \frac{\Phi_{i,j+1}^h + \Phi_{i,j-1}^h}{\delta y^2} + R_{ij} \right) \quad (99a)$$

where $h+1$ represents the advanced values toward convergence of this iteration process.

This method is simply the Gauss-Seidel method of iteration for the solution of a system of simultaneous equations. It has been shown that the method converges toward the values of Φ_{ij} , which exactly satisfy Equation (99a), as the number of iterations approach infinity. In practice, the calculations are truncated to a finite number dependent on the selection of an accuracy criterion. The criterion used in the program is:

$$\left(\frac{|\Phi_{old} - \Phi_{new}|}{|\Phi_{old}| + |\Phi_{new}| + U_{ij}^2 + V_{ij}^2 + gH} \right)_{\max} < 2 \times 10^{-4}$$

The program is written such that a maximum of 1000 iterations is allowed, within any given time increment, for Φ to converge.

Now that the Φ_{ij} field has been established, a new time increment is advanced and steps (a) through (h) are again followed until the steady state criteria are achieved.

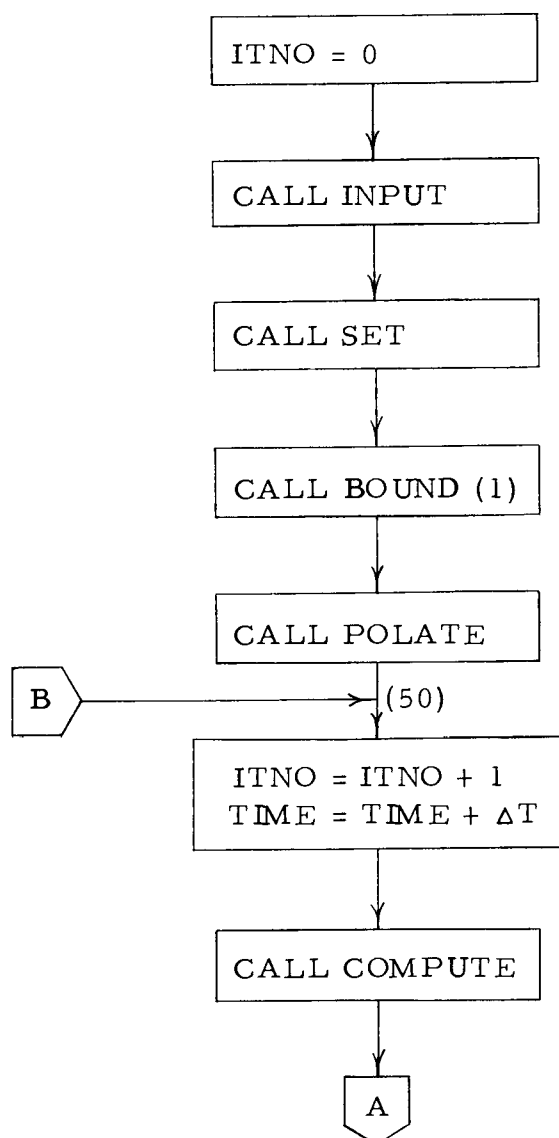


Figure 9. Flow diagram for MAIN.

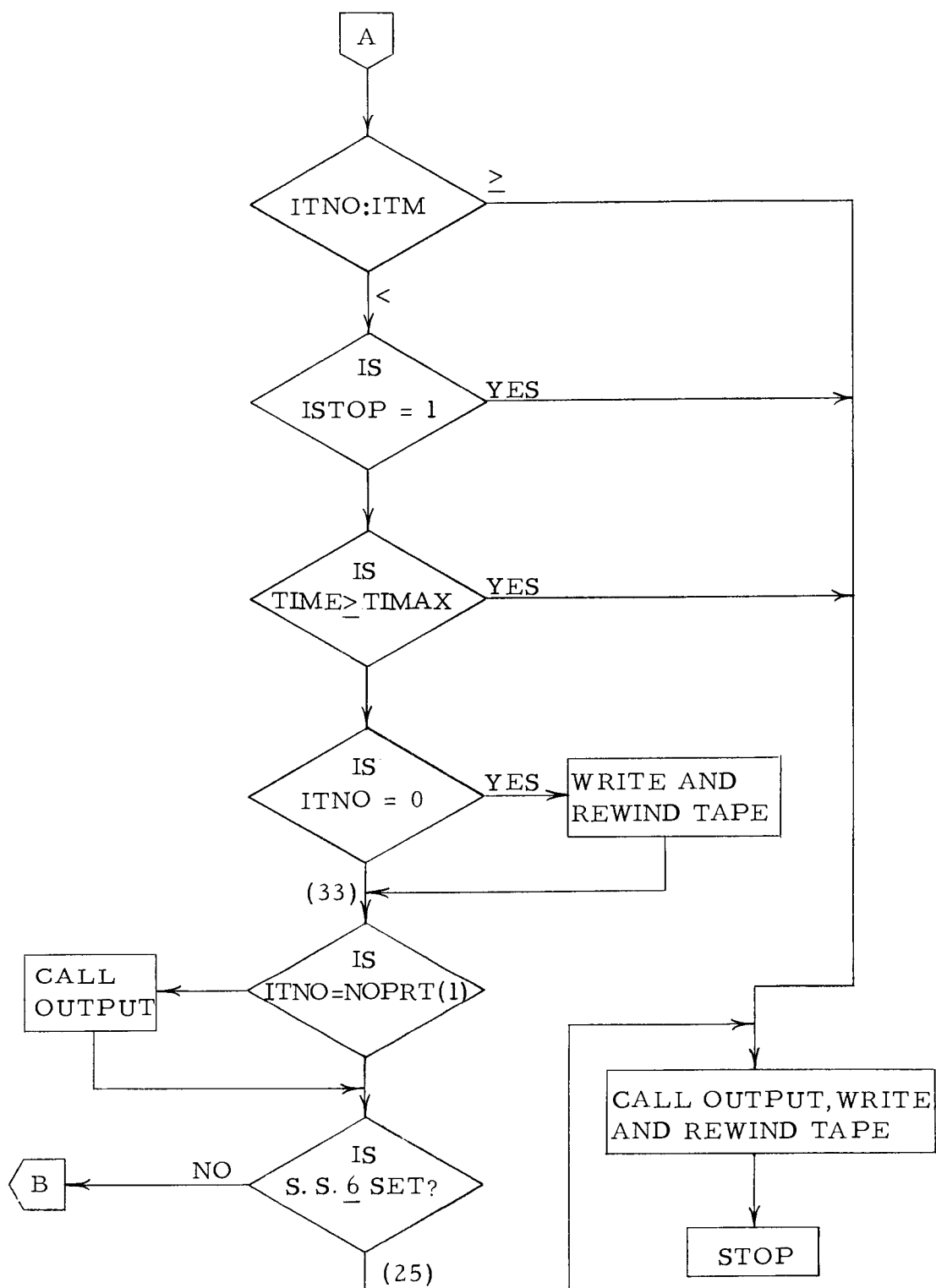


Figure 9. Continued.

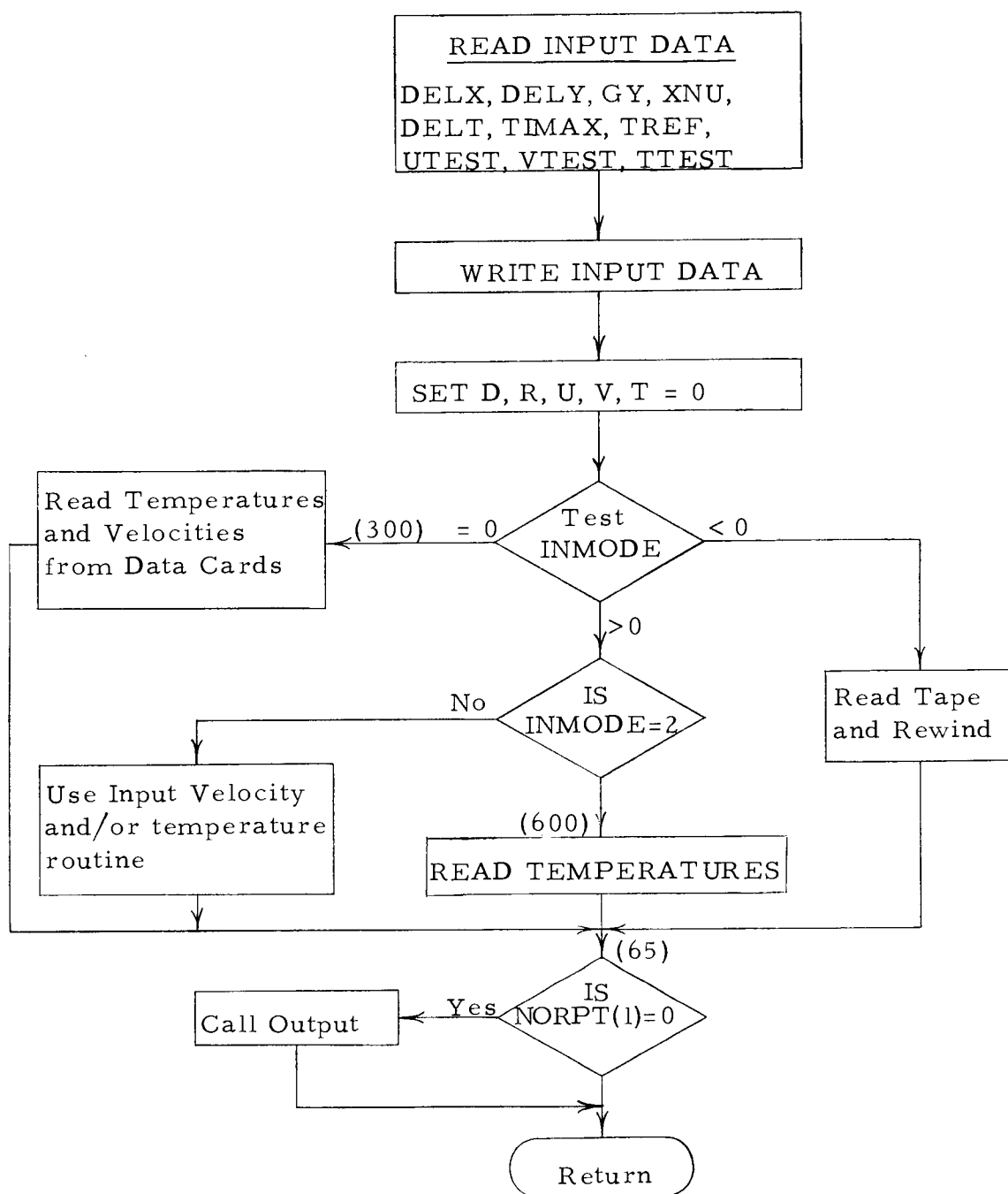


Figure 10. Flow diagram for subroutine INPUT.

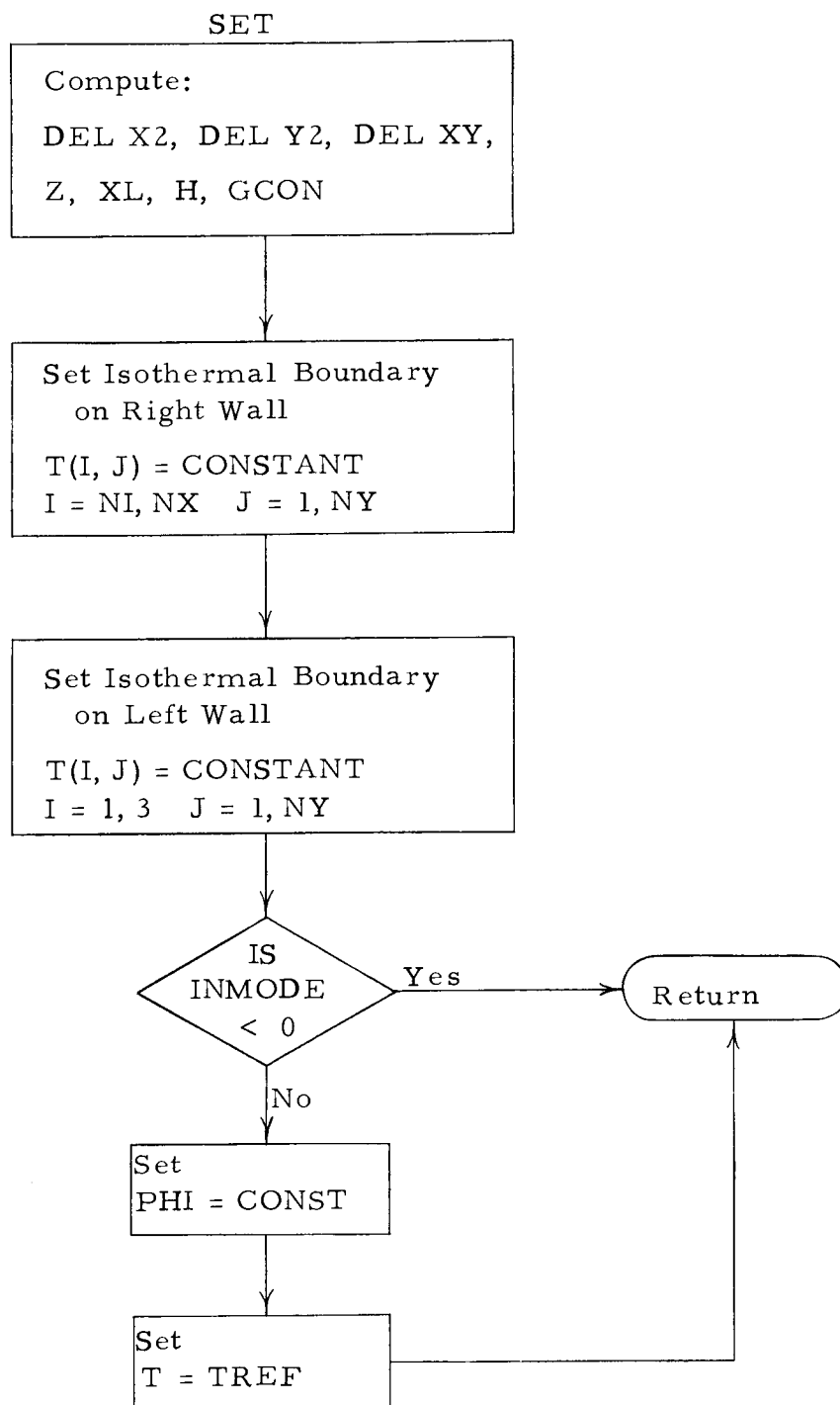


Figure 11. Flow diagram for subroutine SET.

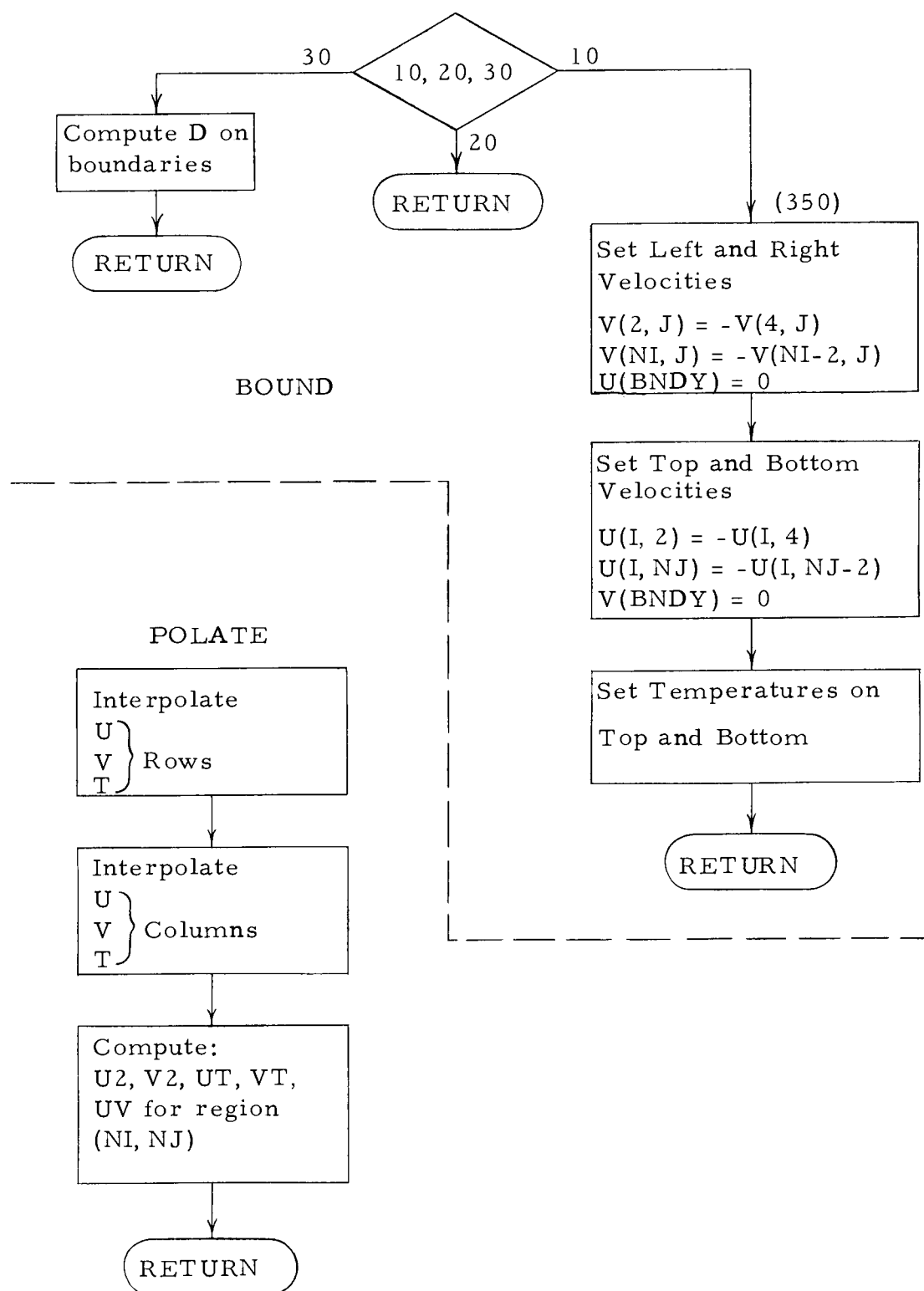


FIGURE 12. Flow diagrams for subroutines BOUND and POLATE.

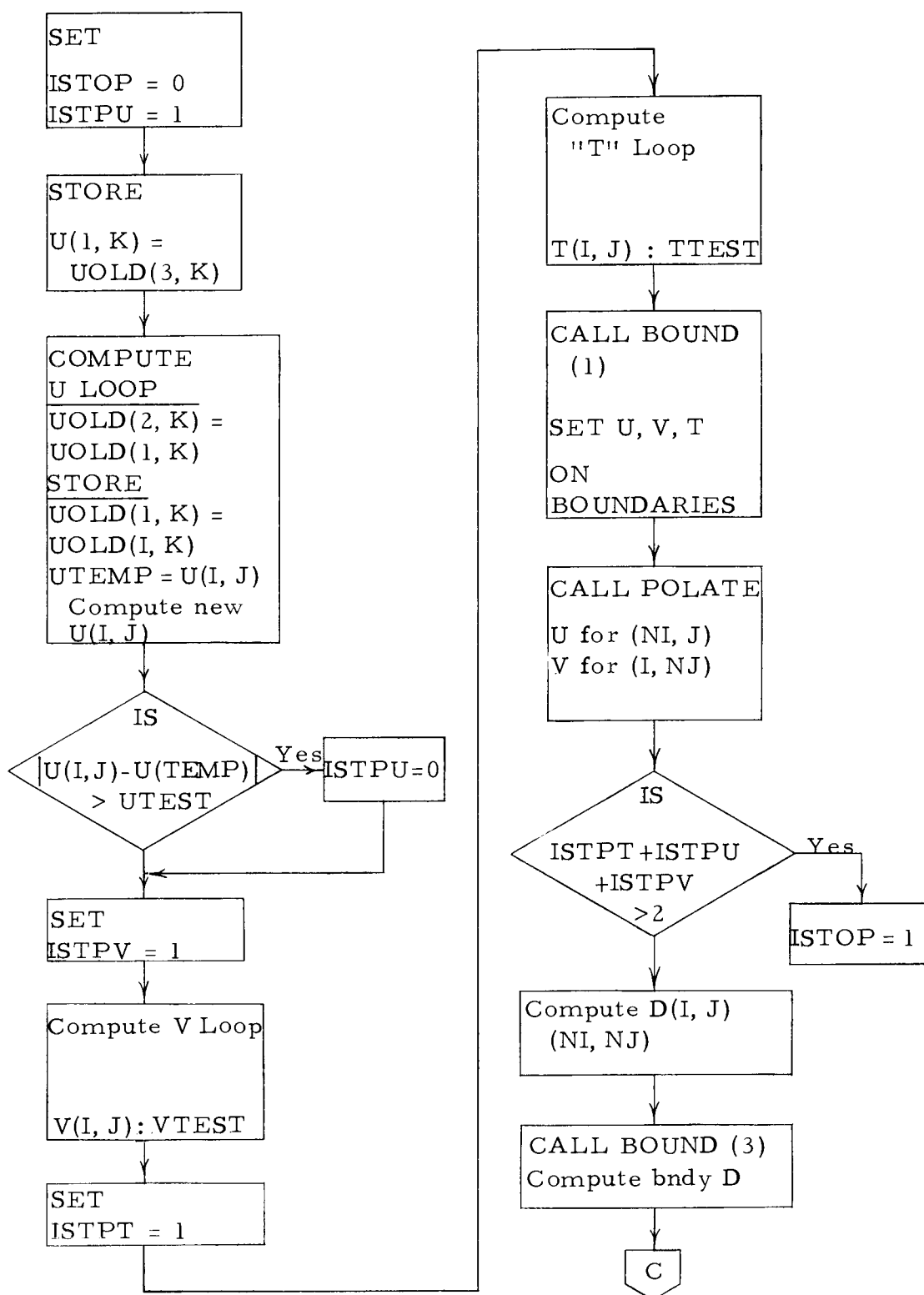


Figure 13. Flow diagram for subroutine COMPUTE.

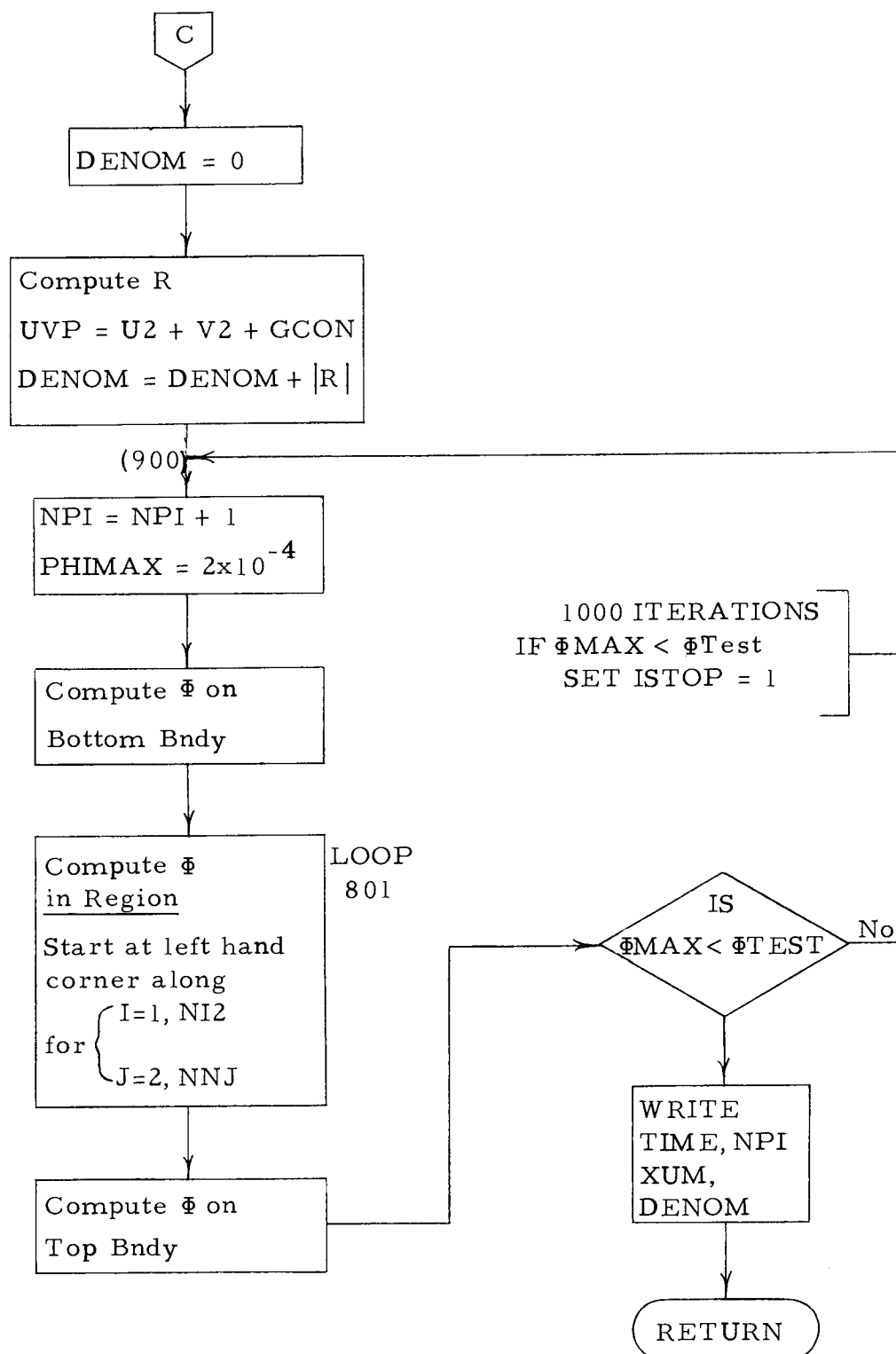


Figure 13. Continued.

IV. RESULTS AND DISCUSSION

General

Computer solutions for the rectangular enclosure problem were obtained for an aspect ratio of 5 over a Rayleigh number range of 3×10^3 to 2.5×10^5 . Additional solutions were obtained for the purposes of providing a direct comparison to previous experimental test data and/or testing the computer program for specific conditions.

Needless to say, it becomes virtually impossible to include all the computed results acquired for this dissertation. In lieu of this, a synopsis of the data is provided in plot form in two basic categories:

- a) those data which are used to validate the computed results and,
- b) those data used to provide an extension to that which exists in the current literature. Supplementing the plotted data are written descriptions of all program tests and their general results.

The majority of the plotted data shown in this chapter are in the form of dimensionless length (x/L) for a given dimensionless height (y/H). In all cases, the dimensionless length and dimensionless height represent distances from the heated wall and from the enclosure bottom, respectively.

In order to evaluate the overall heat transfer characteristics of the enclosure, some consideration must be given to the method of calculating the dimensionless heat transfer coefficient in light of the

calculated data.

This writer chose to define the dimensionless heat transfer coefficient based on one-half the cell length ($L/2$). Since the heat conducted from the hot wall is

$$q/A = k \left(\frac{dT}{dx} \right)_{x=0} \quad (109)$$

if θ_R and \bar{x} be defined as

$$\theta_R = \frac{T - T_R}{T_H - T_R}$$

and

$$\bar{x} = \frac{x}{L/2}$$

then Equation (109) becomes,

$$q/A = \frac{k(T_H - T_R)}{2L} \left(\frac{d\theta_R}{d\bar{x}} \right)_{\bar{x}=0}$$

however

$$T_H - T_R = \frac{T_H - T_C}{2}$$

then, by substitution

$$q/A = \frac{k(T_H - T_C)}{4L} \left(\frac{d\theta_R}{d\bar{x}} \right)_{\bar{x}=0} \quad (110)$$

Based on the total temperature differential of the whole cell,
 q/A is also related to the heat transfer coefficient by the relationship:

$$q/A = h(T_H - T_C) \quad \text{or} \quad h = \frac{q/A}{T_H - T_C} \quad (111)$$

Substituting (111) into (110) yields the average dimensionless heat transfer coefficient for the enclosure

$$Nu_L = \frac{hL}{k} = \frac{1}{4} \left(\frac{d\theta_R}{d\bar{x}} \right)_{\bar{x}=0} \quad (112)$$

Wilkes [50] determined a relationship similar to this, except that he apparently did not consider the half-cell length and, instead, used the full length (L). As a result of this difference, a plot of his calculated Nusselt number versus Rayleigh number shows a greater slope (by a factor of two) than any known empirical or analytical results.

Other points of contention are the manner in which the temperature gradients are measured, the means of averaging and the weight given to those gradients which exist in the proximity of the enclosure ends.

Wilkes attempted to expand $\frac{d\theta_R}{d\bar{x}}$ into a Taylor expansion by using two-, three- and four-point expansions. He found a great variation in the resulting Nusselt number due to the oscillations which occurred in the higher order terms of the polynomial. When the expansions were applied to a trial problem, the variation in $\frac{d\theta_R}{d\bar{x}}$ was on the order of $\pm 30\%$ from the mean value. Wilkes finally used the

four-point expression for calculating $\frac{d\theta_R}{d\bar{x}}$ and used an arithmetic mean to determine the Nusselt number. Temperature gradients in the proximity of the enclosure top and bottom were weighted by a factor of one-half.

MacGregor [27] used a two-point approach for his calculation of the wall temperature gradient. His dimensionless temperature was based on the full enclosure difference $T_H - T_C$. For the calculation of the Nusselt number, MacGregor also used an arithmetic mean and weighed end effects in a manner similar to Wilkes.

The solutions obtained by Wilkes used a space increment, $\frac{\delta x}{L}$, of .1. In the calculation of the temperature gradient, the first and second order terms were based on those chosen increments. The results of this study show that a dimensionless increment $(\frac{\delta x}{L})$ of .1, from the heated wall, is too large to correctly evaluate the gradient at the wall. This is especially true for the higher Rayleigh number computations.

Therefore, for dimensionless heat transfer coefficients calculated in this study, the temperature gradient at the heated wall was measured using a two-point approximation over an interval of $\frac{\delta x}{L} = .025$. The arithmetic averaging technique to obtain Nusselt numbers was also adopted.

A summary of the computer solutions obtained for the

rectangular enclosure problem is shown in Table 2. All computer calculations reported are for a fluid Prandtl number of .72.

For the case of an aspect ratio of 10, two hundred (.1 x .5) "fluid" cells are used, in a 10 x 20 array, and some 40 additional cells are utilized to define the horizontal and vertical boundaries. With an aspect ratio of 5, the number of fluid and boundary cells are doubled, giving a total of 480 cells utilized.

Table 2. Summary of computer results for the vertical rectangular enclosure.

Run	δt	Ra_L	H/L	Nu_L
1	.001	2×10^3	10	1
2	.001	5×10^3	10	1.23
3	.001	6×10^3	10	1.285
4	.001	3×10^3	5	1.13
5	.001	7.5×10^3	5	1.63
6	.001	1.5×10^4	5	2.09
7	.001	3×10^4	5	2.5
8	.0001	6×10^4	5	3.05
9	.0001	9×10^4	5	3.32
10	.0001	1.5×10^5	5	3.89
11	.0001	2.5×10^5	5	4.4

Runs 1 through 8, initialized at $U = V = 0$, required approximately 25 minutes of 7094 computing time to satisfy the steady state criteria. Runs 9 through 11 required a smaller time to satisfy the stability requirements. For these runs, an average of approximately

50 minutes of computer time was required. However, by using the steady solution of Run 9 to initialize Run 10, the total computer time to achieve steady state was halved.

At each printout interval, horizontal and vertical velocity and temperature values are shown for all points surrounding a cell. Therefore, for each fluid cell, ten velocity components are printed. In addition, such terms as U_{ij}^2 , V_{ij}^2 , Φ_{ij} , R_{ij} and D_{ij} are also printed, representing values at the cell center. The term D_{ij} , which represents the residual in the continuity for a cell, never attained a value greater than 10^{-2} in any of the computer printouts.

A typical printout is not shown as part of this dissertation. Due to the number of points being printed out in one time interval, a print format is required which is rather confusing to one not completely familiar with the program. Instead, a portion of the reduced data in tabular form (Appendix B) is shown for the transient and steady state solutions for a Rayleigh number of 1.5×10^5 .

Computer Program Tests

Some preliminary program tests were initiated to determine the effects of differing time increments, cell sizes and boundary condition changes. These tests were conducted to gain some assurance as to the validity of the computed results and to test the stability and/or convergence response of the finite difference equations being used.

The boundary tests were simulated using an aspect ratio of 10, specifically, for Runs 2 and 3 shown in Table 2. These particular runs were chosen since a smaller number of cells were required, somewhat relieving the need for long computational times.

Isothermal wall temperatures for Run 2 were set at the desired levels with U and V initially set equal to zero. With reference temperature (T_R) maintained at the arithmetic mean of the hot and cold walls, calculations were made until the steady state requirement had been fulfilled. The final solution was taped and used as an initialization condition for Run 3. The computational procedure was extended to a second steady state solution. To verify that this Run 3 could have been obtained by starting from $U = V = 0$, an additional run was made with these velocity components initialized at zero. This last run was compared with that obtained by initialization from Run 2, to determine if the final solutions were in close agreement. The point of this exercise was to show that identical solutions could be obtained independent of the initialization point. The result of this study was that the two solutions did agree to the fourth significant figure.

A second program test was initiated to determine the solution differences incurred by altering the chosen cell size ($2\delta x = .1$, $2\delta y = .5$) to smaller and larger values. These tests were performed specifically for a Rayleigh number of 1.5×10^4 and an aspect ratio of

5 (Run 6).

Based on some previous work, it appeared that choosing a $2\delta x = .1$ or $\frac{\delta x}{L} = .05$ was quite respectable. The use of a square mesh (i.e. $2\delta x = .1 = 2\delta y$) was unrealistic on the basis of the number of cells required and the effect on computer time. Therefore, trial runs of $2\delta y = .25$ and $2\delta y = 1.0$ were initiated so that the computed results could be compared, on an overall basis, to the $2\delta y = .5$ case.

For the smaller mesh size, the average Nusselt number was calculated to be some 6% lower than that computed for $2\delta y = .5$. However, the computational time was increased by 35%, due primarily to doubling the total number of cells required to simulate the problem. For a $2\delta y = 1.0$, the calculated Nusselt number was 14% higher than that value at $2\delta y = .5$, with a reduction of approximately 20% in computing time. It appeared that a $2\delta y = .5$ was a reasonable choice when considering the accuracy desired. The increase in computer time for greater accuracies, in this case, was not warranted.

In addition to the boundary and cell size tests, time increment changes were altered (to lower values) to determine if this had any effect on the transient solution. Specifically, δt was changed from .001 to .0001 and identical printouts of total time were compared. Comparisons were made at three periods during the solution: at the beginning, midway and near the steady state solution. In all cases,

printouts for the same total time (from initialization) differed by only negligible amounts.

Validity of Results

Since the finite-difference equations used in this study are not amenable to any strict mathematical proof, the validity of the computed results must be shown by some other means. Aside from the program tests stated in the preceding, further proof is required either by comparison to existing experimental data or comparison to known analytical solutions. The intent is to compare the trends of the computed results obtained here, versus the general trends of the experimental data and those data obtained through other analytical techniques.

Steady state temperature profiles for air in a rectangular enclosure have been experimentally evaluated and reported, but comparable data concerning velocity profiles are not so easily obtained. The temperature data published by Carlson [3] provide a basis for comparing temperature distribution within the enclosure and the general trends of the computer results. Furthermore, since the momentum and energy equations are coupled, a fair agreement of the temperature profiles implies that the velocity components are reasonably correct.

No analytical solutions are known to exist for the set of

difference equations used in this study. However, as stated previously, MacGregor's analytical results for aspect ratios of 1 and 10 can be qualitatively compared to the results of $H/L = 5$ studied here.

On the basis of Carlson's data, a computer study was performed on a model with an aspect ratio of 10 for Rayleigh numbers on the order of 5×10^3 . A rectangular enclosure to the exact dimensions used by Carlson was not attempted since the total number of cells required would have exceeded the storage capabilities of the 7094.

The computer results are shown in dimensionless parameter form in Figures 14 through 17. Comparative experimental results are also shown for the top, mid-height and bottom regions of the enclosure. For a Rayleigh number of 5×10^3 , conduction dominates for most of the mid-height region with convective effects prominent at the top and bottom.

For the most part, the present study indicates a reasonable agreement with existing data and, excepting some very small x/L values (in Figure 14), the computer results are consistently close to interferometric data for $y/H = 0.071$. Similar results for the middle of the cell and the top of the cell are shown in Figures 15 and 16, respectively. One last comparison can be made which portrays the variation of the vertical center line temperature of the cell versus a dimensionless height. In this case, excellent agreement is achieved up to a y/H value of approximately .5. Beyond this a smooth curve

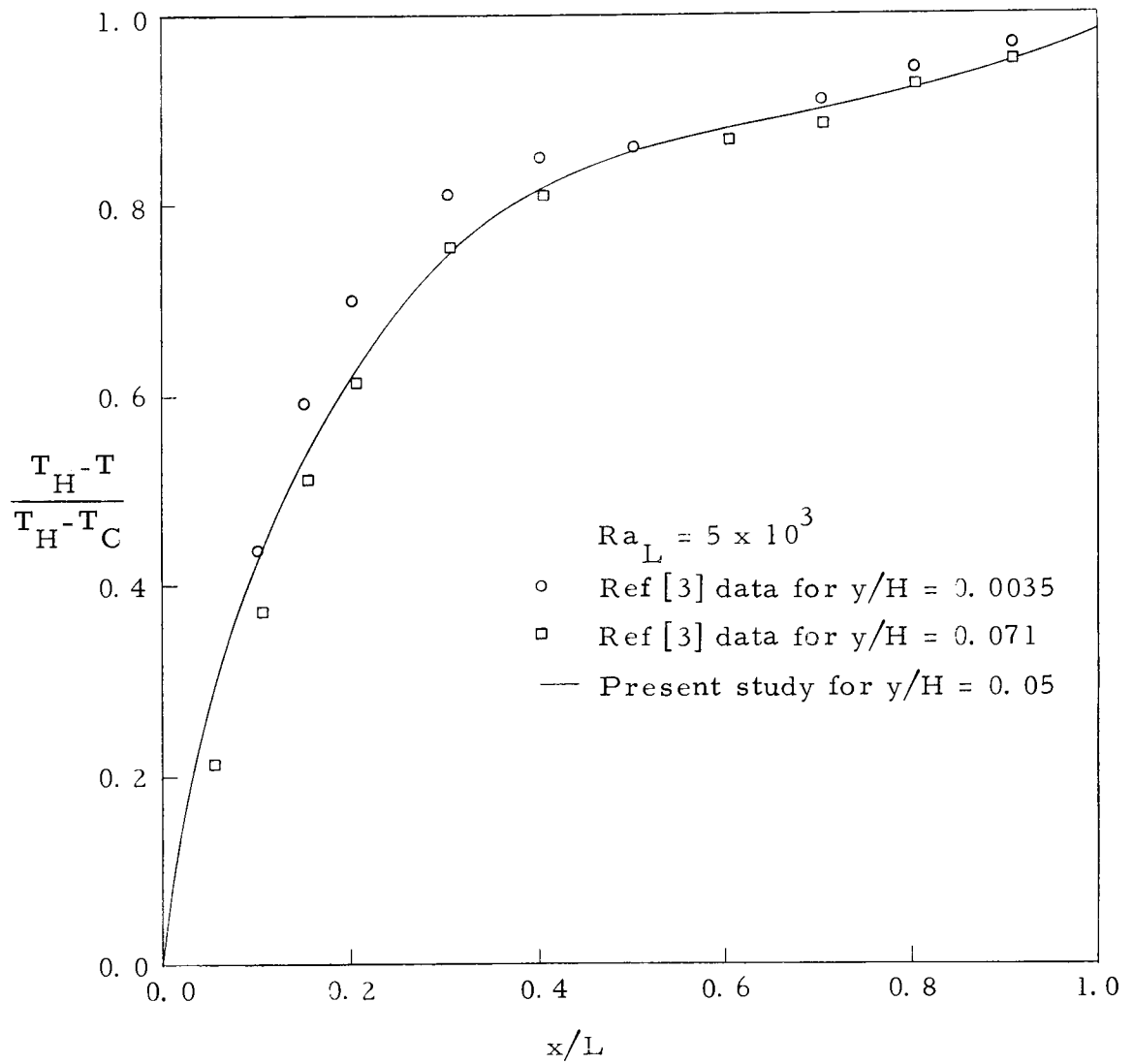


Figure 14. Computed and experimental temperature profiles for small y/H .

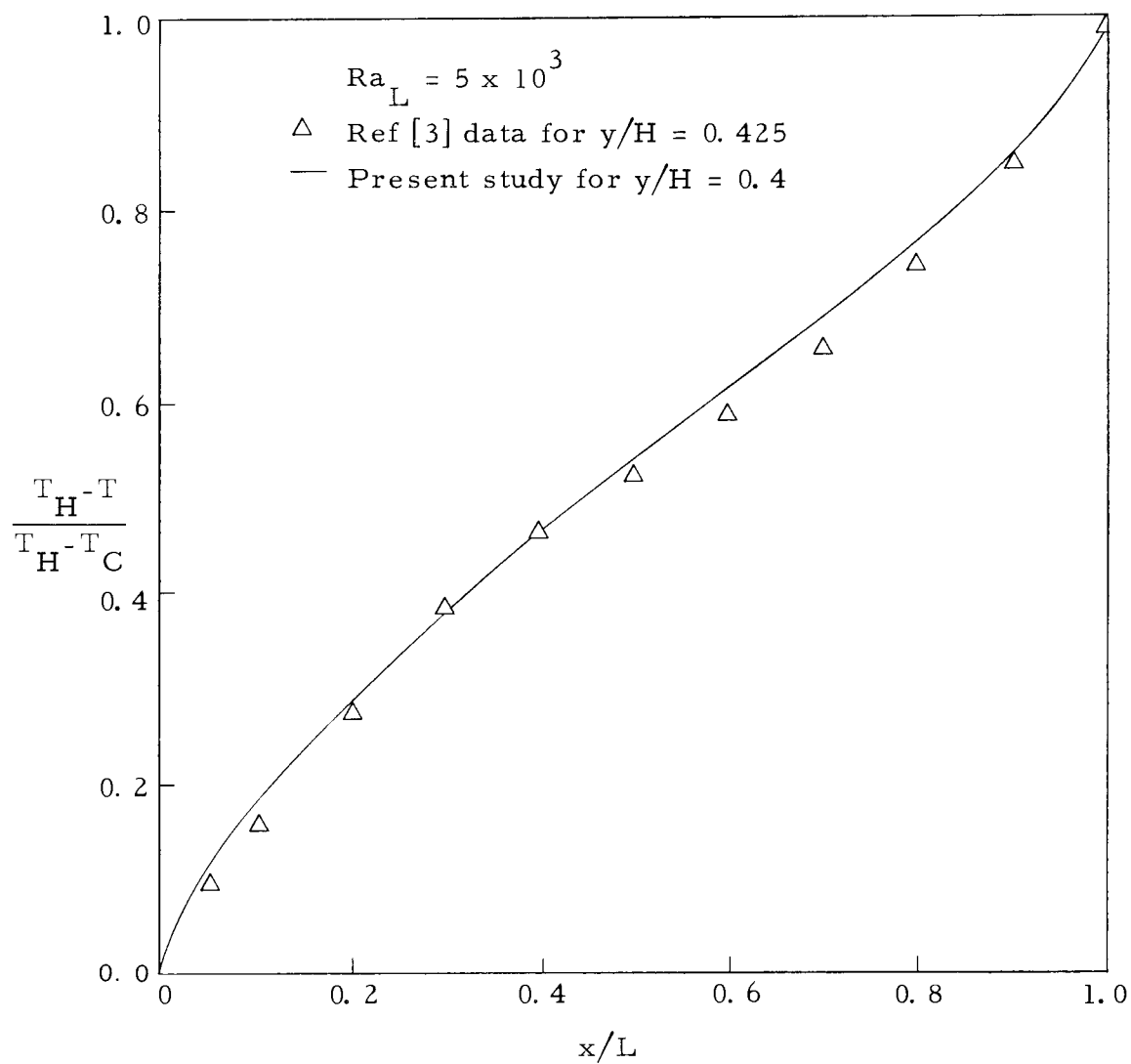


Figure 15. Computed and experimental temperature profiles for $y/H \approx .5$.

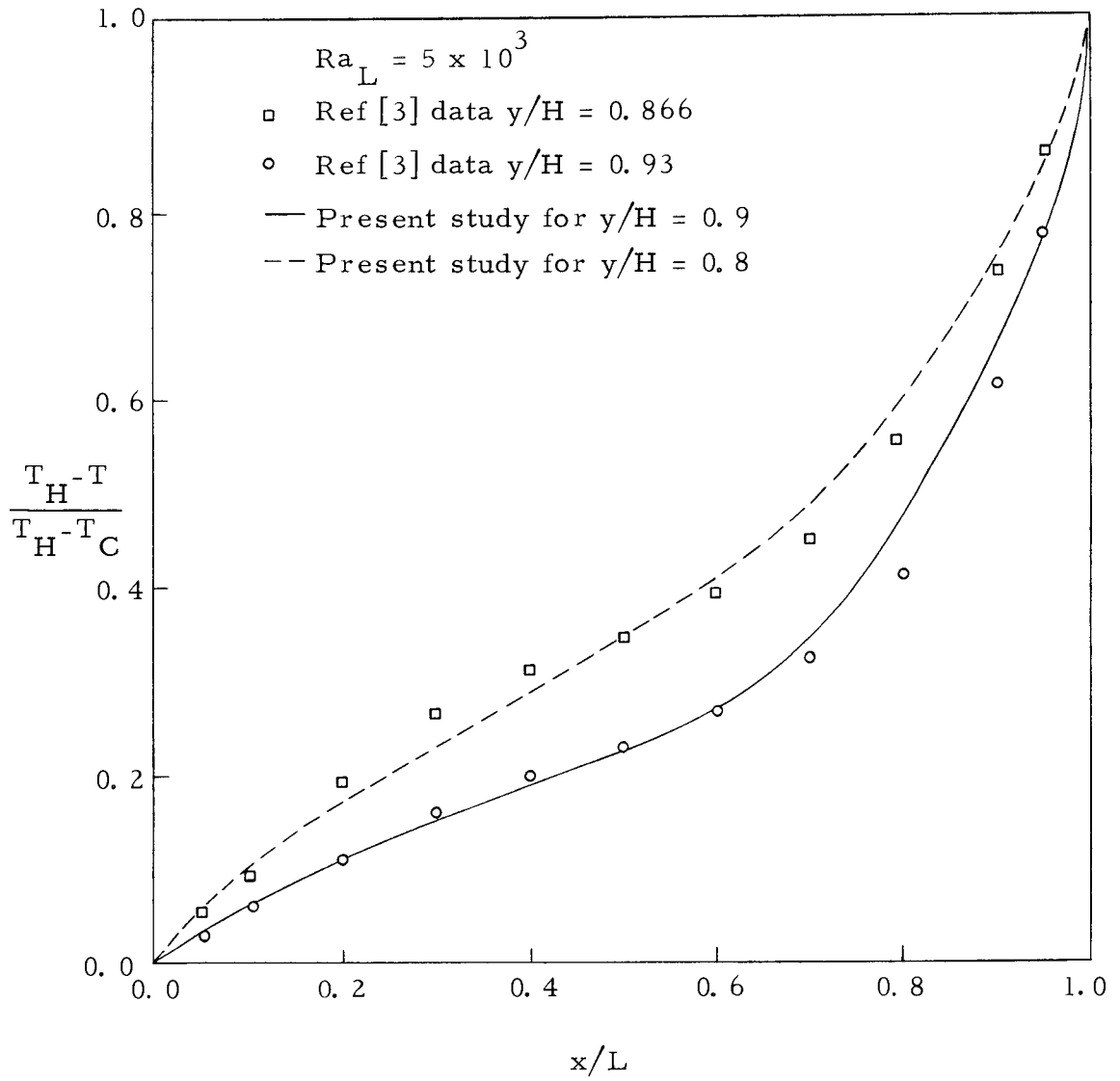


Figure 16. Computed and experimental temperature profiles for $y/H \approx 1.0$.

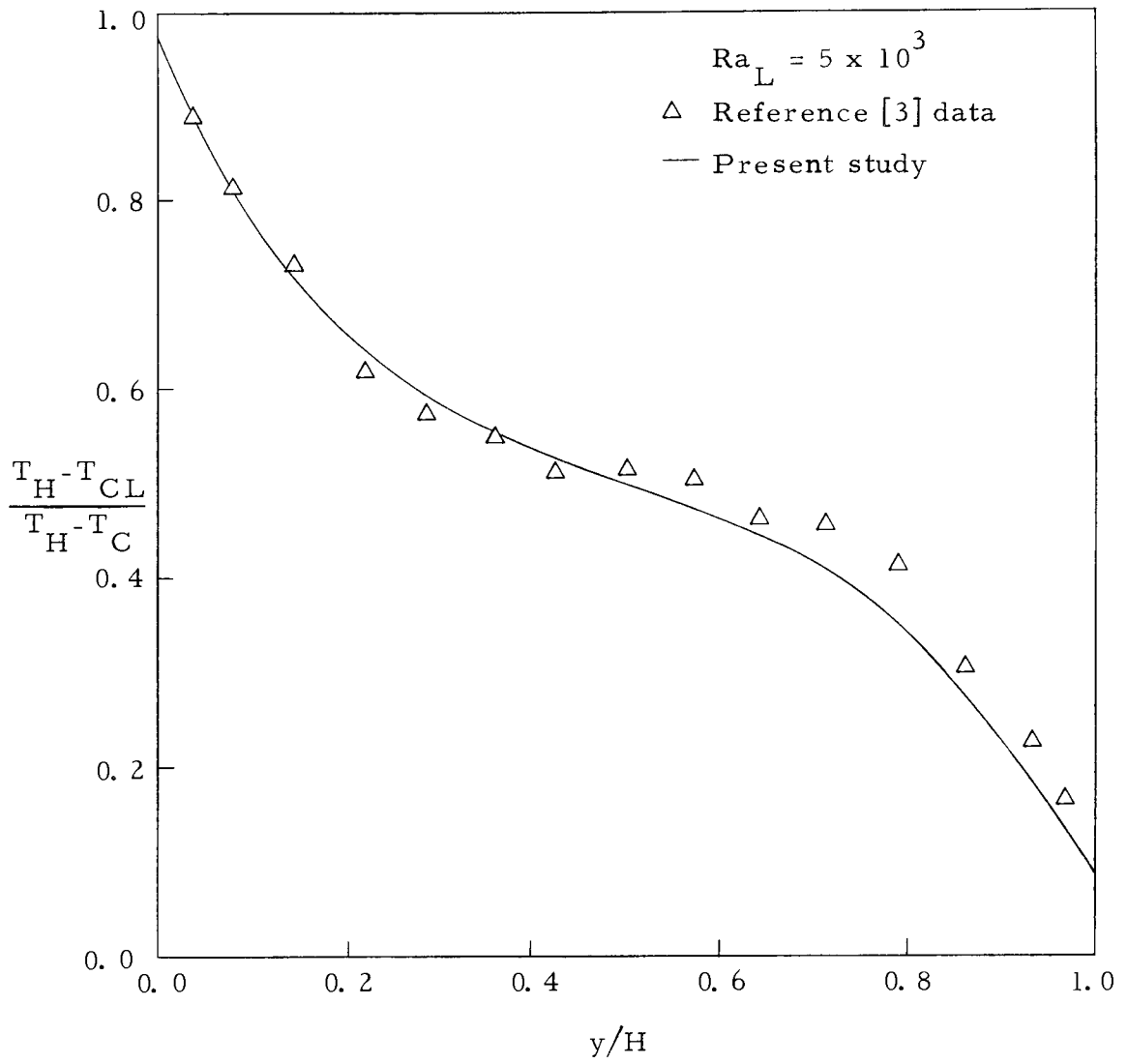


Figure 17. Computed and experimental data for temperature along the enclosure centerline ($\frac{x}{L} = .5$).

exists for the computer results, however, the experimental data are somewhat skewed for some unknown reason, possibly indicating experimental error.

In addition to the preceding, a Grashof number of approximately 200 was used in a run. For this case, one would expect convection effects to be extremely small, if present at all. All experimental data that exist with this Grashof number indicate an average Nusselt number of approximately 1, which is indicative of pure conduction. When this case was run with the computer program, profiles were exactly linear throughout the majority of the enclosure, deviations occurring at y/H values less than .05 and greater than .95.

The average Nusselt number correlation offered by Eckert and Carlson [9] was

$$Nu_L = .119(Gr_L)^{.3}(H/L)^{.1} \quad (113)$$

for a Grashof number range of 3×10^3 to 2×10^5 . For the parameters used in this study, Equation (119) yields values which have a maximum deviation of 9% in comparison to this study. These results, although encouraging, are for a very limited range of Grashof numbers.

Velocity and Temperature Profiles for Specific Rayleigh Numbers

The computer results for an aspect ratio of 5 and a Rayleigh number of 1.5×10^4 are shown in Figures 18 through 20. As would be expected, rather steep profiles occur at the bottom of the heated plate and the top of the cold plate. Referring to the generalized flow regimes shown in Figure 1, a Grashof number of 1.5×10^4 represents the upper portion of the transitory zone from conduction to boundary layer formation.

The temperature profiles are nearly anti-symmetrical with respect to the dimensionless height of .5. The center region ($.3 < \frac{x}{L} < .7$) shows very little change in slope as a result of the fairly high velocities occurring on both the hot and cold walls. This indicates that the primary mode of heat transfer is by convection, and conduction, at least in the central region, is negligible.

Special note is made of the profiles which result for the top and bottom of the enclosure. In both cases, they represent the maximum temperature gradient at the hot and cold wall, respectively. Temperature gradients away from this point (up the heated wall, for example) decrease steadily and approach zero at the top.

The vertical velocity profiles also exhibit an anti-symmetrical arrangement with the dimensionless mid-height. The profiles appear as fairly smooth curves at $y/H = .5$, but then become slightly

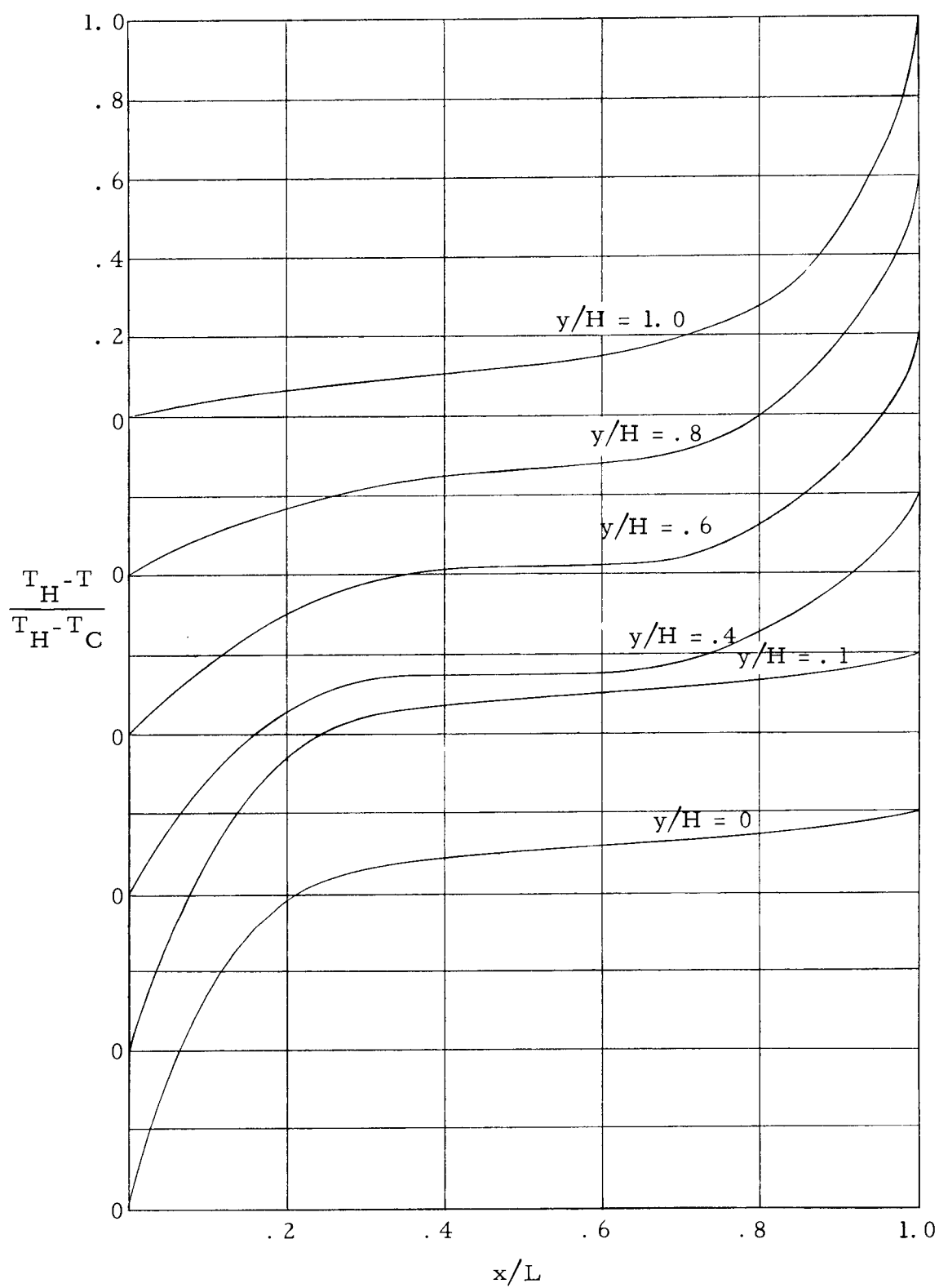


Figure 18. Dimensionless temperature profiles for $Ra_L = 1.5 \times 10^4$.

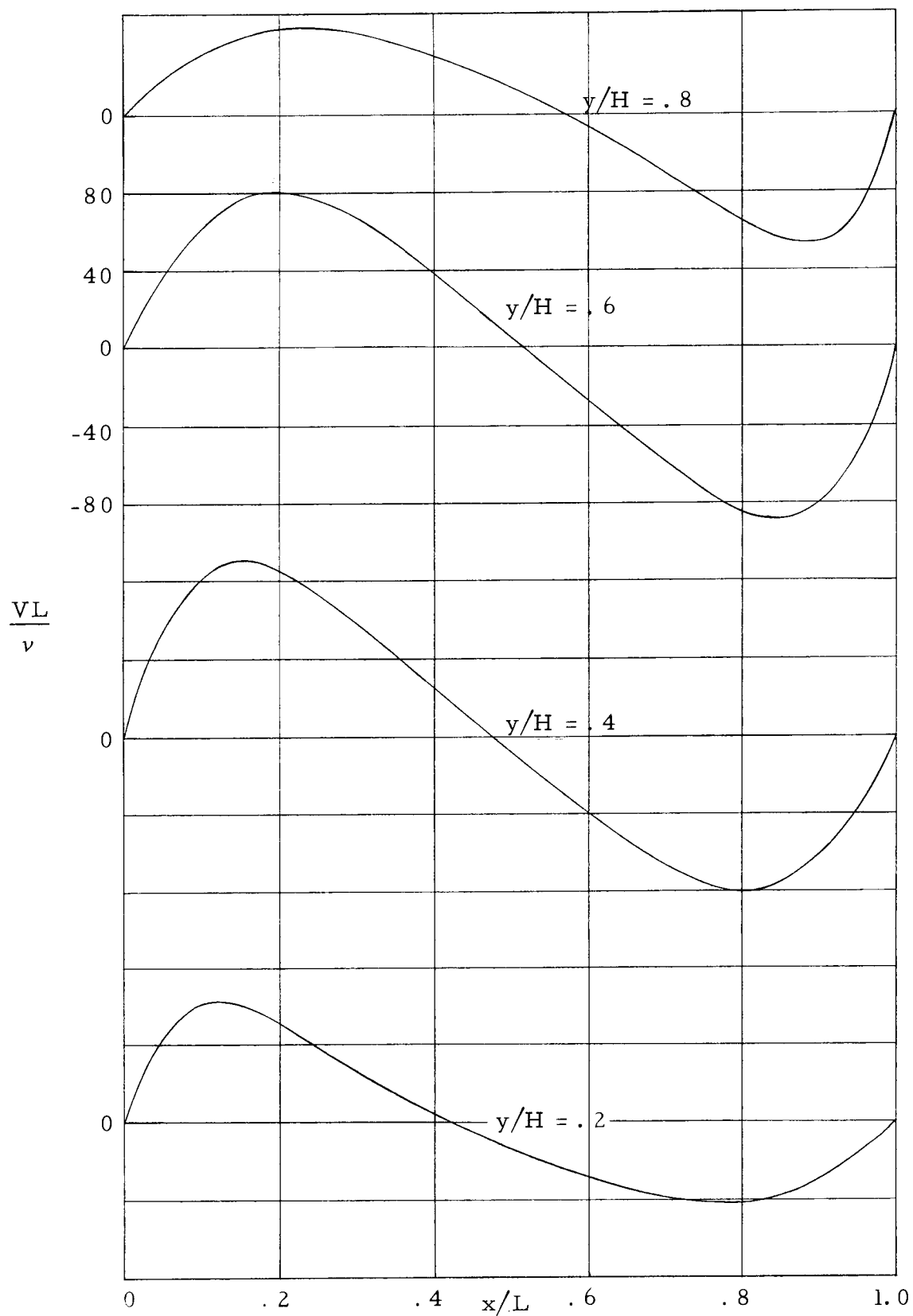


Figure 19. Dimensionless vertical velocities for $Ra_L = 1.5 \times 10^4$.

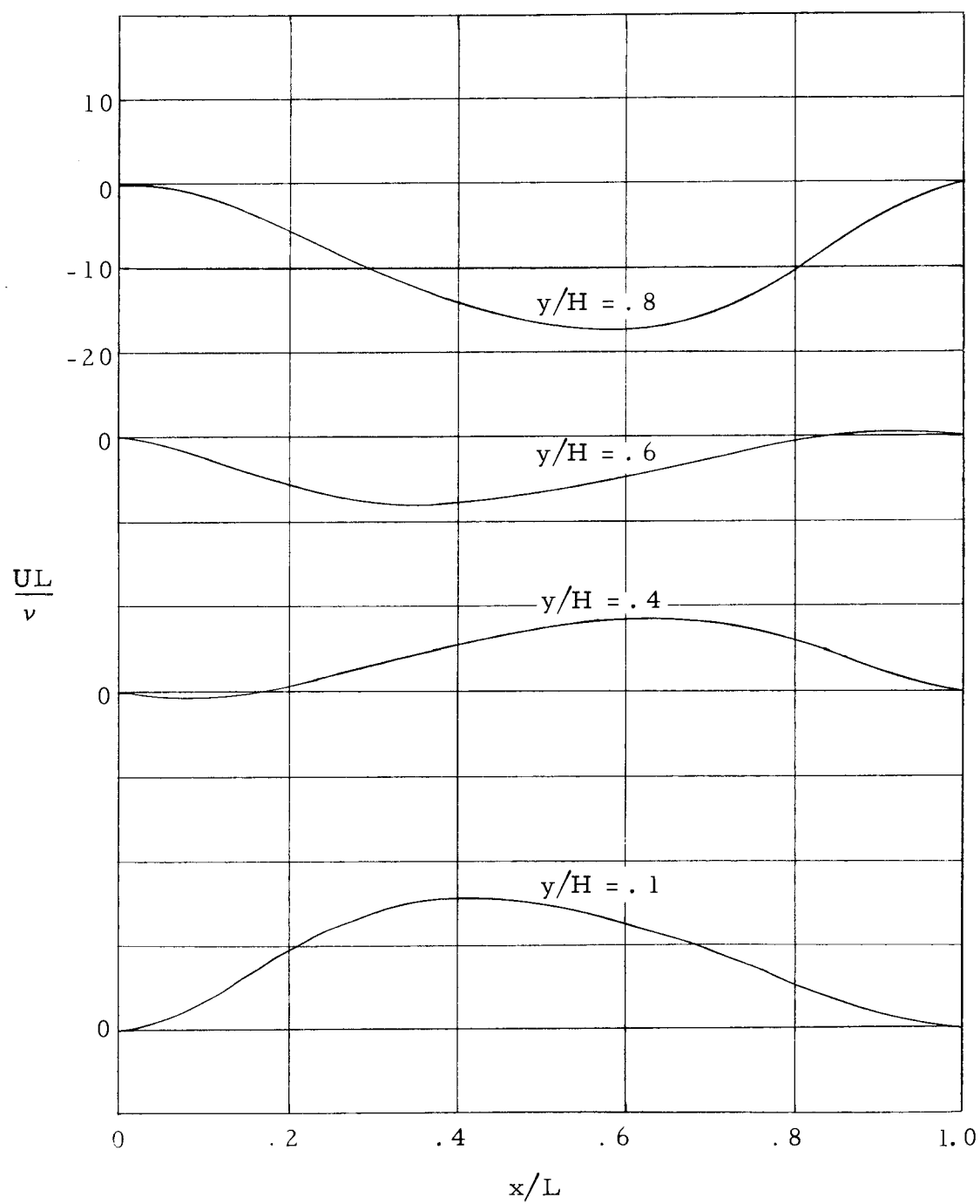


Figure 20. Dimensionless horizontal velocities for $Ra_L = 1.5 \times 10^4$.

distorted at the top and bottom. Notice that as the velocity increases to the mid-height (on the hot wall) and then decelerates to compensate for the approaching horizontal wall. This has a tendency to broaden the velocity profiles at the top wall and cause a shift of the zero point to the right of the centerline. Figure 19 also indicates the identical occurrence for the cold wall.

The horizontal components of velocity exhibit less abrupt changes than the vertical velocity profiles, with maximum values occurring at the top and bottom. At positions near the vertical walls, these components are nearly zero, which indicates that in this region, the horizontal component has very little effect on the vertical component.

The appearance of slightly negative components at the hot wall are not the result of an incomplete steady state solution; they can be explained on the basis of the continuity equation. For positions near the heated wall, attention is directed to the diagram in Figure 21 which represents an element of fluid adjacent to the heated wall. Recall that, as in Figure 7, the heated wall is considered to be the right-hand wall.

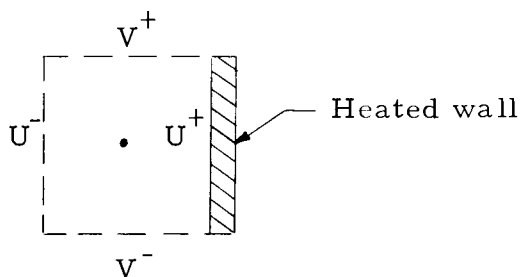


Figure 21. Fluid cell adjacent to heated wall.

From continuity, the relation which must exist between the indicated velocities is

$$\frac{U^+ - U^-}{\delta x} + \frac{V^+ - V^-}{\delta y} = 0$$

At the heated wall, U^+ is zero and solving the above expression for U^- leads to

$$U^- = \frac{\delta x}{\delta y} (V^+ - V^-)$$

At positions near the bottom of the enclosure (i. e. $y/H = 0$) fluid particles near the vertical wall are accelerating upward and therefore $U^- > 0$ since $V^+ > V^-$. At a dimensionless height of approximately .4, a vertical deceleration for particles near the wall begins and continues to be in effect up to $y/H = 1.0$. Therefore, $V^+ < V^-$ and U^- is less than zero.

A similar analysis can be made in considering the slight positive horizontal velocity values that exist on the cold wall.

The center region also reflects the physical occurrence of an accelerating fluid and this is exemplified at a point $\frac{x}{L} = .1$. Again referring to Figures 7 and 21, the continuity expression written as

$$\frac{\partial U}{\partial x} = - \frac{\partial V}{\partial y}$$

or

$$\frac{U^+ - U^-}{\delta x} = - \left(\frac{V^+ - V^-}{\delta y} \right) \quad (114)$$

must be satisfied.

When the slope of $\frac{\partial U}{\partial x}$ is negative, $V^+ > V^-$, indicating an accelerating fluid in the y direction. At a dimensionless height of .4, the slope of $\frac{\partial U}{\partial x}$ is essentially zero, indicating the point at which deceleration begins. Beyond this point, the slope of $\frac{\partial U}{\partial x}$ becomes positive and for this to be true, Equation (114) indicates that V^- must be greater than V^+ and a deceleration of the vertical component begins. With greater positive slopes, the deceleration phase continues up to the top wall.

By comparison, the velocity and temperature profiles (Figures 22 through 24) that exist in the boundary layer region exhibit some characteristics which differ from the transition zone. The slopes of the temperature profiles, for instance, are not maximized at the leading edges of the hot and cold vertical walls. This maximum value now occurs at a position away from the leading edge ($y/H = .1$) and then proceeds to decrease as one would expect. This phenomenon was also analytically derived in the work of MacGregor and was explained to be the result of the cross flow occurring in the vicinity of the ends. In MacGregor's results for an aspect ratio of one, the horizontal and vertical components of velocity were nearly identical. In the case shown here, the horizontal component is approximately one-half that

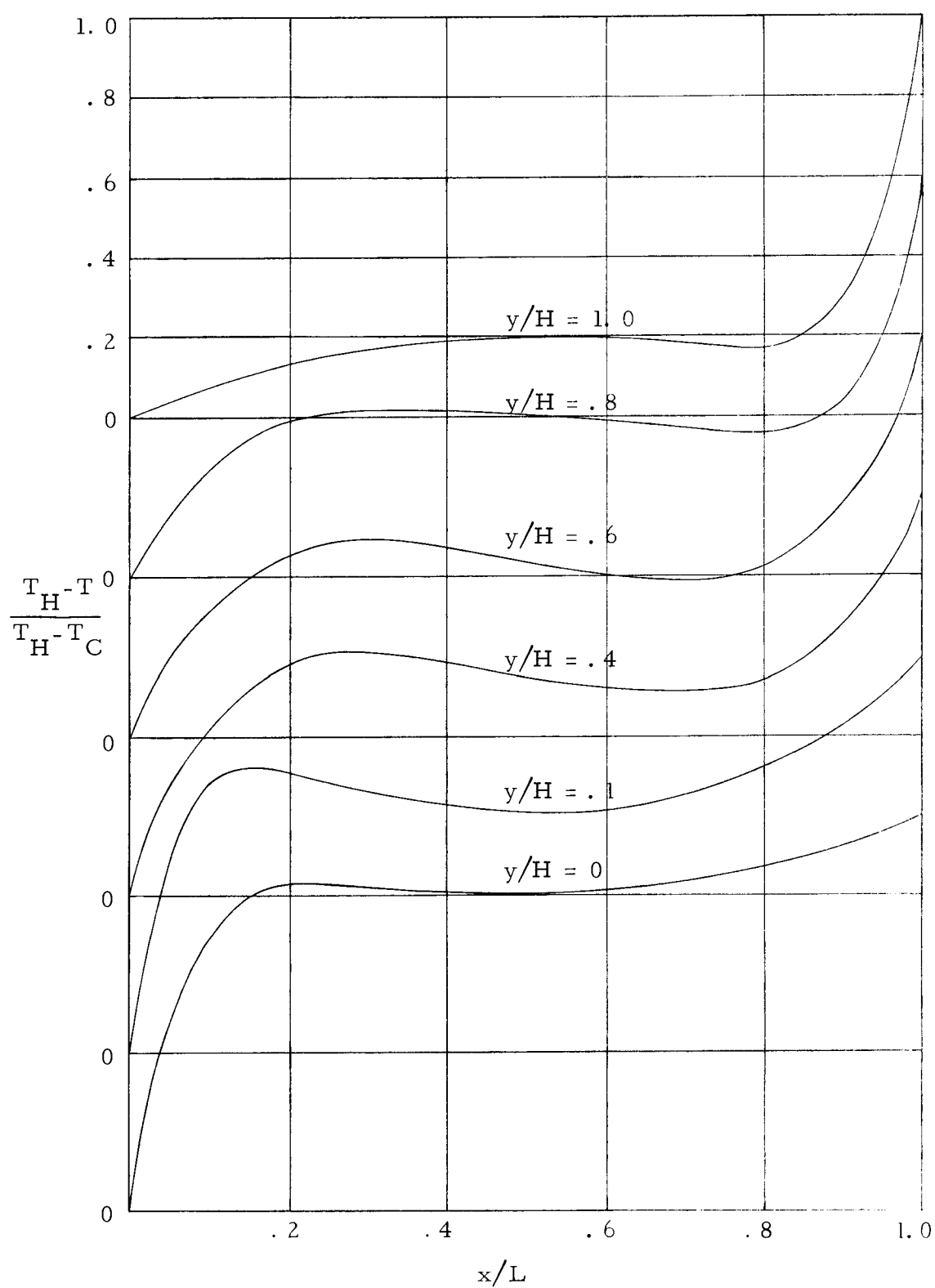


Figure 22. Dimensionless temperature profiles for $Ra_L = 1.5 \times 10^5$.

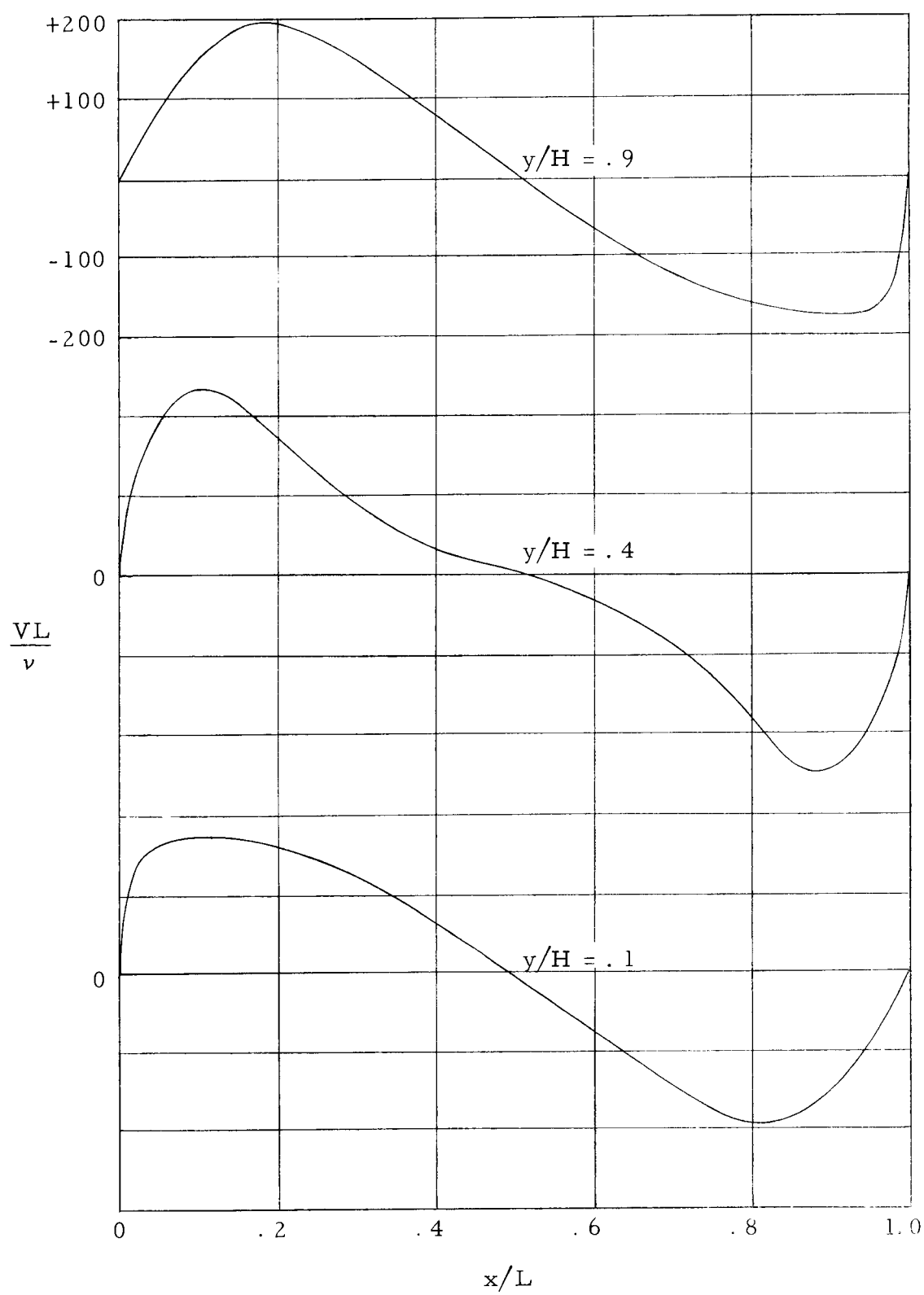


Figure 23. Dimensionless vertical velocities for $Ra_L = 1.5 \times 10^5$.

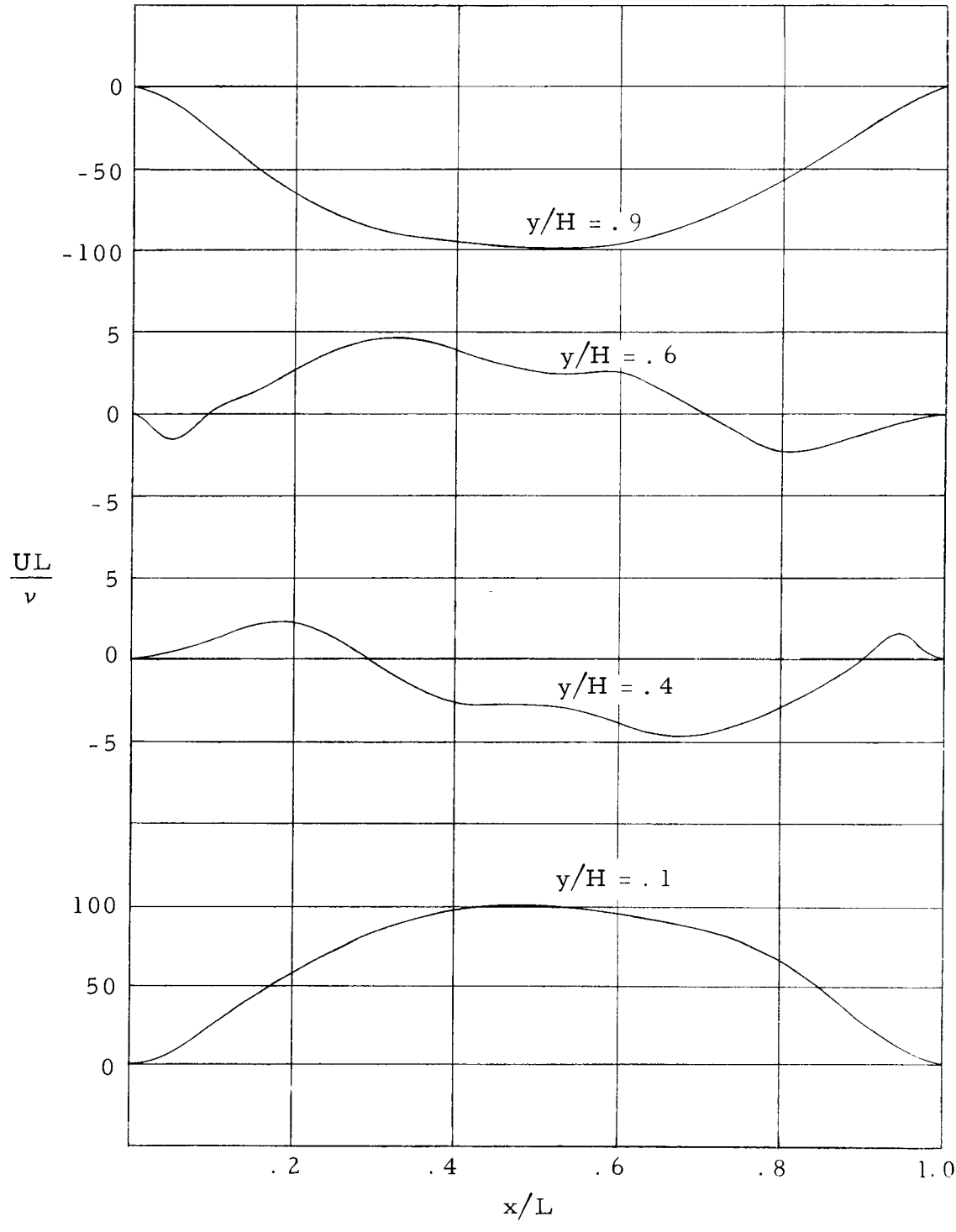


Figure 24. Dimensionless horizontal velocities for $Ra_L = 1.5 \times 10^5$.

of the vertical or in the same proportion exhibited for the transition zone case.

In this region, a phenomenon may be occurring which parallels the forced convection case at the entrance of a conduit. However, in this case the heat transfer coefficients are momentarily retarded due to the cross flow effects. Beyond the leading edge of the hot and cold plates, the expected trend of temperature gradients is re-established.

Another basic difference of the temperature profiles exhibited is the so-called "inversion" effect that occurs from approximately $.3 < x/L < .7$. Recall that in Figure 18, the temperature profiles of the central region exhibited a zero or slightly positive slope. In the boundary layer case, the profile indicates a negative slope for a good portion of the cell height. This phenomenon was also observed by others, and is explained to be the result of constant vorticity in the central core. At higher Grashof numbers, as observed in the computed results of this study, the inversion pattern becomes more accentuated and is apparently proportional to the strength of the vorticity.

With respect to the velocity profiles, note that in the mid-height region, the resulting profile shape simulates those profiles identifiable with laminar boundary layers in forced convection flow. Near the leading edges of both the cold and hot walls, the profiles are skewed, reflecting a rapid acceleration of the flow in that area.

The horizontal velocity components (Figure 24) show about the same trends as indicated in the transition zone, however, there is an appreciable difference in the maximum velocities at $y/H = .1$ versus those at $.2$ and $.4$.

Rayleigh Number Variation

Figures 25 and 26 are shown to portray the difference in temperature and velocity profiles that occur at mid-height at the various flow regimes.

In the conduction region ($Ra \approx 10^2$) temperature profiles are linear, consistent with a negligible convection effect, and vertical velocity components are essentially zero.

Convection effects are slightly noticeable at $Ra = 3 \times 10^3$, resulting in a slight deviation from the linear profile at the vertical walls. The primary mode of heat transfer in the central core is still conduction. At this Rayleigh number value the vertical velocity profiles are small in magnitude and anti-symmetrical about $x/L = .5$.

At a Rayleigh number value of 1.5×10^4 , convection dominance is apparent with the appearance of an isothermal central core. Flows beyond this Rayleigh number are shown to be more distorted and the boundary layer effect close to the walls is more pronounced at still higher Rayleigh numbers.

The appearance of the temperature inversion pattern occurs at

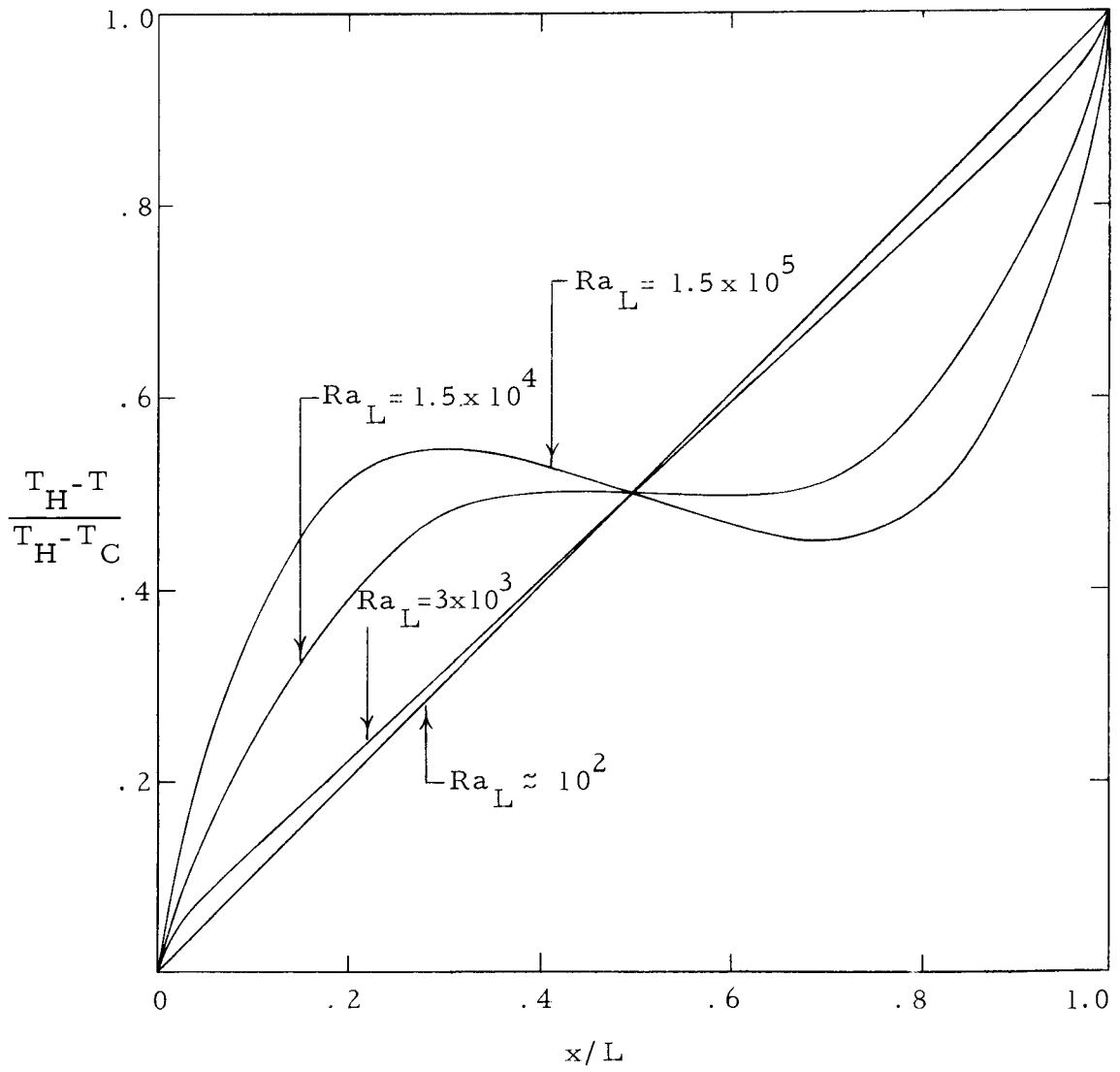


Figure 25. Temperature profiles for various Rayleigh numbers at $y/H = .5$.

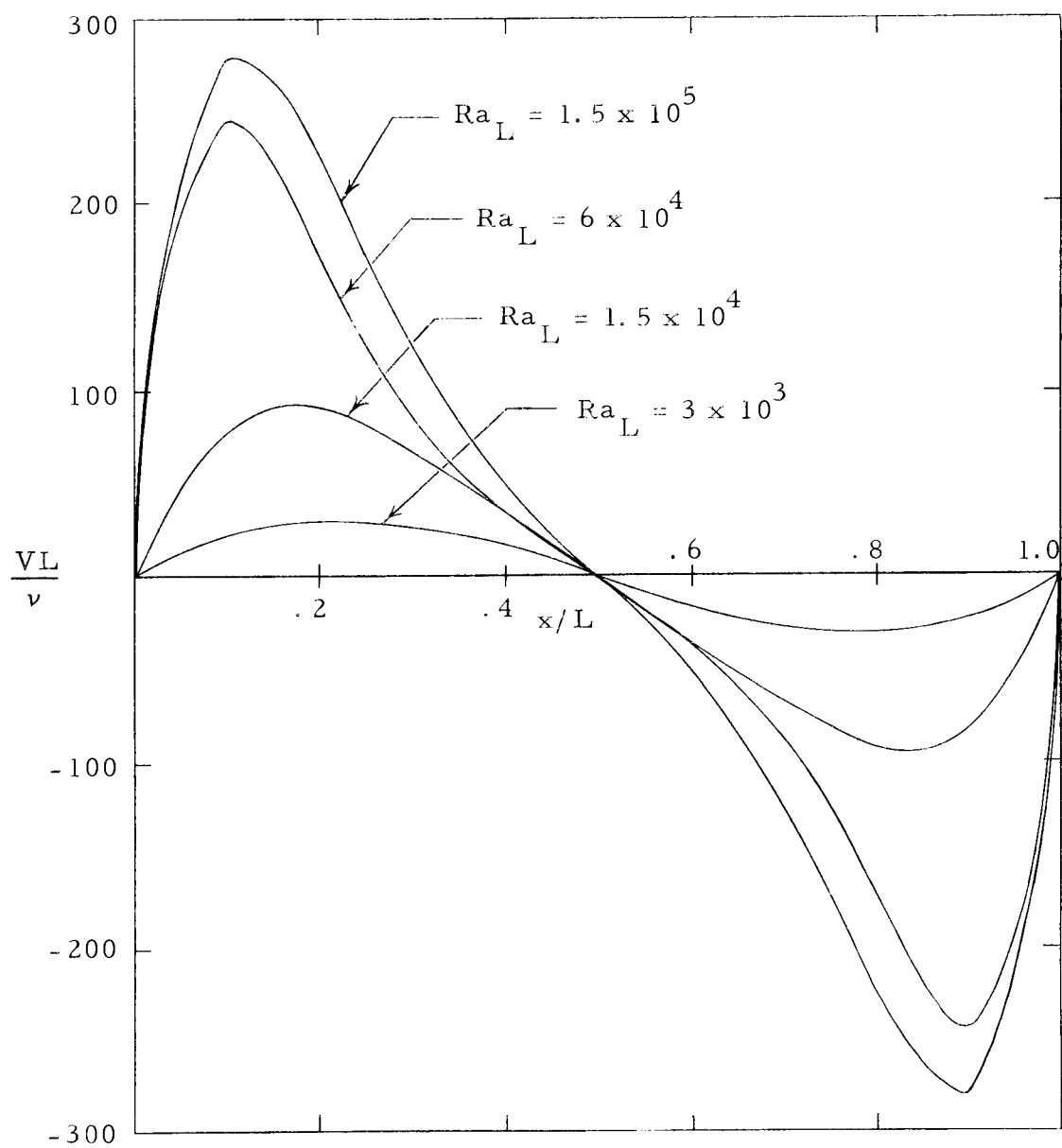


Figure 26. Vertical velocity profiles for various Rayleigh numbers at $y/H = .5$.

approximately 9×10^4 for the aspect ratio of five used in this study.

Aspect Ratio Variation

Although this study is confined primarily to the consideration of one particular aspect ratio, some comparison can be made to an earlier computation for an $H/L = 10$. Figures 27 and 28 represent plots of the velocity and temperature profiles for comparable Rayleigh numbers.

The resulting temperature profiles appear reasonable in that one would expect the convective effects to be more prominent for the lower aspect ratio for a given Rayleigh number. Then, as the aspect ratio is increased, the temperature profiles tend to increase also, and in the limit (i. e. , infinite plate case) approach the linear profile.

Increases in the convection effect are also noted by the overall increase in the velocity field at the lower aspect ratio.

Transient Temperature of Velocity Profiles

Figures 29 and 30 are included to describe the transient stages in the temperature and velocity patterns in obtaining a steady state solution. In an earlier section, reference was made to experimental data by Landis and Yanowitz [24] which exhibited velocity "overshoot" prior to steady state stabilization. This phenomenon was also obtained analytically by MacGregor in his studies. MacGregor also

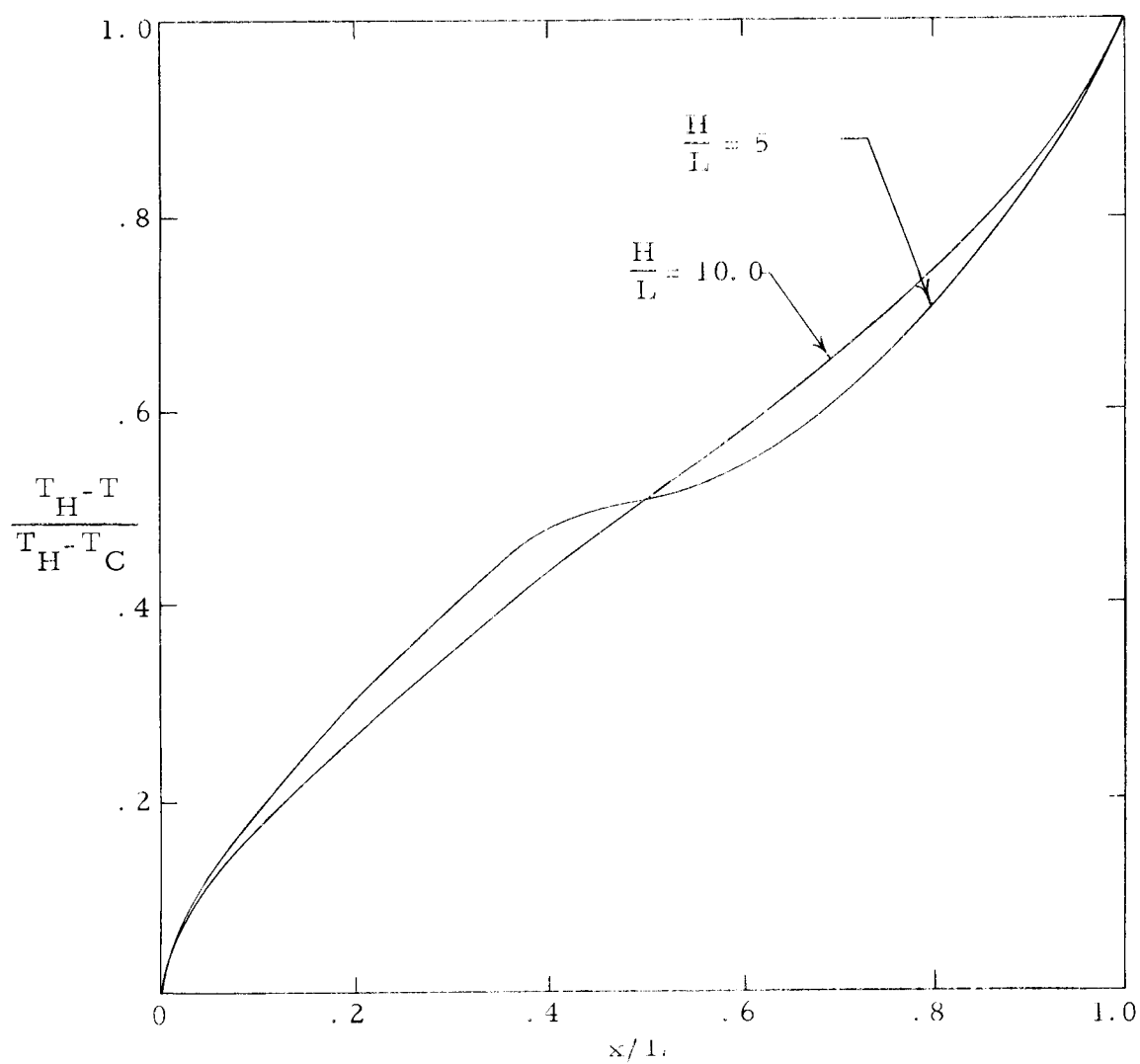


Figure 27. Dimensionless temperature profiles for indicated aspect ratios for $Ra_{1,} \approx 7 \times 10^3$.

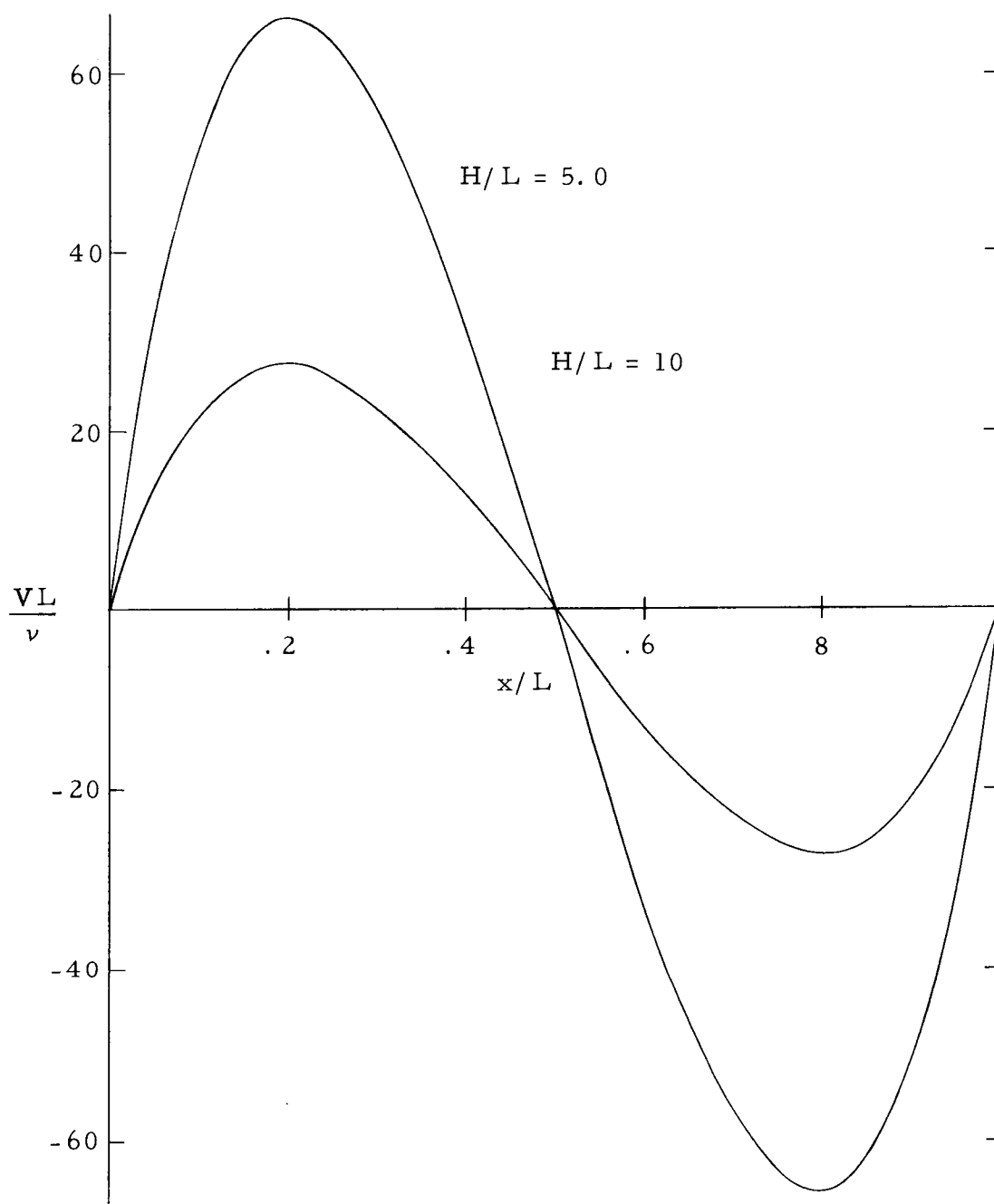


Figure 28. Dimensionless vertical velocity profiles for indicated aspect ratios for $Ra_L \approx 7 \times 10^3$.

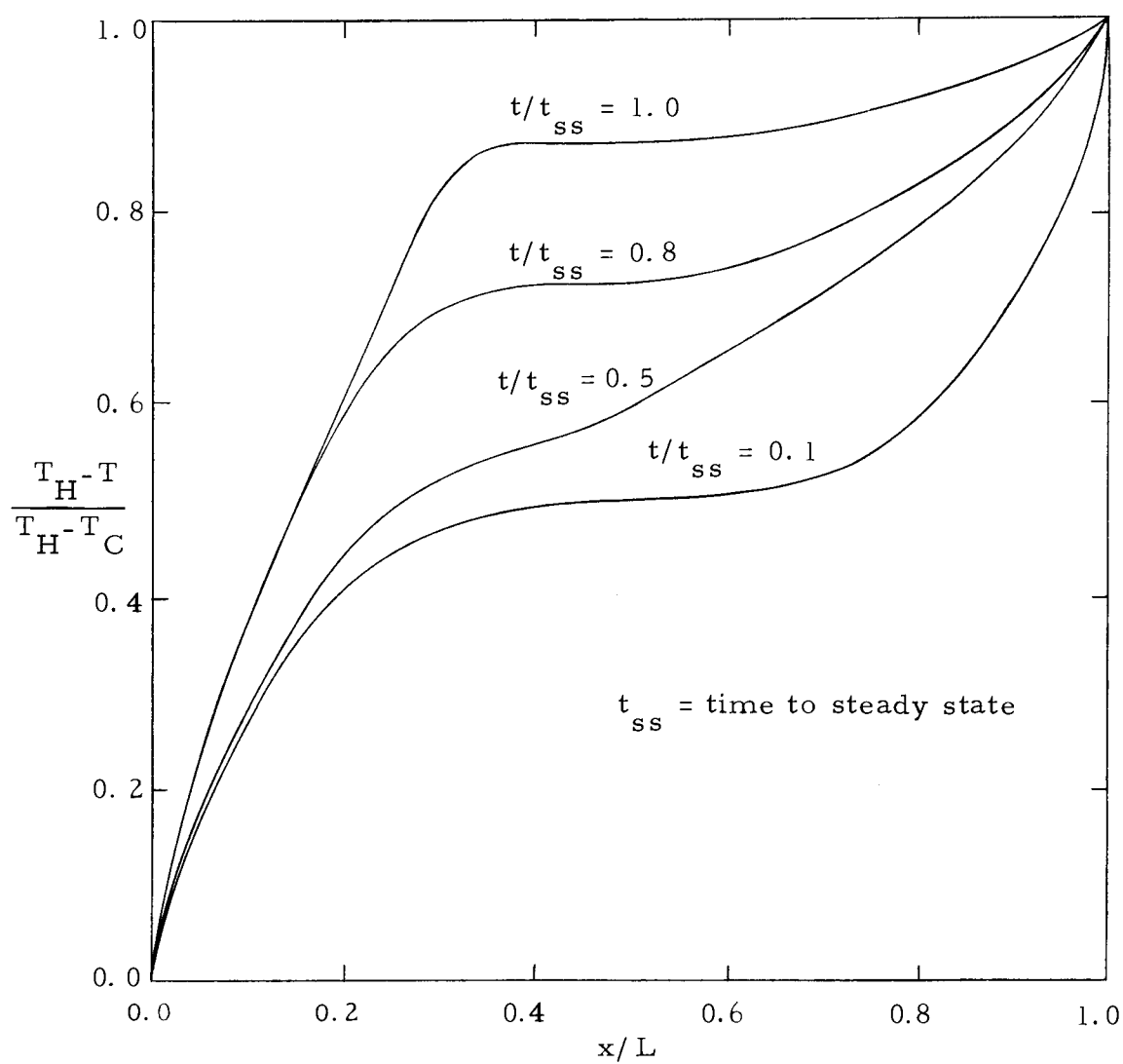


Figure 29. Transient temperature profiles at $y/H = .2$ for $Ra_L = 1.5 \times 10^4$.

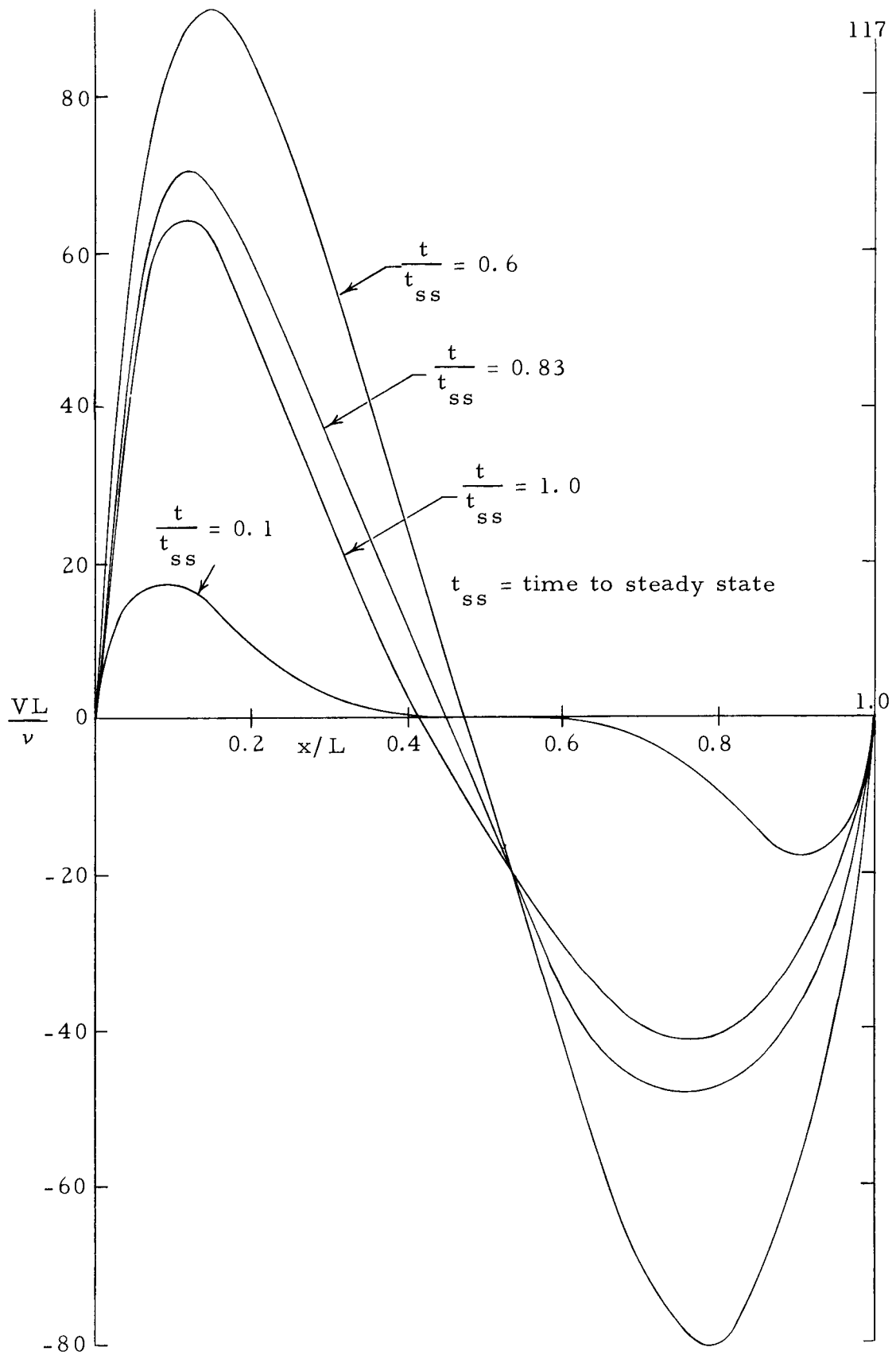


Figure 30. Transient vertical velocity profiles at $y/H = .2$ for a $Ra_L = 1.5 \times 10^4$.

indicated a considerable "overshoot" in temperature for an aspect ratio of one and $Ra_L = 10^4$.

This is not the case for the profiles shown in Figure 29. Note that in this case the temperatures adjacent to the hot wall are fairly well developed after .8 of the required time for steady state has elapsed. In the meantime, a considerable amount of "overshoot" has been experienced in comparison with the finalized velocity profile.

In the case of higher Rayleigh numbers (1.5×10^5), however, this study does show an "overshoot" with respect to velocity profiles and a comparable "overshoot" in temperature values. The phenomena shown in Figures 31 and 32 are typical of both the temperature and velocity profiles throughout this region.

Landis and Yanowitz witnessed the "overshoot" phenomenon for the application of constant flux heating. For the calculations of this study, recall that the system was initialized with zero velocities and at $t = 0$, the temperature boundary conditions were applied. At higher Rayleigh numbers, the temperature differences imposed are of considerable magnitude, which produce high velocity disturbances within the fluid region. This would closely resemble the case of a constant flux boundary condition, where the flux is applied immediately and held constant until the steady state condition is achieved. It would seem that in applying the isothermal boundary condition experimentally, one would gradually apply power to avoid major

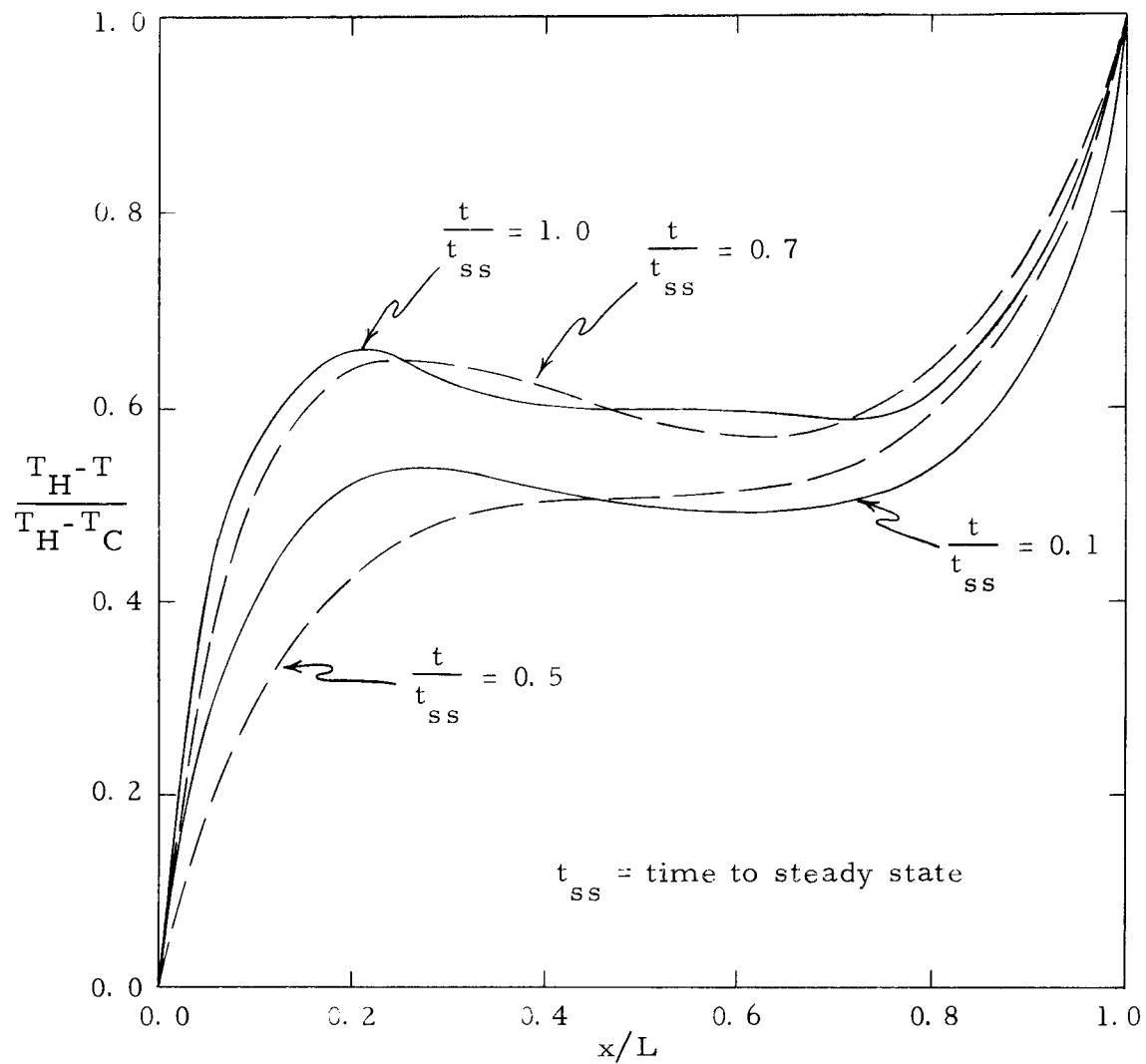


Figure 31. Transient temperature profiles at $y/H = .2$ for $Ra_L = 1.5 \times 10^5$.

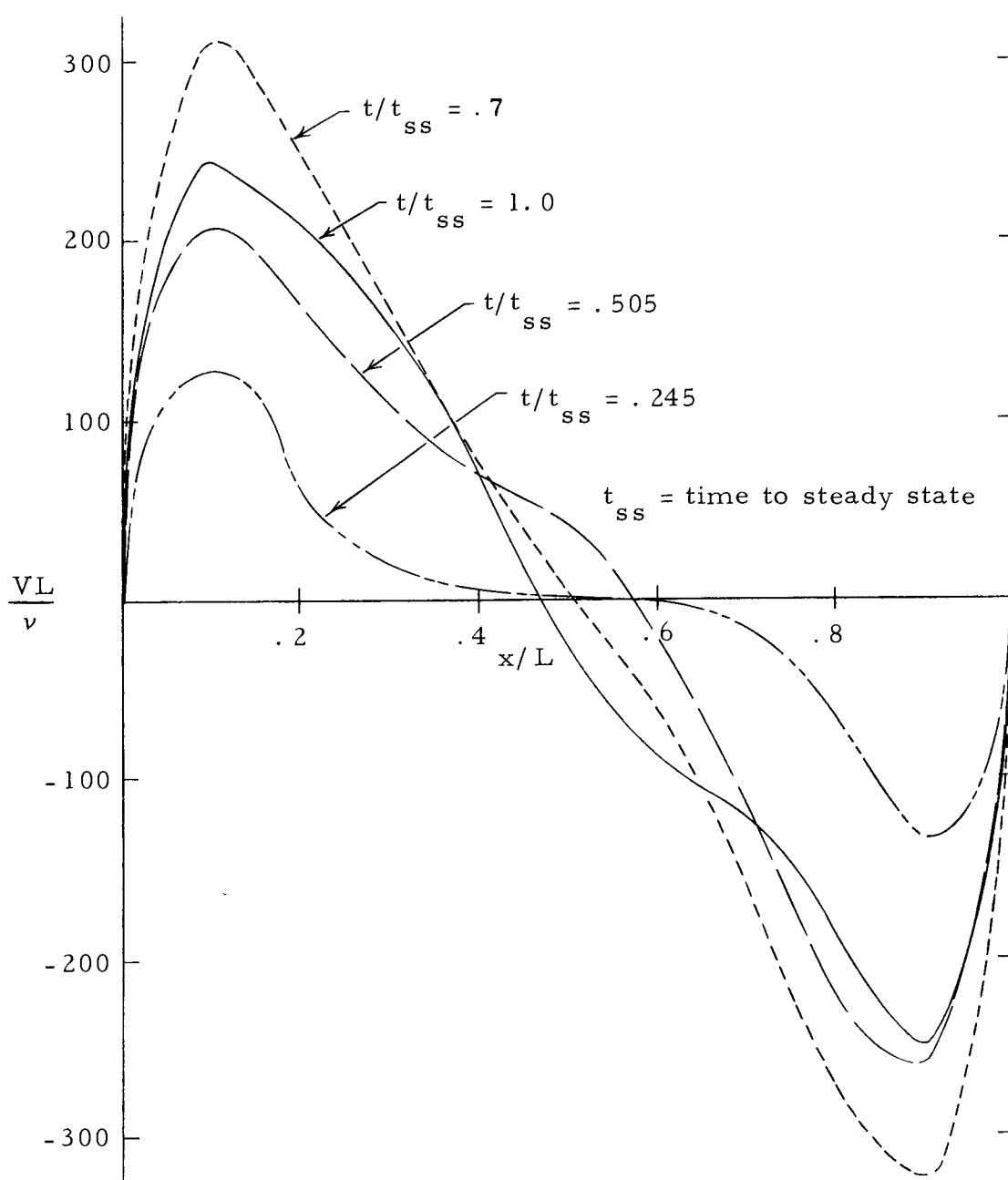


Figure 32. Transient vertical velocity profiles at $y/H = .2$
for $Ra_L = 1.5 \times 10^5$.

temperature differentials within the plate. In this manner gross disturbances in the fluid velocity field would, in all probability, be negated. Therefore, this writer concludes that the resulting transient profiles, shown in Figures 29 through 32, are highly dependent on the manner in which the boundary conditions are applied in the computer program. It is doubtful that the computed results could be experimentally reproduced under the normal practice of applying energy at the boundaries.

Overall Heat Transfer Characteristics

It was noted previously that, for an aspect ratio of ten, the average Nusselt number agreed fairly well with a known experimental correlation for a restricted range of Grashof numbers. Further comparisons, with respect to existing analytical and experimental values, are offered in Figures 33 and 34.

MacGregor's [27] analytical studies included the evaluation of the dimensionless heat transfer coefficient for various aspect ratios. The Nusselt numbers obtained in this study (for an aspect ratio of five) are shown in Figure 33. Included are analytical results for aspect ratios of one and ten, as referenced. Note that in all cases a rapid increase in the Nusselt number is apparent for Rayleigh numbers slightly above the conduction regime. At a point of approximately 2×10^4 , an inflection point is encountered. Beyond this, the rate of

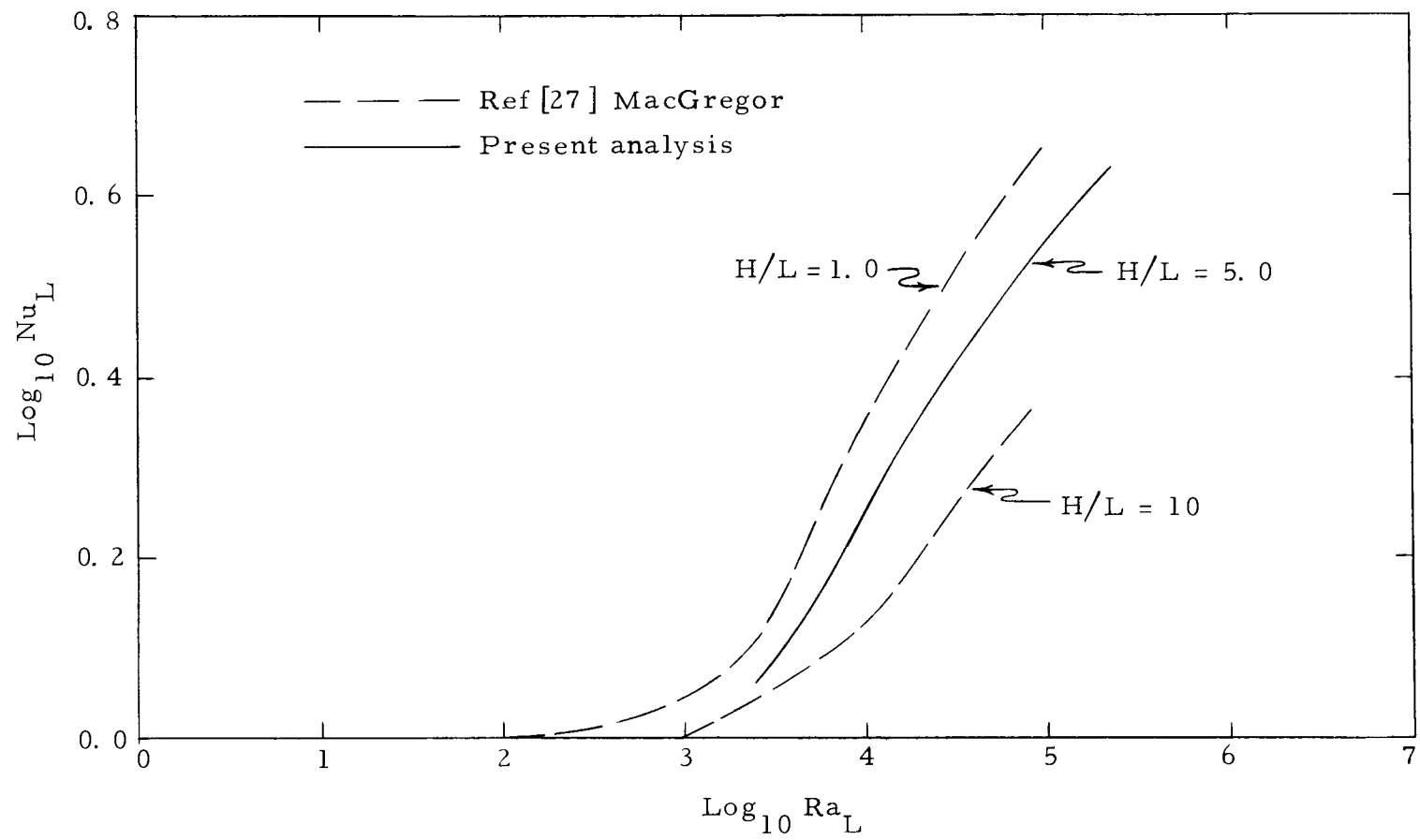


Figure 33. Analytical comparisons of dimensionless heat transfer coefficients.

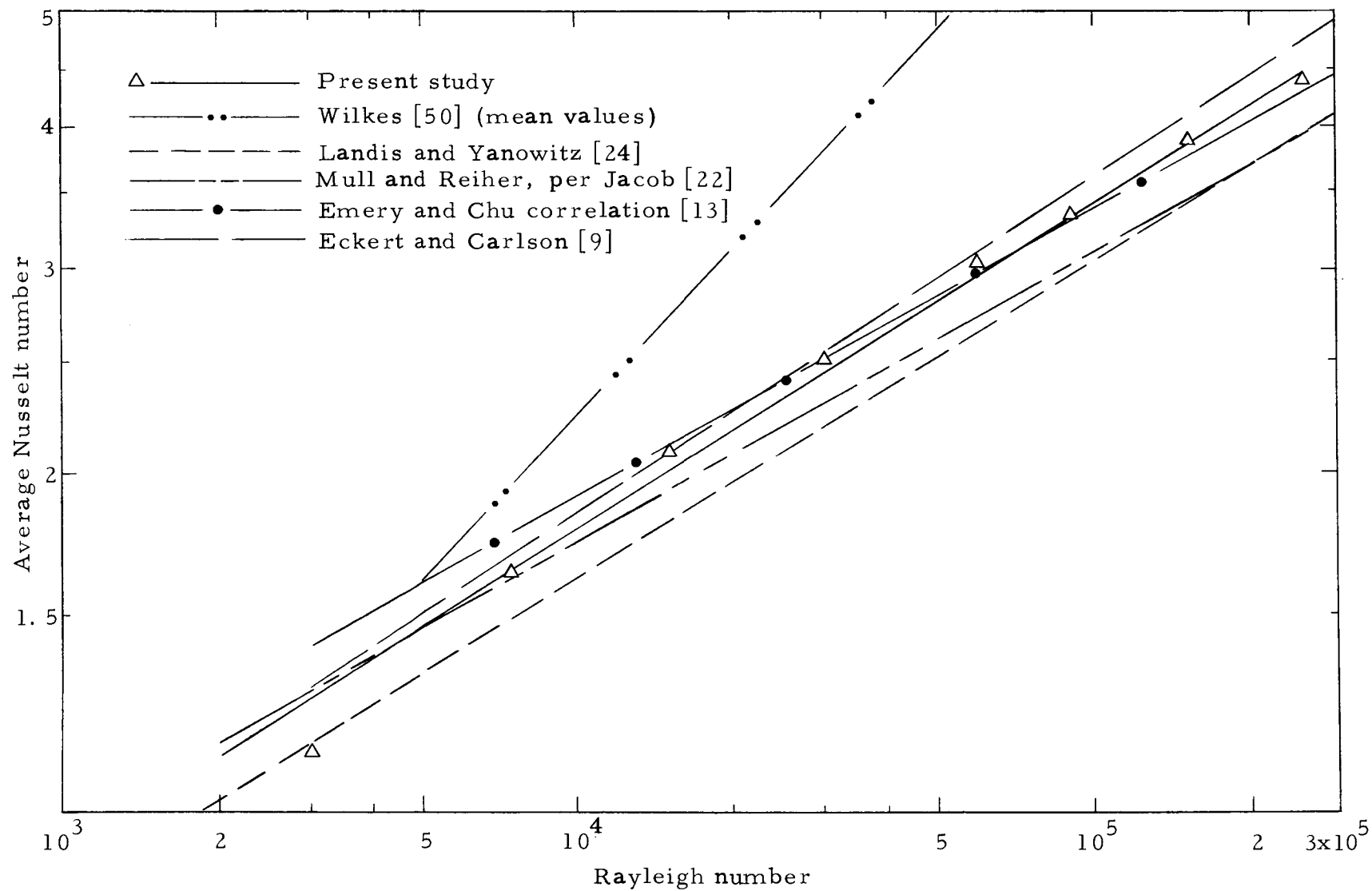


Figure 34. Comparison of this study with previous experimental correlations.

increase in Nusselt number, for larger Rayleigh numbers, is reduced.

Table 3 is a listing of some notable heat transfer correlations for the rectangular enclosure based on the work of various authors. It is apparent from these correlations, that considerable differences exist depending upon which parameters are considered significant in describing the heat transfer condition.

A few of the correlations shown in Table 3 are plotted in Figure 34 for the aspect ratio of interest in this study. Also included are the analytical results of Wilkes for an aspect ratio of one and the results of this study. The straight line representing this study is within $\pm 5\%$ of the calculated values with the maximum deviation occurring at the end point of $Ra_L = 2.5 \times 10^5$.

Some salient points exhibited by Figure 34 worthy of mention are:

The overall correlations of Mull and Reiher (per Jakob), Emery and Chu, and Carlson and Eckert are all reasonable representations of the analytical results of this study. This is to be expected for the correlation of Emery and Chu, since a considerable amount of their data were taken at an aspect ratio of five. Jakob's representation of Mull and Reiher's data is based on a fairly wide range of aspect ratios (see Table 3). However, in reality, the majority of the data points used for this correlation were taken at aspect ratios between 5 and 20. This is also

Table 3. Heat transfer correlations for heat transfer in a rectangular enclosure.

Author (Reference)	Range Correlation	Range Correlation	Range Correlation	Remarks
Jakob [22] (from Mull and Reiher data)	$Gr_L < 2000$ $Nu_L = 1$	$2 \times 10^3 < Gr_L < 2 \times 10^5$ $Nu_L = .18(Gr_L)^{1/4}(H/L)^{-1/9}$	$2 \times 10^4 < Gr_L < 2 \times 10^5$ $Nu_L = .065(Gr_L)^{1/3}(H/L)^{-1/9}$	$3.12 < H/L < 42.2$
DeGraaf and Van der Held [5]	$Gr_L < 7 \times 10^3$ $Nu_L = 1$	$10^4 < Gr_L < 8 \times 10^4$ $Nu_L = .0384Gr_L^{.37}$	$2 \times 10^5 < Gr_L$ $Nu_L = .0317Gr_L^{.37}$	Noted negligible H/L effect
Eckert and Carlson [9]	$Gr_L < 3000$ $Nu_L = 1$	$3000 < Gr_L < 2 \times 10^5$ $Nu_L = .119(Gr_L)^{.3}(H/L)^{-.1}$		$1 < H/L < 47$
Emery [12]		$5 \times 10^3 < Ra_L < 5 \times 10^5$ $Nu_L = .285(H/L)^{-1/4} \left\{ 1 + \frac{.952}{Pr} \right\}^{-1/4} (Ra_L)^{1/4}$	$5 \times 10^5 < Ra_L < 8 \times 10^6$ $Nu_L = .0516(Ra_L)^{1/3}$	$5 < H/L < 10$
Dropkin and Sommercales [7]		$5 \times 10^4 < Ra_L < 7 \times 10^8$ $Nu_L = .049Pr^{.074}Ra_L^{1/3}$		$2 < Pr < 11,560$ $4.4 < H/L < 16.6$
Emery and Chu [13]		$5 \times 10^3 < Ra_L < 10^7$ Overall correlation $Nu = .280(Ra_L)^{1/4}(H/L)^{-1/4}$		$H/L = 5$ and $H/L = 10$ Constant flux heating
Landis and Yanowitz [24]		$2 \times 10^3 < Ra_L < 1.5 \times 10^6$ $Nu = .123(Ra)^{.279}$		$H/L = 20$
MacGregor [27]		$10^4 < Ra_L < 10^7$ Overall correlation $Nu = .42(Ra_L)^{1/4}(H/L)^{-.3}(Pr)^{.012}$	$10^6 < Ra_L$ $Nu = .046(Ra_L)^{1/3}$	$10 < H/L < 40$ $1.0 < Pr < 2 \times 10^3$

the case for the data obtained by Eckert and Carlson.

The correlation of Landis and Yanowitz shows the largest deviation from the results of this study. Their data were obtained for an aspect ratio of 20. Therefore, based on the trend established in Figure 33, test data for higher aspect ratios should yield lower Nusselt numbers for the same Rayleigh number. This trend is apparently adhered to in Figure 34.

The line faired through the analytical results of Wilkes does show a slope difference (greater by approximately two) than the results obtained in this study. An adjustment of his averaging technique, such as that offered by Equation (112), would yield results reasonably close to known experimental data.

For this study, the line shown in Figure 34 in equation form is:

$$\text{Nu}_L = .137(\text{Ra}_L)^{.28} \quad (116)$$

for

$$3 \times 10^3 < \text{Ra}_L < 2.5 \times 10^5$$

The magnitude of the slope (.28) is comparable to .279 obtained by Landis and Yanowitz.

Another possible correlation would be to use two separate curves between Rayleigh numbers of 3×10^3 and 2×10^4 and between 2×10^4 and 2.5×10^5 , respectively. The two curves so obtained

would then be represented by

$$\text{Nu}_L = .046(\text{Ra}_L)^{.403} \quad (117)$$

and

$$\text{Nu}_L = .153(\text{Ra}_L)^{.272} \quad (118)$$

respectively. The correlations shown in Equations(117) and (118) are most representative of the differences in overall heat transfer performance for the transition zone and laminar regimes.

In reviewing the various correlations offered by previous experimentors in this area, it becomes apparent that this study correlates best with data obtained for aspect ratios in the proximity of five. In another case, MacGregor's correlation paralleled that of Landis and Yanowitz and both sets of data were for similar aspect ratios. This would imply that a correlation in the form of

$$\text{Nu}_L = C(\text{Ra}_L)^a(H/L)^b$$

would be more applicable.

V. CONCLUDING REMARKS AND SUGGESTIONS FOR FUTURE WORK

With respect to the objectives of this study, a computing technique has been formulated capable of solving the governing equations, for mass, energy, and momentum in finite difference form which apply to the rectangular enclosure problem. The results of this study compare favorably with recent experimental and analytical data of other workers. In addition to this, the computed results simulate the expected transient conditions, as well as the steady state conditions, based on the written observations of past work.

For the rectangular cell, the present method appears to have merit between Rayleigh numbers of 10^2 to 10^5 . Beyond this, at least, three factors are to be considered:

First is the assumption that constant property fluids are correctly portrayed, for even the isothermal boundary case. An even greater deviation would be encountered for the constant flux problem.

Second are the economic considerations involved in the computational times required to obtain a solution at high Rayleigh numbers. In conjunction with this concern, it is expected that a smaller mesh size will be mandatory in order to reflect the magnitude of the velocities in the vicinity of the vertical walls. This in itself will prohibit the allowable time increment

required to insure stability.

And lastly, beyond the laminar boundary regime, the equations programmed in this study will not, in all probability, correctly portray the physical phenomena. As an example, certain compensations must be made to include turbulent shear stresses.

Within the scope of the present program, solutions for an inclined vertical enclosure up to and including the horizontal case are realizable. It appears that solutions could be studied for a variety of geometrical and fluid property parameters.

It would also be worthwhile to provide solutions for the variable parameter cases, using the basic technique used in this study of retaining the pressure term. This would allow some detailed analyses of the natural convection effect for liquids in which pressure differentials within an enclosure may be of considerable magnitude. Solutions for the cases concerning liquid metals would be of interest in nuclear reactor operations.

However, this writer feels that the most significant feature of this program lies in its adaptability to situations involving in-flow and out-flow boundaries. This provides means for solving a variety of problems concerning "mixed" modes of convection (natural and forced) for either the constant or variable property cases. Along the same line, solutions to various "stationary stall" problems could be attempted to possibly gain a keener understanding of the flow and energy mechanisms that cause this phenomenon.

BIBLIOGRAPHY

1. Albers, L. U. Numerical solution of simplified boundary-value problem. In: Thirty-ninth annual report of the National Advisory Committee for Aeronautics, including technical reports. Technical report no. 1111, Appendix B. Washington, D. C. , U.S. Government Printing Office, 1955. p. 73-75.
2. Batchelor, G. K. Heat transfer by free convection across a closed cavity between vertical boundaries at different temperatures. Quarterly of Applied Mathematics 12:209-233. 1954.
3. Carlson, W. O. Interferometric studies of convective flow phenomena in vertical plane enclosed air layers. Ph. D. thesis. Minneapolis, University of Minnesota, 1956. 298 numb. leaves.
4. Carpenter, L. G. and H. C. Wassell. The loss of heat by natural convection from parallel vertical plates in air. Proceedings of the Institution of Mechanical Engineers 128:439-457. 1934.
5. deGraaf, J. G. A. and E. F. M. van der Held. The relation between the heat transfer and the convective phenomena in enclosed plane layers. Applied Scientific Research 3:393-409. 1953.
6. Davis, C. de Vahl and C. F. Kettleborough. Natural convection in an enclosed rectangular cavity. Institution of Engineers Mechanical and Chemical Engineering Transactions (Australia) MC 1(1):43-49. 1965.
7. Dropkin, D. and E. Somerscales. Heat transfer by natural convection in liquids confined by two parallel plates which are inclined at various angles with respect to the horizontal. Journal of Heat Transfer, Transactions of the American Society of Mechanical Engineers 85:77-84. 1965.
8. DuLong, P. L. and A. T. Petit. Recherches sur la mesure des temperatures, et sur les lois de la communication de la chaleur. Annales de Chemie 7:225-264, 337-367. 1817.
9. Eckert, E. R. G. and W. O. Carlson. Natural convection in an air layer enclosed between two vertical plates with different temperatures. International Journal of Heat and Mass Transfer 2:106-120. 1961.

10. Eckert, E. R. G. and R. M. Drake, Jr. Heat and Mass Transfer. 2d ed. New York, McGraw-Hill, 1959. 530 p.
11. Eckert, E. R. G. and E. E. Soehngen. Studies on heat transfer in laminar free convection with the Zehnder-Mach interferometer. Dayton, Ohio, Air Material Command, (U. S. Air Force Technical Report 5747)
12. Emery, A. F. The effect of a magnetic field upon the free convection of a conducting fluid. Journal of Heat Transfer, Transactions of the American Society of Mechanical Engineers 85: 119-124. 1963.
13. Emery, A. F. and N. C. Chu. Heat transfer across vertical layers. Journal of Heat Transfer, Transactions of the American Society of Mechanical Engineers 84:110-114. 1965.
14. Fromm, J. The time dependent flow of an incompressible viscous fluid. Method in Computational Physics 3:345-382. 1964.
15. Gebhart, B. Transient convection from vertical elements. Journal of Heat Transfer, Transactions of the American Society of Mechanical Engineers 83:61-70. 1961.
16. Gebhart, B. Transient convection from vertical elements, appreciable thermal capacity. Journal of Heat Transfer, Transactions of the American Society of Mechanical Engineers 85:10-14. 1963.
17. Griffiths, E. and A. H. Davis. The transmission of heat by radiation and convection. London, 1931. 26 p. (Great Britain. Department of Scientific and Industrial Research. Food Investigation Board. Special Report 9)
18. Hayday, A. A., D. A. Bowles and R. A. McGraw. Free convection from a vertical flat plate with step discontinuities. Journal of Heat Transfer, Transactions of the American Society of Mechanical Engineers 89:244-250. 1967.
19. Held, E. F. M. van der. (Chart: Heat transfer in horizontal and vertical air layers). Warmetechnik 2:54. 1931. Reproduced in: The relation between the heat transfer and the convective phenomena in enclosed plane layers, by J. G. A. deGraaf and E. F. M. van der Held. Applied Scientific Research 3:395-409. 1953.

20. Hellums, J. D. and S. W. Churchill. Transient and steady state, free and natural convection, numerical solutions. American Institute of Chemical Engineering Journal 8:879-886. 1958.
21. Jakob, M. Heat transfer vol. I. New York, Wiley, 1936. 758 p.
22. Jakob, M. Free heat convection through enclosed plane gas layers. Transactions of the American Society of Mechanical Engineers 68:189-193. 1946.
23. Kreith, F. Principles of heat transfer. Scranton, International Textbook, 1958. 536 p.
24. Landis, F. and H. Yanowitz. Transient natural convection in a narrow vertical cell. In: Proceedings of the Third International Heat Transfer Conference, Chicago, August 1966. Vol. 2. New York, American Institute of Chemical Engineers, 1966. p. 139-151.
25. Leary, J. W. An analytical solution of free convection in a closed cavity. Master's thesis. Seattle, University of Washington, 1965. 82 numb. leaves.
26. Lorenz, L. Über das leitungsvermögen der metalle fuer warme und electricitat. Wiedemanns Annalender Physik and Chemie 13:581-582. 1881.
27. MacGregor, R. K. The natural convection of fluids in rectangular vertical enclosures. Ph. D. thesis. Seattle, University of Washington, 1967. 274 numb. leaves.
28. Mull, W. and H. Reiher. Der warmeschutz von Luftschichten. Beihefte Zum Gesundheits-Ingenieure, Reihe 1, 28:126. 1930.
29. Nusselt, W. Die varmeleitfähigkeit von warmeisolierstoffen. Mitteilungen über Forschungsarbeiten herausgegeben vom Verein deutscher Ingenieure 63 and 64:1-23. 1909.
30. Nusselt, W. and W. Juerges. Das temperaturfeld über einer lotrecht stehenden geheizten platte. Zeitschrift des Vereines deutscher Ingenieure 72:597-603. 1928.

31. Ostrach, S. An analysis of laminar free convection flow and heat transfer about a flat plate parallel to the direction of the generating body force. Washington, D. C., 1952. 47 p. (U.S. National Advisory Committee for Aeronautics Technical Note 2635)
32. Ostrach, S. An analysis of laminar free convection flow and heat transfer above a flat plate parallel to the direction of the generating body force. In: Thirty-ninth annual report of the National Committee of Aeronautics, including technical reports. Technical report no. 1111. Washington, D. C., U.S. Government Printing Office, 1955. p. 75-79.
33. Poots, G. Heat transfer by laminar free convection in enclosed plane gas layers. Quarterly Journal of Mechanics and Applied Mathematics 11:257-273. 1958.
34. Queer, E. R. Importance of radiation in heat transfer through air spaces. Transactions of the American Society of Heating and Ventilating Engineers 38:77-96. 1932.
35. Rayleigh, Lord. On convective currents in a horizontal layer of fluid, when the higher temperature is on the underside. Philosophical Magazine 32:529-546. 1916.
36. Richtmyer, R. D. Difference methods for initial value problems. New York, Interscience. 1957. 405 p.
37. Rohsenow, W.M. and H. Choi. Heat, mass and momentum transfer. Englewood Cliffs, Prentice-Hall, 1961. 537 p.
38. Saunders, O. A. Effect of pressure on free convection from a heated plate to the air inside a pressurized vessel. Proceedings of the Royal Society of London, ser. A., 157:278-291. 1936.
39. Schmidt, E. Warmeschutz durch aluminum folie. Zeitschrift des Vereines Deutscher Ingenieure 71:1395-1400. 1927.
40. Schmidt, E. and W. Beckmann. Das temperature-und Geschwindigkeitfeld vor einer warme abgebenden senkrechten platte bei natuerlicher konvektion. Technische Mechanik und Thermodynamik 10:341-349; 11:391-405. 1930.

41. Schmidt, E. and O. A. Saunders. On the motion of a fluid heated from below. Proceedings of the Royal Society of London, ser. A, 165:216-228. 1938.
42. Shetz, J. A. and R. Eichhorn. Natural convection with discontinuous wall temperature variations. Journal of Fluid Mechanics 18:167-176. 1964.
43. Smith, G. D. Numerical solution of partial differential equations. London, Oxford University, 1965. 175 p.
44. Sparrow, E. M. Laminar free convection on a vertical plate with prescribed non-uniform wall heat flux or prescribed non-uniform wall temperature. Washington, D. C., 1955. 34 p. (U. S. National Advisory Committee for Aeronautics Technical Note 3508)
45. Sparrow, E. M. and J. L. Gregg. Laminar free convection from a vertical plate with a uniform surface heat flux. Transactions of the American Society of Mechanical Engineers 78:435-550. 1956.
46. Sparrow, E. M. and J. L. Gregg. The variable fluid property problem in free convection. Transactions of the American Society of Mechanical Engineers 80:879-886. 1958.
47. Timo, D. P. Discussion: Laminar free convection from a vertical plate with a uniform heat flux, by E. M. Sparrow and J. L. Gregg. Transactions of the American Society of Mechanical Engineers 78:435-440. 1956.
48. Weise, R. Waermeuebergeng durch freie konvektion an quadratischen platte. Forschung im Ingenieurwesens, verein Deutscher Ingenieure 6:281-286. 1935.
49. Welch, J. E. et al. The MAC method, a computing technique for solving viscous, incompressible, transient fluid-flow problems involving free surfaces. Los Alamos, New Mexico, Los Alamos Scientific Laboratory, 1965. 146 p. (Los Alamos Report 3425)
50. Wilkes, J. O. The finite difference computation of natural convection in an enclosed rectangular cavity. Ph. D. thesis. Ann Arbor, University of Michigan, 1963. 177 numb. leaves.

51. Wilkes, G. B. and C. M. F. Peterson. Radiation and convection across air spaces in frame construction. Heating, Piping and Air Conditioning Journal 9:505-510. 1937.
52. Wilkes, G. B. and C. M. F. Peterson. Radiation and convection from surfaces in various positions. Heating, Piping and Air Conditioning Journal 10:477-480. 1938.
53. Yang, K-T. Possible similarity solutions for laminar free convection on vertical plates and cylinders. Journal of Applied Mechanics, Transactions of the American Society of Mechanical Engineers 82:230-236. 1960.

APPENDICES

APPENDIX A

Stability Criteria

There exist two classic methods for examining the stability of finite-difference equations. The easier of the two is accomplished by substituting a Fourier series expansion of the dependent variables into the equations and examining the resulting form for maximum and minimum values. The second method involves expressing the equations in matrix form and examining the resulting form of the eigenvalues. Stability analyses shown in this section are predominantly the Fourier substitution type except for the von Neumann analysis which is a combination of both methods.

Fromm [14] analyzed the momentum equation in vorticity form for two separate cases, with the transport terms omitted and zero viscosity. In both these cases, the pressure term had been deleted since it was automatically eliminated by taking cross partials.

For the first case, Fromm started with the momentum equation written in finite difference form with $\delta x = \delta y = a$.

$$\begin{aligned} \omega_{ij}^{n+1} = \omega_{ij}^n + \frac{\delta t}{2a} [(U\omega)_{i-1,j}^n - (U\omega)_{i+1,j}^n + (V\omega)_{i,j-1}^n - (V\omega)_{i,j+1}^n] \\ + \frac{\nu \delta t}{a^2} [\omega_{i+1,j}^n + \omega_{i-1,j}^n + \omega_{i,j+1}^n + \omega_{i,j-1}^n - 4\omega_{ij}^n] \end{aligned} \quad (A-1)$$

With the transport terms deleted, (A-1) now takes the form of:

$$\omega_{ij}^{n+1} = \omega_{ij}^n + \frac{\nu \delta t}{a} [\omega_{i+1,j}^n + \omega_{i-1,j}^n + \omega_{i,j+1}^n + \omega_{i,j-1}^n - 4\omega_{ij}^n] \quad (\text{A-2})$$

The Fourier analysis of stability assumes that at any time, t , within the computation scheme, the dependent variables, (x, y) may be expanded into a series in the form,

$$\omega_{ij}^n = \omega_0 r^n e^{i\alpha x} e^{i\beta y} \quad (\text{A-3})$$

where i is the imaginary number $\sqrt{-1}$ and r^n is the amplification factor at some arbitrary n advancement in time. From the expression in (A-3), it is mandatory that $|r| < 1$.

Now using the assumed expression in (A-3), components of Equation (A-2) become:

$$\begin{aligned} \omega_{ij}^{n+1} &= \omega_0 r^{n+1} e^{i\alpha x} e^{i\beta y} \\ \omega_{i+1,j}^n &= \omega_0 r^n e^{i\alpha(x+1)} e^{i\beta y} \\ \omega_{i-1,j}^n &= \omega_0 r^n e^{i\alpha(x-1)} e^{i\beta y} \\ \omega_{i,j+1}^n &= \omega_0 r^n e^{i\alpha x} e^{i\beta(y+1)} \\ \omega_{i,j-1}^n &= \omega_0 r^n e^{i\alpha x} e^{i\beta(y-1)} \end{aligned}$$

Substitution into Equation (A-2) leads to:

$$\begin{aligned}
& \omega_0 r^{n+1} e^{iax} e^{i\beta y} - \omega_0 r^n e^{iax} e^{i\beta y} \\
&= \frac{\nu \delta t}{a} \omega_0 r^n e^{iax} e^{i\beta y} (e^{ia} + e^{-ia} + e^{i\beta} + e^{-i\beta} - 4) \quad (\text{A-4})
\end{aligned}$$

but

$$e^{ia} + e^{-ia} = 2 \cos a$$

and

$$e^{i\beta} + e^{-i\beta} = 2 \cos \beta$$

therefore, Equation (A-4) reduces to:

$$r - 1 = \frac{\nu \delta t}{a} (2 \cos a + 2 \cos \beta - 4)$$

or

$$r = 1 + \frac{2\nu \delta t}{a} (\cos a + \cos \beta - 2)$$

The maximum absolute value of the term $(\cos a + \cos \beta - 2)$ occurs when $a = \beta = \pi$ or, in reference to the Argand diagram, when r lies along the negative real axis. In this case, r must be chosen such that $r \geq -1$ to minimize the amplification at any given computational step.

Therefore,

$$1 - \frac{8\nu \delta t}{a} \geq -1$$

or

$$\frac{8\nu\delta t}{a^2} \leq 2$$

and finally

$$\frac{\nu\delta t}{a^2} \leq \frac{1}{4} \quad (\text{A-5})$$

Equation (A-5) represents the stability relationship for the case of deleted transport terms in the vorticity-momentum equations.

Fromm then proceeded to analyze Equation (A-1) under the condition of zero viscosity by linearizing the velocity terms.

By allowing

$$U_{ij}^n = U_0(1 + \delta_{ij}^n)$$

and

$$V = V_0(1 + \Delta_{ij}^n) \quad (\text{A-6})$$

where both

$$\delta_{ij}^n \quad \text{and} \quad \Delta_{ij}^n \ll 1$$

and V_0 and U_0 are velocity values which would be obtained if the exact solution of the partial differential equations existed.

Now, applying Fourier expansions as in the previous case, a final expression results:

$$\frac{\delta t^2}{a^2} (U_0 \sin \alpha + V_0 \sin \beta)^2 \leq 0$$

which cannot be satisfied for all α and β . Fromm concluded that for the case of zero viscosity, Equation (A-1) is unconditionally unstable.

It is interesting to note at this point that an analysis identical to that used in the preceding case, applied to the momentum equation

$$\frac{\partial U}{\partial t} + U \frac{\partial U}{\partial x} + V \frac{\partial V}{\partial y} = \nu \left(\frac{\partial^2 U}{\partial x^2} + \frac{\partial^2 U}{\partial y^2} \right) \quad (\text{A-7})$$

for the condition of zero viscosity, can be shown to be stable under certain conditions. To show this, the central finite difference form must be used and linearized as shown in Equation (A-6). A Fourier expansion of the resulting expression leads to a stability criterion in the form

$$\frac{U_0 \delta t}{\delta x \delta y} \leq \frac{1}{2} \quad (\text{A-8})$$

Again using the central difference method, an examination of the required criteria for the case of deleted transport terms in Equation (A-7) results in the following:

$$2\nu \delta t \leq \frac{\delta x^2 \delta y^2}{\delta x^2 + \delta y^2} \quad (\text{A-9})$$

A stability expression similar to that of Equation (A-9) may be

achieved for the energy equation, written in form:

$$\frac{\partial T}{\partial t} + U \frac{\partial T}{\partial x} + V \frac{\partial T}{\partial y} = \frac{\nu}{Pr} \left(\frac{\partial^2 T}{\partial x^2} + \frac{\partial^2 T}{\partial y^2} \right)$$

For the case where $U \frac{\partial T}{\partial x}$ and $V \frac{\partial T}{\partial y}$ have been deleted, the stability criterion can be established as:

$$2\nu\delta t \leq Pr \left(\frac{\delta x^2 \delta y^2}{\delta x^2 + \delta y^2} \right) \quad (\text{A-10})$$

which, for air, is only slightly more stringent on the time step for a given grid size.

All the preceding criteria establish the stability requirements on a single equation basis with the stipulation of certain conditions imposed to provide a tractable analysis. For the type of solutions required for this dissertation, it was important to determine the stability requirements of the momentum and energy equations as a set. This type of analysis invariably becomes quite complex since the velocity and temperature terms are coupled.

Hellums and Churchill [20] analyzed the set of momentum and energy Equations (20) and (21), as shown in Chapter II, to establish a relationship for the stability criteria. Their analysis considered the finite difference equations in explicit form. A Fourier expansion of the temperature and vorticity function were substituted in Equations

(20) and (21). The resulting forms could then be written in matrix form and the amplification matrix was then examined for limiting cases.

Hellums and Churchill obtained a stability relationship of

$$\frac{|\bar{u}|\Delta\bar{t}}{\Delta\bar{x}} + \frac{|\bar{v}|\Delta\bar{t}}{\Delta\bar{y}} + \frac{2\Delta\bar{t}}{\text{Pr}(\Delta\bar{x})^2} + \frac{2\Delta\bar{t}}{\text{Pr}(\Delta\bar{y})^2} \leq 1 \quad (\text{A-11})$$

for fluid Prandtl numbers less than 1. The terms in Equation (A-11) represent dimensionless quantities identical in form to those shown in Equation (21a), Chapter II.

The above criterion has since been used by Wilkes [50] and MacGregor [27] to establish allowable time increments for a given mesh size and the expected magnitude of velocities. Wilkes, however, used an implicit form of the equations and experienced instability problems at high Grashof number ($\approx 10^5$).

MacGregor used the identical criteria, but he used a factor of .7 rather than 1.0.

At best, Equation (A-11) can only be offered as a guide in selecting an allowable time increment. By substituting the various dimensionless terms into Equation (A-11), the following results

$$\frac{|\mathbf{U}|\delta t}{\delta x} + \frac{|\mathbf{V}|\delta t}{\delta y} + \frac{2\nu\delta t}{\text{Pr}\delta x^2} + \frac{2\nu\delta t}{\text{Pr}\delta y^2} \leq 1$$

For this particular study, the criterion used for the majority of the temperature calculations was:

$$\frac{|U|_{\max} \delta t}{\delta x} + \frac{|V|_{\max} \delta t}{\delta y} + \frac{2\nu \delta t}{Pr \delta x^2} + \frac{2\nu \delta t}{Pr \delta y^2} \leq .3 \quad (A-12)$$

APPENDIX B

Reduced Computational Data for $Ra_L = 1.5 \times 10^5$ Case

Dimensionless temperature (θ); $t/t_{ss} = .1$; $Ra_L = 1.5 \times 10^5$

y/H \ x/L	x/L																
	.025	.05	.1	.15	.2	.25	.3	.35	.4	.45	.5	.6	.7	.8	.9	.95	.975
0	.195	.274	.395	.46	.49	.494	.500	.500	.500	.500	.500	.500	.512	.564	.694	.8	.855
.1	.173	.243	.36	.434	.473	.491	.500	.500	.500	.500	.500	.500	.508	.539	.651	.772	.816
.2	.169	.237	.351	.426	.468	.491	.500	.500	.500	.500	.500	.500	.503	.534	.646	.77	.816
.3	.169	.237	.351	.426	.468	.491	.500	.500	.500	.500	.500	.500	.503	.534	.646	.77	.816
.4	.169	.237	.351	.426	.468	.491	.500	.500	.500	.500	.500	.500	.503	.534	.646	.77	.816
.5	.169	.237	.351	.426	.468	.491	.500	.500	.500	.500	.500	.500	.503	.534	.646	.77	.816
.6	.169	.237	.351	.426	.468	.491	.500	.500	.500	.500	.500	.500	.503	.534	.646	.77	.816
.7	.169	.237	.351	.426	.468	.491	.500	.500	.500	.500	.500	.500	.503	.534	.646	.77	.816
.8	.169	.237	.351	.426	.468	.491	.500	.500	.500	.500	.500	.500	.503	.534	.646	.77	.816
.9	.167	.234	.347	.421	.465	.487	.49	.500	.500	.500	.500	.500	.503	.53	.638	.764	.812
1.0	.149	.2	.304	.378	.438	.47	.486	.494	.500	.500	.500	.500	.498	.512	.604	.734	.79

Dimensionless vertical velocity ($\frac{vL}{\nu}$); $t/t_{ss} = .1$; $Ra_L = 1.5 \times 10^5$

y/H \ x/L	x/L																
	.025	.05	.1	.15	.2	.25	.3	.35	.4	.45	.5	.6	.7	.8	.9	.95	.975
.1	56	57	45.5	22	6.85	0.25	-1.5	-1.23	-0.26	0.85	2.1	4.26	4.25	-8.7	-51.5	-61	-58
.2	60.5	64	54.5	30.5	13.2	4.3	1.7	0.09	-0.002	-0.17	0.41	0.76	-0.61	-13.6	-55.5	-64.5	-61
.3	61	65	56.5	32.2	14.5	5.45	1.72	0.44	0.11	0.05	0.08	0.032	-1.65	-14.6	-56.5	-65.4	-61.5
.4	61.5	65.5	56.6	32.6	14.7	5.65	1.85	0.52	0.13	0.03	0.01	-0.11	-1.85	-14.8	-57	-65.5	-61.8
.5	61.5	65.5	56.6	32.6	14.8	5.7	1.87	0.53	0.13	0.02	-0.005	-0.14	-1.9	-14.8	-57	-65.5	-61.8
.6	61.5	65.5	56.6	32.6	14.8	5.65	1.85	0.5	0.1	0.003	-0.02	-0.14	-1.88	-14.8	-56.5	-65.5	-61.5
.7	61	65	56.5	32.4	14.6	5.45	1.64	0.32	-0.04	-0.1	-0.085	-0.12	-1.75	-14.5	-56	-65	-61.4
.8	60.5	64.5	55.5	31.4	13.6	4.4	0.61	-0.56	-0.78	-0.65	-0.42	-0.009	-1.1	-15.2	-54.5	-64	-60.5
.9	58	61	51.5	27	8.65	-0.7	-4.25	-4.9	-4.3	-3.25	-2.08	0.25	1.47	-6.85	-45.3	-57	-56

Dimensionless horizontal velocity ($\frac{UL}{\nu}$); $t/t_{ss} = .1$; $Ra_L = 1.5 \times 10^5$

x/L y/H	.025	.05	.1	.15	.2	.25	.3	.35	.4	.45	.5	.6	.7	.8	.9	.95	.975
.1	0.64	1.27	3.56	5.67	7.1	7.95	8.4	8.65	3.75	8.65	8.55	7.77	6.33	4.32	2.26	0.1	0.51
.2	-0.09	0.18	0.54	0.94	1.31	1.55	1.73	1.83	1.89	1.88	1.82	1.57	1.16	0.7	0.3	0.11	0.06
.3	0.017	0.03	0.1	0.2	0.25	0.3	0.33	0.36	0.37	0.37	0.36	0.31	0.23	0.14	0.06	0.02	0.011
.4	.003	.006	.02	.035	.05	.06	.06	.07	.071	.071	.07	.06	.04	.026	.011	.004	.002
.5	.0002	.0004	.0018	.003	.004	.04	.004	.003	.002	.001	.0005	-.002	-.04	-.004	-.002	-.0004	-.0002
.6	-.002	-.004	-.011	-.018	-.03	-.03	-.04	-.05	-.06	-.06	-.07	-.07	-.06	-.048	-.02	-.006	-.003
.7	-.01	-.02	-.06	-.095	-.14	-.2	-.23	-.27	-.31	-.33	-.36	-.37	-.33	-.25	-.10	-.03	-.017
.8	-0.06	-0.11	-0.3	-0.5	-0.72	-0.93	-1.13	-1.38	-1.57	-1.72	-1.81	-1.88	-1.73	-1.31	-.56	-.18	-.09
.9	-.515	-1.01	-2.3	-3.3	-4.32	-5.35	-6.3	-7.1	-7.7	-8.25	-8.55	-8.75	-8.42	-7.1	-3.55	-1.27	-.64

Dimensionless temperature (θ); $t/t_{ss} = .4$; $Ra_L = 1.5 \times 10^5$

x/L y/H	.025	.05	.1	.15	.2	.25	.3	.35	.4	.45	.5	.6	.7	.8	.9	.95	.095
0	.205	.282	.408	.47	.49	.494	.5	.503	.51	.521	.542	.609	.68	.741	.83	.885	.92
.1	.153	.221	.338	.417	.46	.481	.491	.495	.5	.5	.504	.512	.535	.595	.725	.825	.881
.2	.130	.187	.295	.373	.43	.46	.431	.489	.496	.5	.5	.503	.525	.585	.72	.82	.877
.3	.121	.178	.282	.355	.416	.456	.478	.486	.496	.5	.5	.503	.525	.581	.72	.82	.877
.4	.121	.178	.277	.355	.416	.45	.472	.486	.496	.5	.5	.503	.525	.581	.72	.82	.877
.5	.121	.178	.277	.355	.416	.45	.472	.486	.496	.5	.5	.503	.521	.581	.72	.82	.877
.6	.121	.178	.277	.351	.416	.45	.472	.486	.496	.5	.5	.503	.521	.581	.72	.82	.877
.7	.121	.178	.277	.351	.412	.45	.472	.486	.496	.495	.5	.503	.521	.581	.717	.82	.877
.8	.121	.178	.277	.351	.412	.45	.472	.486	.496	.495	.5	.503	.517	.568	.704	.81	.871
.9	.117	.174	.269	.343	.402	.44	.46	.477	.486	.49	.496	.5	.508	.538	.66	.778	.846
1.0	.078	.118	.169	.217	.256	.287	.318	.351	.39	.426	.456	.49	.5	.508	.59	.716	.788

Dimensionless vertical velocity ($\frac{vL}{\nu}$); $t/t_{ss} = .4$; $Ra_L = 1.5 \times 10^5$

x/L																	
y/H \	.025	.05	.1	.15	.2	.25	.3	.35	.4	.45	.5	.6	.7	.8	.9	.95	.975
.1	84	96.5	95	65.2	39.6	25.1	19.3	17.9	18.7	19.7	20	14	-10	- 66	-129.5	-111.5	-86
.2	93.5	116	130	97.5	62	35.3	19.3	11	7.46	6.1	5.25	1.34	-17	-69.8	-136.5	-119.5	-94
.3	95.5	120	136	107	70	39.9	20.6	10.1	4.88	2.54	1.29	- 2.8	-20.2	-72	-138	-121.5	-95.5
.4	96	121	138	109.5	72	41.3	21.2	10	4.38	1.71	0.29	- 3.9	-21.2	-72.6	-139	-122	-96
.5	96	122	138.5	110.5	72.5	41.6	21.3	9.95	4.2	1.47	- 0.103	- 4.2	-21.5	-72.6	-139	-122	-96
.6	95.5	121.5	138.5	110	72.5	41.5	21	9.7	3.88	1.15	- 0.3	- 4.35	-21.2	-72	-138.5	-121.5	-96
.7	95	121	138	109	71.8	40.6	20.2	8.6	2.76	0.05	- 1.31	- 4.95	-20.7	-70	-136.5	-121	-95.5
.8	94	119	136	107	69.7	38.1	17	4.85	-1.36	- 4.2	- 5.36	- 7.55	-19.3	-62	-128	-116	-94.5
.9	96	111	129	103	66	33.7	10.3	- 5	-14	-18.5	-20.1	-18.6	-19.3	-39.7	- 95	- 96.5	-84

Dimensionless horizontal velocity ($\frac{uL}{\nu}$); $t/t_{ss} = .4$; $Ra_L = 1.5 \times 10^5$

x/L y/H	.025	.05	.1	.15	.2	.25	.3	.35	.4	.45	.5	.6	.7	.8	.9	.95	.975
.1	1.34	2.68	8.6	14.75	19.1	21.3	21.8	21.3	20	18.2	16.1	11.7	98.5	10.2	7.3	3.37	1.68
.2	0.185	0.37	1.82	3.75	5.45	6.53	6.1	6.8	6.3	5.65	4.9	3.3	1.99	1.2	0.62	0.28	0.13
.3	0.04	0.08	0.43	0.95	1.45	1.79	1.97	2	1.91	1.76	1.57	1.13	0.72	0.41	0.2	0.08	0.04
.4	0.01	0.02	0.1	0.24	0.36	0.45	0.50	0.51	0.49	0.46	0.42	0.31	0.2	0.11	0.06	0.026	0.013
.5	-0.0009	-0.002	0.009	0.03	0.05	0.06	0.07	0.06	0.04	0.02	0.0002	- 0.04	- 0.07	- 0.05	-0.009	0.002	0.01
.6	-0.013	-0.026	-0.06	- 0.09	- 0.12	- 0.15	- 0.19	- 0.24	- 0.29	- 0.35	- 0.41	- 0.48	- 0.5	- 0.35	-0.1	-0.02	-0.01
.7	-0.041	-0.081	-0.19	- 0.3	- 0.41	- 0.5	- 0.7	- 0.89	- 1.13	- 1.35	- 1.57	- 1.9	- 1.97	- 1.45	-0.42	-0.08	-0.04
.8	-0.13	-0.26	-0.6	- 0.88	- 1.2	- 1.54	- 1.99	- 2.6	- 3.3	- 4.07	- 4.9	- 6.34	- 6.9	- 5.45	-1.82	-0.36	-0.18
.9	-1.68	-3.37	-7.3	- 9.65	-10.3	-10	- 9.9	-10.4	-11.75	-13.8	-16.1	-20	-21.8	-19	-8.65	-2.7	-1.34

Dimensionless temperature (θ); $t/t_{ss} = .7$; $Ra_L = 1.5 \times 10^5$

x/L																	
$y/H \backslash$.025	.05	.1	.15	.2	.25	.3	.35	.4	.45	.5	.6	.7	.8	.9	.95	.975
0	.382	.525	.726	.791	.795	.788	.785	.782	.782	.782	.785	.798	.823	.858	.91	.945	.97
.1	.387	.517	.68	.705	.517	.677	.66	.642	.625	.615	.612	.637	.677	.75	.858	.917	.945
.2	.242	.348	.52	.61	.643	.648	.642	.633	.621	.604	.59	.569	.578	.63	.761	.855	.905
.3	.187	.274	.42	.518	.573	.598	.6	.593	.58	.562	.551	.541	.549	.597	.703	.833	.89
.4	.163	.246	.379	.461	.515	.535	.538	.534	.528	.524	.524	.524	.534	.58	.707	.817	.88
.5	.139	.208	.323	.41	.461	.482	.493	.497	.497	.497	.5	.5	.507	.541	.677	.795	.861
.6	.125	.184	.288	.372	.428	.455	.469	.476	.479	.489	.489	.472	.465	.486	.629	.763	.84
.7	.111	.167	.264	.347	.402	.434	.448	.455	.458	.455	.448	.42	.4	.427	.58	.729	.812
.8	.097	.146	.236	.316	.372	.406	.423	.43	.431	.424	.41	.379	.369	.369	.48	.65	.757
.9	.055	.083	.142	.202	.25	.292	.323	.347	.365	.379	.389	.376	.34	.306	.319	.545	.962
1.0	.038	.056	.091	.118	.142	.16	.177	.191	.201	.208	.215	.219	.215	.205	.274	.476	.97

Dimensionless vertical velocity ($\frac{VL}{\nu}$); $t/t_{ss} = .7$; $Ra_L = 1.5 \times 10^5$

x/L																	
$y/H \backslash$.025	.05	.1	.15	.2	.25	.3	.35	.4	.45	.5	.6	.7	.8	.9	.95	.975
.1	217	250	271	250	221	187	147	105	59.5	12.5	35	-130	-215	-249	-165	-79	-31
.2	171	234	302	294	259	213	164	116	76.5	43	13	-62.2	-160	-275	-325	-231	-153
.3	141	195	257	248	214	175	143	118	98	79	51	-33.3	-143	-258	-318	-238	-166
.4	146	197	252	240	205	173	147	124	97.5	68	32.6	-50	-142	-241	-296	-225	-160
.5	153	211	273	260	223	183	146	120	74	37	- .08	-74	-146	-223	-274	-212	-154
.6	160	225	295	284	241	191	141	95	50	7.05	-32.8	-98.6	-147	-205	-253	-198.5	-146
.7	166	237	316	306	258	200	143	86.5	33	-13.9	-51.4	-98	-143	-214	-257	-196	-142
.8	153	230	325	313	275	216	159	109	62	20.6	-13.1	-76.5	-165	-258	-303	-234	-171
.9	31	78	165	225	247	241	214	175	130	82	34.4	-59.5	-148	-222	-271	-249	-219

Dimensionless horizontal velocity ($\frac{U}{v}$); $t/t_{ss} = .7$; $Ra_L = 1.5 \times 10^5$

x/L y/H	.025	.05	.1	.15	.2	.25	.3	.35	.4	.45	.5	.6	.7	.8	.9	.95	.975
.1	6.6	13.2	37	57.8	73.8	86.5	96	104	109	114	119	126	118	85	33.7	10	5.15
.2	-3.3	-6.6	-12.3	-15.7	-15.1	-20.3	-22.4	-23.6	-23.8	-23.	-21.4	-15	-3.2	8.45	11	6	3
.3	-0.22	-0.45	-2.3	-5.3	-8.9	-12.2	-13.9	-13.7	-12.2	-10.5	-9.5	-10.9	-11.5	-6.9	-1.35	-0.07	-0.03
.4	0.36	0.72	2.03	3.23	4.25	5.18	5.8	5.7	4.5	2.2	.86	-6.8	-9.7	-7.9	-2.6	-0.62	-0.3
.5	0.4	0.75	2.85	5.6	8.15	9.7	9.86	8.7	6.4	3.4	-0.02	-6.4	-9.85	-8.2	-2.85	-0.73	-0.41
.6	0.33	0.65	2.62	5.3	7.85	9.45	9.75	8.8	6.8	4.05	-0.84	-4.5	-5.8	-4.25	-2.1	-0.72	-0.36
.7	0.03	0.06	1.37	3.9	7	9.8	11.5	11.7	10.9	9.85	9.5	12.1	14	8.9	2.31	0.45	0.21
.8	-3	-6	-11.1	-11.6	-8.45	-3.17	3.15	9.6	15	18.9	21.3	23.8	22.2	18.1	12.3	6.6	3.3
.9	-5.15	-10.2	-33.7	-61	-85	-104	-117	-124	-126	-123	-118	-108	-96	-73.5	-37	-13.2	-6.6

Dimensionless temperature (θ); $t/t_{ss} = 1.0$; $Ra_L = 1.5 \times 10^5$

x/L y/H	.025	.05	.1	.15	.2	.25	.3	.35	.4	.45	.5	.6	.7	.8	.9	.95	.975
0	.342	.485	.704	.804	.83	.828	.82	.82	.83	.832	.832	.815	.836	.872	.923	.955	.97
.1	.37	.503	.69	.735	.715	.688	.663	.642	.63	.621	.685	.62	.65	.71	.826	.895	.93
.2	.267	.381	.557	.64	.654	.64	.623	.607	.6	.597	.598	.592	.586	.607	.732	.832	.89
.3	.21	.306	.464	.562	.61	.628	.631	.629	.628	.618	.604	.573	.556	5.8	.712	.82	.879
.4	.187	.27	.419	.521	.58	.605	.61	.6	.59	.57	.55	.515	.505	.538	.68	.8	.865
.5	.157	.236	.367	.464	.52	.545	.548	.542	.53	.514	.5	.471	.452	.481	.634	.768	.843
.6	.147	.201	.32	.407	.462	.486	.493	.49	.48	.465	.448	.403	.389	.42	.58	.73	.817
.7	.121	.18	.288	.372	.424	.444	.448	.441	.431	.417	.4	.376	.369	.385	.538	.697	.778
.8	.111	.167	.267	.347	.392	.41	.413	.41	.407	.402	.402	.4	.378	.347	.444	.621	.733
.9	.066	.104	.174	.236	.292	.33	.354	.372	.379	.382	.382	.368	.333	.281	.309	.496	.684
1.0	.031	.045	.077	.104	.129	.146	.163	.177	.184	.19	.191	.191	.184	.17	.299	.518	.66

Dimensionless vertical velocity ($\frac{VL}{\nu}$); $t/t_{ss} = 1.0$; $Ra_L = 1.5 \times 10^5$

x/L y/H	.025	.05	.1	.15	.2	.25	.3	.35	.4	.45	.5	.6	.7	.8	.9	.95	.975
.1	152	167.5	176	166.5	160	146	125.5	98	66.2	31.2	- 4.97	-77	-146.5	-194.5	-157.5	- 85	- 45.5
.2	154	199	243	232	210	185	153	113.5	68.2	18.6	-27	-87.7	-122.5	-193	-254	-190.5	-132
.3	136.5	182	229	216	186	152.5	117.5	81.2	44.8	11.9	-14.4	-52.2	- 95	-173.5	-243	-189	-136
.4	144	191.5	238	216	173	128	88.2	56.6	33.5	17.2	3.35	-31.9	- 87.5	-174.5	-244	-191.5	-139
.5	143.	195	268	222	179	125	86	57	35	16.9	- .05	-34.9	- 85	-179	-267	-195	-143.
.6	139.	191.5	245	222.5	174	126	87.5	56.6	33	12.2	- 3.43	-33.5	- 88	-173.5	-238	-191.5	-143
.7	136	189	242	222	174.5	128.5	95	71	52	34.6	14.4	-44.8	-117.5	-185.5	-230	-182	-136
.8	132	190.5	253	237	192	152	122.5	104	87.6	63.5	27	-67.3	-152.5	-210	-243	-198	-153.5
.9	45.5	88.5	158	192	195	175	146	112.5	77	41.2	5	-66	-125.5	-159.5	-176	-168	-152.5

Dimensionless horizontal velocity ($\frac{UL}{\nu}$); $t/t_{ss} = 1.0$; $Ra_L = 1.5 \times 10^5$

x/L y/H	.025	.05	.1	.15	.2	.25	.3	.35	.4	.45	.5	.6	.7	.8	.9	.95	.975
.1	4.77	9.56	27.3	44.6	58.5	72.5	83	91	96.5	99.1	99.4	95	85.6	65.2	27.9	8.98	4.5
.2	-1.63	-3.26	- 4.22	- 3.94	- 4.6	- 6.3	- 8.32	-10.1	-11.55	-12.4	-12.1	- 7.92	- 1.0	4.6	6.52	3.81	1.9
.3	.083	.165	.31	.051	- 1.30	- 4.0	- 7.7	-11.85	-15.50	-17.4	-17.4	-13.6	- 8.75	- 4.32	- 1.55	- .51	- .26
.4	.175	.34	1.37	2.3	2.36	1.37	- .26	- 1.75	- 2.51	- 2.65	- 2.67	- 3.88	- 4.6	- 2.72	- .3	.155	.072
.5	- .22	- .43	- .145	- .82	1.77	2.37	2.68	2.58	2.12	1.24	- .01	- 2.14	- 2.68	- 1.75	- .145	.41	.21
.6	- .072	- .155	.31	1.34	2.74	3.92	4.6	4.55	3.87	3.07	2.65	2.6	.27	- 2.35	- 1.37	- .34	- .175
.7	.26	.515	1.5	2.76	4.36	6.4	8.75	11.2	13.6	15.85	17.4	15.45	7.7	1.34	- .31	- .21	- .08
.8	-1.9	-3.8	- 6.5	- 6.5	- 4.74	- 1.95	1.03	4.43	7.92	10.8	11.5	11.6	8.35	5.15	4.2	3.3	1.65
.9	-4.5	-9	-28	-48.3	-65.2	-77.5	-85.6	-91	-95	-98	-99.5	-96.5	-83	-59.5	-27.4	-9.6	-4.8

APPENDIX C

Computer Program Listing

8IBFTC MAIN DECK

COMMON/MOOSE/D(53,53),R(53,53),PHI(26,26),U(53,53)

1 ,V(53,53),T(53,53),UV(27,27),U2(26,26)

2 ,V2(26,26),UVP(26,26),NOPRT(20),TITLE(12)

3 ,UT(26,26),VT(26,26)

COMMON Z ,DELX ,DELY ,DELX2 ,DELY2 ,DELXY

1 ,GX ,GY ,NX ,NY ,H ,XL

2 ,GCON ,NOIT ,DELT ,TIME ,TIMAX ,XNU

3 ,ALPHA ,UTEST ,VTEST ,TTEST ,PHITST ,INMODE

4 ,ISTOP ,ITOUT ,DTEST ,TREF ,NPI

5 ,PHICON ,ITM ,ITNO

6 ,LP , INC ,NPX ,NPY

C

C

C D E F I N I T I O N O F C O M M O N T E R M S

C D - DIVERGENCE

C R - RESIDUAL IN PRESSURE COMPUTATION

C PHI - PRESSURE

C U - VELOCITY (X COMPONENT)

C V - VELOCITY (Y COMPONENT)

C T - ABOLUTE TEMPERATURE

C UV - U*V FACTOR

C U2 - U**2 FACTOR

C V2 - V**2 FACTOR

C UVP - U*V FACTOR FOR PRESSURE TEST

C NOPRT - ITERATION NUMBER FOR PRINTING

C Z - 2*(1/DELX2 + 1/DELY2)

C DELX - X SPACE INCREMENT

C DELY - Y SPACE INCREMENT

C DELX2 - DELX**2

C DELY2 - DELY**2

C DELXY - DELX*DELY

C GX - GRAVITATIONAL COMPONENT IN X DIRECTION

C GY - GRAVITATIONAL COMPONENT IN Y DIRECTION

C NX - NUMBER OF HALF GRIDS IN X DIRECTION

C NY - NUMBER OF HALF GRIDS IN Y DIRECTION

C H - TOTAL HEIGHT OF COMPUTATION REGION (CM)

C XL - TOTAL LENGTH OF COMPUTATION REGION (CM)

C GCON - CONSTANT USED IN PRESSURE TEST

C NOIT - NUMBER OF ITERATIONS TAKEN IN PRESSURE COMPUTATIONS (MAX)

```

C      DELT      - TIME INCREMENT
C      TIME      - CURRENT TIME (SIMULATION)
C      TIMAX     - UPPER BOUND ON SIMULATION TIME
C      XNU       - GREEK NU, COMPUTATION CONSTANT
C      ALPHA     - COMPUTATION CONSTANT
C      UTEST     - USED IN CONVERGENCE TEST ON U
C      VTEST     - USED IN CONVERGENCE TEST ON V
C      TTEST     - USED IN CONVERGENCE TEST ON T
C      PHITST    - USIN IN CONVERGENCE TEST ON PHI
C      INMODE    - MODE OF INITIALIZING RUN
C      ITNO      - ITERATION NUMBER
C      ISTOP     - TERMINATION FLAG (SET IF NOIT EXCEEDED)
C      ITOUT     - CHECK-POINT TAPE EVERY ITOUT-TH ITERATION
C      TITLE     - TITLE TO APPEAR ON PRINT-OUT
C      DTEST     - VALUE USED AS ACCEPTABLE DIVERGENCE TERM
C      TREF      - REFERENCE TEMPERATURE
C      NPI       - NUMBER OF PRESSURE ITERATIONS
C      UT        - U*T FACTOR
C      VT        - V*T FACTOR
C      PHICON    - INITIALIZATION VALUE OF PRESSURE TO DENSITY RATIO
C      LP        - LOWEST NODE VALUE FOR PRINTING
C      INC       - EVERY ** INC ** NODES PRINT
C      NPX       - NUMBER OF LAST NODE IN X DIRECTION
C      NPY       - NUMBER OF LAST NODE IN Y DIRECTION
C      ITM       - MAXIMUM NO. OF ITERATIONS IN RUN
C
C      * * * * *
C      ITNO=0
C      SATISFY INITIAL DATA REQUIREMENTS
C      CALL INPUT
C      NX2=NX/2
C      NY2=NY/2
C      COMPUTES SYSTEM CONSTANTS
C
C      CALL SETUP
C
C      INITIALIZES BOUNDARY
C      CALL BOUND(1)
C      INTERPOLATES FOR MISSING DATA
C      CALL POLATE

```

```

50 ITNO = ITNO + 1
   TIME = TIME + DELT
C
C   UPDATE SIMULATION TIME AND ITERATION NUMBER
C
C   CALL COMPUT
C
C   COMPUTES BASIC U,V,T AND PHI FOR CURREN SIMULATION TIME
C
C   IF(ITNO .GE. ITM) GO TO 25
C   IF(ISTOP .EQ. 1) GO TO 25
C   IF(TIME .GE. TIMAX) GO TO 25
C
C   MAXIMUM SIMULATION TIME EXCEEDED OR NOIT EXCEEDED
C   OR CONVERGENCE SATISFIED
C
C   IF( MOD(ITNO,ITOUT) .NE. 0 ) GO TO 33
C   WRITE(8,60) ((U(I,J),V(I,J),T(I,J),D(I,J), I=1,NX),J=1,NY),
C   1 ((PHI(I,J),UV(I,J),U2(I,J),V2(I,J),UT(I,J),VT(I,J),
C   2 I=1,NX2), J=1,NY2)
60 FORMAT(1P10E13.6)
C   WRITE CHECK POINT TAPE
C   ENDFILE 8
C   REWIND 8
33 DO 100 I = 1,20
100 IF(ITNO .EQ. NOPRT(I)) CALL OUTPUT
C
C   TEST TO SEE IF IT IS TIME TO PRINT
C
C   CALL SSWTCH(6,NIC)
C   IF(NIC.EQ.1) GO TO 25
C   GO TO 50
25 CALL OUTPUT
C   WRITE(8,60) ((U(I,J),V(I,J),T(I,J),D(I,J), I=1,NX),J=1,NY),
C   1 ((PHI(I,J),UV(I,J),U2(I,J),V2(I,J),UT(I,J),VT(I,J),
C   2 I=1,NX2), J=1,NY2)
C   WRITE RESTART TAPE
C   ENDFILE 8
C   REWIND 8
C   STOP

```

```

      END
$ISFTC IN      DECK
      SUBROUTINE INPUT
      COMMON/MOOSE/D(53,53),R(53,53),PHI(26,26),U(53,53)
1         ,V(53,53),T(53,53),UV(27,27),U2(26,26)
2         ,V2(26,26),UVP(26,26),NOPRT(20),TITLE(12)
3         ,UT(26,26),VT(26,26)
      COMMON      Z      ,DELX      ,DELY      ,DELX2      ,DELY2      ,DELXY
1         ,GX      ,GY      ,NX      ,NY      ,H      ,XL
2         ,GCON      ,NOIT      ,DELT      ,TIME      ,TIMAX      ,XNU
3         ,ALPHA      ,UTEST      ,VTEST      ,TTEST      ,PHITST      ,INMODE
4         ,ISTOP      ,ITOUT      ,DTEST      ,TREF      ,NPI
5         ,PHICON      ,ITM      ,ITNO
6         ,LP      , INC      ,NPX      ,NPY

```

```

C * * * * *

```

```

C
C      D E F I N I T I O N      O F      C O M M O N      T E R M S
C      D      - DIVERGENCE
C      R      - RESIDUAL IN PRESSURE COMPUTATION
C      PHI - PRESSURE
C      U      - VELOCITY (X COMPONENT)
C      V      - VELOCITY (Y COMPONENT)
C      T      - ABOLUTE TEMPERATURE
C      UV      - U*V FACTOR
C      U2      - U**2 FACTOR
C      V2      - V**2 FACTOR
C      UVP - U*V FACTOR FOR PRESSURE TEST
C      NOPRT - ITERATION NUMBER FOR PRINTING
C      Z      - 2*(1/DELX2 + 1/DELY2)
C      DELX      - X SPACE INCREMENT
C      DELY      - Y SPACE INCREMENT
C      DELX2      - DELX**2
C      DELY2      - DELY**2
C      DELXY      - DELX*DELY
C      GX      - GRAVITATIONAL COMPONENT IN X DIRECTION
C      GY      - GRAVITATIONAL COMPONENT IN Y DIRECTION
C      NX      - NUMBER OF HALF GRIDS IN X DIRECTION
C      NY      - NUMBER OF HALF GRIDS IN Y DIRECTION
C      H      - TOTAL HEIGHT OF COMPUTATION REGION (CM)
C      XL      - TOTAL LENGTH OF COMPUTATION REGION (CM)

```

```

C      GCON  -  CONSTANT USED IN PRESSURE TEST
C      NOIT  -  NUMBER OF ITERATIONS TAKEN IN PRESSURE COMPUTATIONS (MAX)
C      DELT  -  TIME INCREMENT
C      DELT  -  TIME INCREMENT
C      TIME  -  CURRENT TIME (SIMULATION)
C      XNU   -  GREEK NU, COMPUTATION CONSTANT
C      ALPHA -  COMPUTATION CONSTANT
C      UTEST -  USED IN CONVERGENCE TEST ON U
C      INMODE - MODE OF INITIALIZING RUN
C      ITNO  -  ITERATION NUMBER
C      ISTOP -  TERMINATION FLAG (SET IF NOIT EXCEEDED)
C      ITOUT -  CHECK-POINT TAPE EVERY ITOUT-TH ITERATION
C      TITLE -  TITLE TO APPEAR ON PRINT-OUT
C      DTEST -  VALUE USED AS ACCEPTABLE DIVERGENCE TERM
C      TREF  -  REFERENCE TEMPERATURE
C      NPI   -  NUMBER OF PRESSURE ITERATIONS
C      UT    -  U*T FACTOR
C      VT    -  V*T FACTOR
C      PHICON -  INITIALIZATION VALUE OF PRESSURE TO DENSITY RATIO
C      LP    -  LOWEST NODE VALUE FOR PRINTING
C      INC   -  EVERY ** INC ** NODES PRINT
C      NPX   -  NUMBER OF LAST NODE IN X DIRECTION
C      NPY   -  NUMBER OF LAST NODE IN Y DIRECTION
C      ITM   -  MAXIMUM NO. OF ITERATIONS IN RUN
C
C * * * * *

```

```

      READ (5,20) TITLE
20  FORMAT(12A6)
      WRITE (6,30) TITLE
80  FORMAT(1H1,20X,12A6//)
      READ (5,10) NOPRT
10  FORMAT(12I6)
      WRITE (6,90) NOPRT
90  FORMAT(21X, 16HPRINT ITERATIONS /11X,20I6 // )
      READ (5,10) NX ,NY ,NOIT ,INMODE,ITOUT,ITM,LP,NPX,NPY,INC
      WRITE (6,110) NX ,NY ,NOIT ,INMODE ,ITOUT ,ITM
110  FORMAT(28X, 2HNX, 3X, 2HNY, 7X, 4HNOIT, 5X, 6HINMODE, 4X, 5HITOUT,
1      6X, 3HITM / 19X,6I10 // )
      READ (5,75) DELX ,DELY ,GX ,GY ,DELT
1      ,TIME ,TIMAX ,XNU ,ALPHA ,UTEST

```



```

2          ,VTEST ,TTEST ,PHITST ,DTEST ,TREF
3          ,PHICON
75 FORMAT(5E14.7)
WRITE (6,120) DELX ,DELY ,GX ,GY ,DELT
1          ,TIME ,TIMAX ,XNU ,ALPHA ,UTEST
2          , VTEST ,TTEST ,PHITST ,DTEST ,TREF
3          ,PHICON
120 FORMAT(21X,4HDELX,16X,4HDELY,18X,2HGX,18X,2HGY,16X,4HDELT/3X,5E20.
18 // 21X,4HTIME,15X,5HTIMAX,17X,3HXNU,15X,5HALPHA,15X,5HUTEST/3X,
25E20.8 //20X,5HVTEST,15X,5HTTEST,14X,6HPHITST,15X,5HDTEST,16X,
34HTREF/3X,5E20.8// 19X,6HPHICON
4 / 3X,5E20.8 // )
DO 15 I = 1,NX
DO 15 J = 1,NY
D(I,J) = 0.
R(I,J) = 0.
U(I,J) = 0.
V(I,J) = 0.
T(I,J) = 0.
15 CONTINUE
C INMODE = 0 IMPLIES INPUT NODAL VALUE SATISFING DIVERGENCE
C * * * OF PAPER GIVING CLOSED FORM SOLUTION OF A SIMILAR PROBLEM
C
IF(INMODE) 200, 300, 400
400 IF(INMODE .NE. 2) GO TO 450
600 READ (5,70) I1,J1,T1,I2,J2,T2,I3,J3,T3
70 FORMAT(3(2I4,E16.7))
IF(I1 .EQ. 0) GO TO 65
T(I1,J1) = T1
T(I2,J2) = T2
T(I3,J3) = T3
GO TO 600
450 CALL INVEL
GO TO 65
300 READ (5,50) I ,J ,UTEMP ,VTEMP ,TTEMP
50 FORMAT(2I2,3E14.8)
IF(I .EQ. 99) GO TO 65
J = 2*J+ 2
I = 2*I+ 2
IP=I+1

```

```

      JM=J-1
      U(IP,J) = UTEMP
      V(I,JM) = VTEMP
      T(I,J) = TTEMP
      GO TO 300
200  CONTINUE
      NX2=NX/2
      NY2=NY/2
      READ (8,60) ((U(I,J),V(I,J),T(I,J),D(I,J), I=1,NX),J=1,NY),
1    ((PHI(I,J),UV(I,J),U2(I,J),V2(I,J),UT(I,J),VT(I,J),
2    I=1,NX2), J=1,NY2)
60  FORMAT(1P10E13.6)
      REWIND 8
65  IF(NOPRT(1) .EQ. 0) CALL OUTPUT
      RETURN
      END
$IBFTC OUT      DECK
      SUBROUTINE OUTPUT
      COMMON/MOOSE/D(53,53),R(53,53),PHI(26,26),U(53,53)
1      ,V(53,53),T(53,53),UV(27,27),U2(26,26)
2      ,V2(26,26),UVP(26,26),NOPRT(20),TITLE(12)
3      ,UT(26,26),VT(26,26)
      COMMON
1      Z      ,DELX      ,DELY      ,DELX2      ,DELY2      ,DELXY
2      ,GX      ,GY      ,NX      ,NY      ,H      ,XL
3      ,GCON      ,NOIT      ,DELT      ,TIME      ,TIMAX      ,XNU
4      ,ALPHA      ,UTEST      ,VTEST      ,TTEST      ,PHITST      ,INMODE
5      ,ISTOP      ,ITOUT      ,DTEST      ,TREF      ,NPI
6      ,PHICON      ,ITM      ,ITNO
      ,LP      , INC      ,NPX      ,NPY
C * * * * *
C
C  D E F I N I T I O N      O F      C O M M O N      T E R M S
C  D      - DIVERGENCE
C  R      - RESIDUAL IN PRESSURE COMPUTATION
C  PHI - PRESSURE
C  U      - VELOCITY (X COMPONENT)
C  V      - VELOCITY (Y COMPONENT)
C  T      - ABSOLUTE TEMPERATURE
C  UV      - U*V FACTOR
C  U2      - U**2 FACTOR

```

C V2 - V**2 FACTOR
 C UVP - U*V FACTOR FOR PRESSURE TEST
 C NOPRT - ITERATION NUMBER FOR PRINTING
 C Z - 2*(1/DELX2 + 1/DELY2)
 C DELX - X SPACE INCREMENT
 C DELY - Y SPACE INCREMENT
 C DELX2 - DELX**2
 C DELY2 - DELY**2
 C DELXY - DELX*DELY
 C GX - GRAVITATIONAL COMPONENT IN X DIRECTION
 C GY - GRAVITATIONAL COMPONENT IN Y DIRECTION
 C NX - NUMBER OF HALF GRIDS IN X DIRECTION
 C NY - NUMBER OF HALF GRIDS IN Y DIRECTION
 C H - TOTAL HEIGHT OF COMPUTATION REGION (CM)
 C XL - TOTAL LENGTH OF COMPUTATION REGION (CM)
 C GCON - CONSTANT USED IN PRESSURE TEST
 C NOIT - NUMBER OF ITERATIONS TAKEN IN PRESSURE COMPUTATIONS (MAX)
 C DELT - TIME INCREMENT
 C TIME - CURRENT TIME (SIMULATION)
 C TIMAX - UPPER BOUND ON SIMULATION TIME
 C XNU - GREEK NU, COMPUTATION CONSTANT
 C ALPHA - COMPUTATION CONSTANT
 C UTEST - USED IN CONVERGENCE TEST ON U
 C VTEST - USED IN CONVERGENCE TEST ON V
 C TTEST - USED IN CONVERGENCE TEST ON T
 C PHITST - USED IN CONVERGENCE TEST ON PHI
 C INMODE - MODE OF INITIALIZING RUN
 C ITNO - ITERATION NUMBER
 C ITNO - ITERATION NUMBER
 C ISTOP - TERMINATION FLAG (SET IF NOIT EXCEEDED)
 C ITOUT - CHECK-POINT TAPE EVERY ITOUT-TH ITERATION
 C TITLE - TITLE TO APPEAR ON PRINT-OUT
 C DTEST - VALUE USED AS ACCEPTABLE DIVERGENCE TERM
 C TREF - REFERENCE TEMPERATURE
 C NPI - NUMBER OF PRESSURE ITERATIONS
 C UT - U*T FACTOR
 C VT - V*T FACTOR
 C PHICON - INITIALIZATION VALUE OF PRESSURE TO DENSITY RATIO
 C LP - LOWEST NODE VALUE FOR PRINTING
 C INC - EVERY ** INC ** NODES PRINT

```

C      NPX      - NUMBER OF LAST NODE IN X DIRECTION
C      NPY      - NUMBER OF LAST NODE IN Y DIRECTION
C      ITN      - MAXIMUM NO. OF ITERATIONS IN RUN
C
C * * * * *
      INC2=2*INC
      LI=LP+1
      WRITE (6,5)
5  FORMAT(1H1,20X,1HU// )
      DO 100 I = LP,NPX,INC
      WRITE (6,15) (U(I,J), J = LP,NPY,INC )
15  FORMAT(8E16.8)
      100 CONTINUE
      WRITE (6,25)
      25  FORMAT(1H1,20X,1HV// )
      DO 200 I = LP,NPX,INC
      WRITE (6,15) (V(I,J) , J = LP,NPY,INC )
      200 CONTINUE
      WRITE (6,35)
      35  FORMAT(1H1,20X,1HT// )
      DO 300 I = LP,NPX,INC
      WRITE (6,15) (T(I,J), J = LP,NPY,INC)
      300 CONTINUE
      IF(KIP.NE.0 .AND.INMODE.NE.-1) GO TO 1000
      NPX2=NPX/2
      NPY2=NPY/2
      WRITE (6,45)
      45  FORMAT(1H1,20X,3HPHI //)
      DO 400 I = LP,NPX2,INC
      WRITE (6,95) (PHI(I,J), J = LP,NPY2,INC)
      400 CONTINUE
      WRITE(6,101)
101  FORMAT(1H0,20X,3HU2 //)
      DO 401 I=LP,NPX2,INC
      WRITE(6,15) (U2(I,J), J=LP,NPY2,INC)
      401 CONTINUE
      WRITE(6,102)
102  FORMAT(1H0,20X,3HV2 //)
      DO 402 I=LP,NPX2,INC
      WRITE(6,15) (V2(I,J), J=LP,NPY2,INC)

```

```

402  CONTINUE
    WRITE(6,103)
103  FORMAT(1H0,20X,3HUV //)
    DO 403 I=LP,NPX2,INC
        WRITE(6,15) (UV(I,J), J=LP,NPY2,INC)
403  CONTINUE
    WRITE(6,104)
104  FORMAT(1H0,20X,3HVT //)
    DO 404 I=LP,NPX2,INC
        WRITE(6,15) (VT(I,J), J=LP,NPY2,INC)
404  CONTINUE
    WRITE(6,105)
105  FORMAT(1H0,20X,3HUT //)
    DO 405 I=LP,NPX2,INC
        WRITE(6,15) (UT(I,J), J=LP,NPY2,INC)
405  CONTINUE
    WRITE (6,55)
    55  FORMAT(1H1,20X,1HD //)
    DO 500 I = L1,NPX,INC2
        WRITE (6,15) (D(I,J), J = L1,NPY,INC2)
    500 CONTINUE
    WRITE (6,65)
    65  FORMAT(1H1,20X,1HR //)
    DO 600 I = L1,NPX,INC2
        WRITE (6,95) (R(I,J), J = L1,NPY,INC2)
    95  FORMAT(8E16.8)
    600 CONTINUE
    1000 CONTINUE
    KIP=0
    RETURN
    END
*IEFTC SET      DECK
SUBROUTINE SETUP
COMMON/ROOSE/D(53,53),R(53,53),PHI(26,26),U(53,53)
1      ,V(53,53),T(53,53),UV(27,27),U2(26,26)
2      ,V2(26,26),UVP(26,26),NOPRT(20),TITLE(12)
3      ,UT(26,26),VT(26,26)
COMMON      Z      ,DELX      ,DELY      ,DELX2      ,DELY2      ,DELXY
1      ,GX      ,GY      ,NX      ,NY      ,H      ,XL
2      ,GCON      ,NOIT      ,DELT      ,TIME      ,TIMAX      ,XNU

```

3	,ALPHA	,UTEST	,VTEST	,TTEST	,PHITST	,INMODE
4	,ISTOP	,ITOUT	,DTEST	,TREF	,NPI	
5	,PHICON	,ITM	,ITNO			
6	,LP	,INC	,NPX	,NPY		

C * * * *

C

C D E F I N I T I O N O F C O M M O N T E R M S

C D - DIVERGENCE

C R - RESIDUAL IN PRESSURE COMPUTATION

C PHI - PRESSURE

C U - VELOCITY (X COMPONENT)

C V - VELOCITY (Y COMPONENT)

C T - ABSOLUTE TEMPERATURE

C UV - U*V FACTOR

C U2 - U**2 FACTOR

C V2 - V**2 FACTOR

C UVP - U*V FACTOR FOR PRESSURE TEST

C NOPRT - ITERATION NUMBER FOR PRINTING

C Z - $2*(1/DELX2 + 1/DELY2)$

C DELX - X SPACE INCREMENT

C DELY - Y SPACE INCREMENT

C DELX2 - DELX**2

C DELY2 - DELY**2

C DELXY - DELX*DELY

C GX - GRAVITATIONAL COMPONENT IN X DIRECTION

C NX - NUMBER OF INCREMENTS IN X DIRECTION

C GY - GRAVITATIONAL COMPONENT IN Y DIRECTION

C NY - NUMBER OF INCREMENTS IN Y DIRECTION

C H - TOTAL HEIGHT OF COMPUTATION REGION (CM)

C XL - TOTAL LENGTH OF COMPUTATION REGION (CM)

C GCON - CONSTANT USED IN PRESSURE TEST

C NCIT - NUMBER OF ITERATIONS TAKEN IN PRESSURE COMPUTATIONS (MAX)

C DELT - TIME INCREMENT

C TIME - CURRENT TIME (SIMULATION)

C TIMAX - UPPER BOUND ON SIMULATION TIME

C XNU - GREEK NU, COMPUTATION CONSTANT

C ALPHA - COMPUTATION CONSTANT

C UTEST - USED IN CONVERGENCE TEST ON U

C VTEST - USED IN CONVERGENCE TEST ON V

C TTEST - USED IN CONVERGENCE TEST ON T

999

```

C      PHITST - USIN IN CONVERGENCE TEST ON PHI
C      INMODE - MODE OF INITIALIZING RUN
C      ITNO   - ITERATION NUMBER
C      ISTOP  - TERMINATION FLAG (SET IF NOIT EXCEEDED)
C      ITOUT  - CHECK-POINT TAPE EVERY ITOUT-TH ITERATION
C      TITLE  - TITLE TO APPEAR ON PRINT-OUT
C      DTEST  - VALUE USED AS ACCEPTABLE DIVERGENCE TERM
C      TREF   - REFERENCE TEMPERATURE
C      NPI    - NUMBER OF PRESSURE ITERATIONS
C      UT     - U*T FACTOR
C      VT     - V*T FACTOR
C      PHICON - INITIALIZATION VALUE OF PRESSURE TO DENSITY RATIO
C      LP     - LOWEST NODE VALUE FOR PRINTING
C      INC    - EVERY ** INC ** NODES PRINT
C      NPX    - NUMBER OF LAST NODE IN X DIRECTION
C      NPY    - NUMBER OF LAST NODE IN Y DIRECTION
C      ITM    - MAXIMUM NO. OF ITERATIONS IN RUN
C
C      * * * * *
C      INITIALIZE PHI
C
C      INDEX (I,J) CORRESPONDS TO (I/2 - 1, J/2 - 1)
      DELX2 = DELX**2
      DELY2 = DELY**2
      DELXY=DELX*DELY
      Z = 2.*(1./DELX2 + 1./DELY2)
      XL=FLOAT(NX-5)*DELX/2.
      H = FLOAT(NY-5)*DELY/2.
      GCON = GY*H + GX*XL
      NI = NX - 2
      DO 300 I = NI,NX
      DO 300 J = 1,NY
500    T(I,J)=345.6
      DO 301 I=1,3
      DO 301 J=1,NY
301    T(I,J)=230.4
      IF (INMODE.LT.0) RETURN
      NX2=NX/2
      NY2=NY/2
      DO 100 I=1,NX2

```

```

      DO 100 J=1,NY2
      PHI(I,J) = PHICON
100  CONTINUE
      NI = NX - 3
      DO 200 I = 4,NI
      DO 200 J = 1,NY
      T(I,J) = TREF
200  CONTINUE
1000 RETURN
      END
$IBFTC INV      DECK
      SUBROUTINE INVEL
      RETURN
      END
$IBFTC COMP      DECK
      SUBROUTINE COMPUT
      COMMON/MOOSE/D(53,53),R(53,53),PHI(26,26),U(53,53)
1      ,V(53,53),T(53,53),UV(27,27),U2(26,26)
2      ,V2(26,26),UVP(26,26),NOPRT(20),TITLE(12)
3      ,UT(26,26),VT(26,26)
      COMMON
1      ,Z      ,DELX      ,DELY      ,DELX2      ,DELY2      ,DELXY
2      ,GX      ,GY      ,NX      ,NY      ,H      ,XL
3      ,GCON      ,NOIT      ,DELT      ,TIME      ,TIMAX      ,XNU
4      ,ALPHA      ,UTEST      ,VTEST      ,TTEST      ,PHITST      ,INMODE
5      ,ISTOP      ,ITOUT      ,DTEST      ,TREF      ,NPI
6      ,PHICON      ,ITM      ,ITNO
      ,LP      ,INC      ,NPX      ,NPY
      DIMENSION      UOLD(2,53),VOLD(2,53),TOLD(2,53)
      NAMELIST/LOOK/TOLD,DELT,DELX,DELY,ALPHA,DELX2,DELY2,UOLD,VOLD
C * * * * *
C
C      D E F I N I T I O N      O F      C O M M O N      T E R M S
C      D      - DIVERGENCE
C      R      - RESIDUAL IN PRESSURE COMPUTATION
C      PHI - PRESSURE
C      U      - VELOCITY (X COMPONENT)
C      V      - VELOCITY (Y COMPONENT)
C      T      - ABSOLUTE TEMPERATURE
C      UV      - U*V FACTOR
C      U2      - U**2 FACTOR

```


C V2 - V**2 FACTOR
 C UVP - U*V FACTOR FOR PRESSURE TEST
 C NOPRT - ITERATION NUMBER FOR PRINTING
 C Z - 2*(1/DELX2 + 1/DELY2)
 C DELX - X SPACE INCREMENT
 C DELY - Y SPACE INCREMENT
 C DELX2 - DELX**2
 C DELY2 - DELY**2
 C DELXY - DELX*DELY
 C GX - GRAVITATIONAL COMPONENT IN X DIRECTION
 C GY - GRAVITATIONAL COMPONENT IN Y DIRECTION
 C NX - NUMBER OF HALF GRIDS IN X DIRECTION
 C NY - NUMBER OF HALF GRIDS IN Y DIRECTION
 C H - TOTAL HEIGHT OF COMPUTATION REGION (CM)
 C XL - TOTAL LENGTH OF COMPUTATION REGION (CM)
 C GCON - CONSTANT USED IN PRESSURE TEST
 C NOIT - NUMBER OF ITERATIONS TAKEN IN PRESSURE COMPUTATIONS (MAX)
 C DELT - TIME INCREMENT
 C TIME - CURRENT TIME (SIMULATION)
 C TIMAX - UPPER BOUND ON SIMULATION TIME
 C XNU - GREEK NU, COMPUTATION CONSTANT
 C ALPHA - COMPUTATION CONSTANT
 C UTEST - USED IN CONVERGENCE TEST ON U
 C VTEST - USED IN CONVERGENCE TEST ON V
 C TTEST - USED IN CONVERGENCE TEST ON T
 C PHITST - USIN IN CONVERGENCE TEST ON PHI
 C INMODE - MODE OF INITIALIZING RUN
 C ITNO - ITERATION NUMBER
 C ISTOP - TERMINATION FLAG (SET IF NOIT EXCEEDED)
 C ITOUT - CHECK-POINT TAPE EVERY ITOUT-TH ITERATION
 C TITLE - TITLE TO APPEAR ON PRINT-OUT
 C DTEST - VALUE USED AS ACCEPTABLE DIVERGENCE TERM
 C TREF - REFERENCE TEMPERATURE
 C NPI - NUMBER OF PRESSURE ITERATIONS
 C UT - U*T FACTOR
 C VT - V*T FACTOR
 C PHICON - INITIALIZATION VALUE OF PRESSURE TO DENSITY RATIO
 C LP - LOWEST NODE VALUE FOR PRINTING
 C INC - EVERY ** INC ** NODES PRINT
 C NPX - NUMBER OF LAST NODE IN X DIRECTION

```

C      NPY      - NUMBER OF LAST NODE IN Y DIRECTION
C      ITM      - MAXIMUM NO. OF ITERATIONS IN RUN
C
C * * * * *
C * * * * *
C      INTEGRATE VELOCITY IN X DIRECTION
C                                     REFER TO VALUES COMPUTED THIS COMP TIME
C      ALL OTHER VALUES WERE COMPUTED LAST COMP CYCLE
C * * * * *
      MMM=0
      IF(KIP.NE.0) GO TO 1000
      ISTOP = 0
      NJ = NY - 3
      NI = NX - 4
      ISTPU = 1
      NI = NX - 4
      NJ = NY - 3
      DO 503 K=2,NJ,2
503    UOLD(1,K)=U(3,K)
      DO 500 I = 5,NI,2
      DO 501 K=2,NJ,2
      UOLD(2,K)=UOLD(1,K)
501    UOLD(1,K)=U(I,K)
      K=(I-1)/2
      K1=K+1
      DO 500 J = 4,NJ,2
      L=J/2
      L1=L+1
      UTEMP = U(I,J)
      GXA=GX*(T(I ,J)-TREF)/TREF
      U(I,J) = U(I,J) + DELT*( (U2(K,L ) - U2(K1,L ))/DELX + (UV(K1,L )
1        - UV(K1,L1 ))/DELY + GXA+ (PHI(K,L)  - PHI(K1,L ))/DELX
2        + XNU*( (U(I+2,J) +UOLD(2,J) - 2.*U(I,J) )/DELX2 +
3        (U(I,J+2) +UOLD(1,J-2)-2.*U(I,J) )/DELY2 ) )
      IF(ABS(U(I,J) - UTEMP).GT. UTEST) ISTPU = 0
500 CONTINUE
C * * * * *
C      INTEGRATE VELOCITY IN Y DIRECTION
C                                     COMPUTED THIS COMP CYCLE
C * * * * *

```

```

NJ = NY - 4
NI = NX - 3
ISTPV = 1
DO 504 K=3,NJ,2
504  VOLD(1,K)=V(2,K)
DO 600 I = 4,NI,2
DO 502 K=3,NJ,2
VOLD(2,K)=VOLD(1,K)
502  VOLD(1,K)=V(I,K)
K=I/2
K1=K+1
DO 600 J = 3,NJ,2
L=(J-1)/2
L1=L+1
VTEMP = V(I,J)
GYA=GY*(T(I,J)-TREF)/TREF
V(I,J) = V(I,J) + DELT*( (V2(K,L) - V2(K,L1))/DELY
1      + (UV(K,L1) - UV(K1,L1))/DELX
2      + GYA*(PHI(K,L) - PHI(K,L1))/DELY
3      +XNU*( (V(I,J+2) +VOLD(1,J-2)-2.*V(I,J))/DELY2
4      + (V(I+2,J) +VOLD(2,J) - 2.*V(I,J))/DELY2 ) )
IF(ABS(V(I,J) - VTEMP) .GT. VTEST) ISTPV = 0
600 CONTINUE
C      INTERPOLATE U,V,U2,V2, ETC.
C      ADD UT, VT TO COMMON
C      * * * * *
C      INTEGRATE TEMPERATURE
C
C      COMPUTED THIS COMP CYCLE
C      ALL OTHER TERMS WERE COMPUTED LAST COMP CYCLE
C      * * * * *
NI = NX - 3
NJ = NY - 3
ISTPT = 1
DO 505 K=2,NJ,2
505  TOLD(1,K)=T(2,K)
DO 700 I = 4,NI,2
DO 530 K=2,NJ,2
TOLD(2,K)=TOLD(1,K)
530  TOLD(1,K)=T(I,K)
K=I/2

```

```

      K1=K+1
      DO 700 J = 4,NJ,2
      L=J/2
      L1=L+1
      TTEMP = T(I,J)
      T(I,J) = T(I,J) + DELT*( (UT(K,L ) - UT(K1,L ))/DELX
1      + (VT(K,L ) -VT(K,L1 ))/DELY
2      + ALPHA*((T(I+2,J) +TOLD(2,J) - 2.*T(I,J))/DELX2
3      + (T(I,J+2) +TOLD(1,J-2)-T(I,J)*2.)/DELY2 ))
      IF(ABS(T(I,J) - TTEMP) .GT. TTEST) ISTPT = 0
700  CONTINUE
1001  CONTINUE
      CALL BOUND (1)
      CALL POLATE
      IF(ISTPU + ISTPV + ISTPT .GT. 2) ISTOP = 1
1000  CONTINUE
      KIP=0
      NI=NX-3
      NJ=NY-3
      DO 850 I = 4,NI,2
      DO 850 J = 4,NJ,2
      D(I,J) = ( U(I+1,J) - U(I-1,J) )/DELX
1      + ( V(I,J+1) - V(I,J-1) )/DELY
850  CONTINUE
      CALL BOUND (3)
C    GENERATE BOUNDARY FOR DIVERGENCE
      DENOM=0.
      NI = NX - 3
      NJ = NY - 3
      DO 100 J = 4,NJ,2
      JJ = J/2 - 1
      L=J/2
      L1=L+1
      DO 100 I = 4,NI,2
      II = I/2 - 1
      K=I/2
      K1=K+1
      R(I,J) = 1./DELX2*(U2(K1,L ) + U2(II,L ) - 2.*U2(K,L) )
1      + 1./DELY2*(V2(K,L1 ) + V2(K,JJ ) - 2.*V2(K,L) )
2      + 2./DELXY*(UV(K,L ) + UV(K1,L1 ) - UV(K1,L ) )

```

```

3          -UV(K,L1  ) )
4      - XNU*( 1./DELX2*(D(I+2,J) + D(I-2,J) - 2.*D(I,J) )
5          + 1./DELY2*(D(I,J+2) + D(I,J-2) - 2.*D(I,J) ) )
6          -GY/(DELY*TREF)*(T(I,J+1)-T(I,J-1))
7          -D(I,J)/DELT
      UVP(K-1,L-1)=U2(K,L) + V2(K,L) + GCON
      DENOM=DENOM+ABS(R(I,J))
100 CONTINUE
      NPI = 0
      NNI=NI/2
      NNJ=NJ/2
      NI2=NNI+1
      NJ2=NNJ+1
C      CALL BOUND (2)
      DO 900 K = 1,NOIT
      NPI=NPI+1
      PHIMAX = 0.
C      CALCULATE PHI ON BOTTOM NO SLIP BOUNDARY
      IF(NPI.NE.1.AND.ITNO.LE.MMM) GO TO 800
      DO 775 I=2,NNI
      GYA=GY*(T(2*I,2)-TREF)/TREF
775  PHI(I,1)=PHI(I,2)-GYA*DELY-2.*XNU/DELY*(V(2*I,5)-V(2*I,3))
800  CONTINUE
      DO 801 J=2,NNJ
      DO 801 I=1,NI2
      PHITMP = PHI(I,J)
      IF(I.EQ.1 ) GO TO 1
      IF(I.EQ.NI2 ) GO TO 2
      PHI(I,J) = ((PHI(I+1,J) + PHI(I-1,J))/DELX2
1          +{PHI(I,J+1) + PHI(I,J-1)}/DELY2 + R(2*I,2*J))/2
      PHIVAL = ABS(PHI(I,J) - PHITMP) /
1          (ABS(PHI(I,J)) + ABS(PHITMP) + UVP(I-1,J-1))
      IF( PHIVAL .GT. PHIMAX ) PHIMAX = PHIVAL
      GO TO 3
1      CONTINUE
      IF(ITNO.LE.MMM.AND.NPI.NE.1) GO TO 801
C      CALCULATE PHI IN LEFT HAND (IN) BOUNDARY
C      CALCULATE PHI ON LEFT NO SLIP BOUNDARY
      PHI(1,J)=PHI(2,J)-GX*DELX-2.*XNU/DELX*(U(5,2*J)-U(3,2*J))
      GO TO 3

```

```

2      CONTINUE
      IF(ITNO.LE.MMM.AND.NPI.NE.1) GO TO 801
C      CALCULATE PHI IN RIGHT HAND (NOSLIP) BOUNDARY
      PHI(NI2,J)= PHI(NI2-1,J)+ GX*DELX + 2.*XNJ/DELX*U(NI-1,2*J)
3      CONTINUE
      IF(MOD(NPI,5).EQ.0) PHI(I,J)=PHITMP+1.55*(PHI(I,J)-PHITMP)
801     CONTINUE
      IF(NPI.NE.1.AND.ITNO.LE.MMM) GO TO 802
C      CALCULATE PHI ON UP NO SLIP BOUNDARY
      DO 778 I=2,NPI
      GYA=GY*(T(2*I,NY-1)-TREF)/TREF
778     PHI(I,NJ2)=PHI(I,NJ2-1)+2.*XNU/DELY*(V(NJ-1,2*I)-V(NJ+1,2*I))
      1 +GYA*DELY
802     CONTINUE
      NJ2=NJ/2
      NI2=NI/2
      XUM=0.
      DO 133 I=2,NI2
      DO 133 J=2,NJ2
133     XUM=XUM+ABS((PHI(I+1,J)+PHI(I-1,J)-2.*PHI(I,J))/DELX2
      1 + (PHI(I,J+1)+PHI(I,J-1)-2.*PHI(I,J))/DELY2)
      RAT=ABS(XUM/DENOM-1.)
      RAT=0.
      IF(PHIMAX.LT.PHITST.AND.RAT.LT.PHITST) GO TO 250
900     CONTINUE
      ISTOP=1
250     WRITE (6,10) TIME,NPI,XUM,DENOM
      10 FORMAT(1H0,20X,6HTIME =, E15.7, 10X, 19HPHI ITERATION NO. = , I6/
      1 2E15.8)
      RETURN
      END
$IBFTC BND      DECK
      SUBROUTINE BOUND(K)
      COMMON/MOOSE/D(53,53),R(53,53),PHI(26,26),U(53,53)
      1 ,V(53,53),T(53,53),UV(27,27),U2(26,26)
      2 ,V2(26,26),UVP(26,26),NOPRT(20),TITLE(12)
      3 ,UT(26,26),VT(26,26)
      COMMON      Z      ,DELX      ,DELY      ,DELX2      ,DELY2      ,DELXY
      1      ,GX      ,GY      ,NX      ,NY      ,H      ,XL
      2      ,GCON      ,NOIT      ,DELT      ,TIME      ,TIMAX      ,XNU

```

100

3	,ALPHA	,UTEST	,VTEST	,TTEST	,PHITST	,INMODE
4	,ISTOP	,ITOUT	,DTEST	,TREF	,NPI	
5	,PHICON	,ITM	,ITNO			
6	,LP	,INC	,NPX	,NPY		

C * * * * *

C

C D E F I N I T I O N O F C O M M O N T E R M S

C D - DIVERGENCE

C R - RESIDUAL IN PRESSURE COMPUTATION

C PHI - PRESSURE

C U - VELOCITY (X COMPONENT)

C V - VELOCITY (Y COMPONENT)

C T - ABSOLUTE TEMPERATURE

C UV - U*V FACTOR

C U2 - U**2 FACTOR

C V2 - V**2 FACTOR

C UVP - U*V FACTOR FOR PRESSURE TEST

C NOPRT - ITERATION NUMBER FOR PRINTING

C Z - 2*(1/DELX2 + 1/DELY2)

C DELX - X SPACE INCREMENT

C DELY - Y SPACE INCREMENT

C DELX2 - DELX**2

C DELY2 - DELY**2

C DELXY - DELX*DELY

C GX - GRAVITATIONAL COMPONENT IN X DIRECTION

C GY - GRAVITATIONAL COMPONENT IN Y DIRECTION

C NX - NUMBER OF HALF GRIDS IN X DIRECTION

C NY - NUMBER OF HALF GRIDS IN Y DIRECTION

C H - TOTAL HEIGHT OF COMPUTATION REGION (CM)

C XL - TOTAL LENGTH OF COMPUTATION REGION (CM)

C GCON - CONSTANT USED IN PRESSURE TEST

C NOIT - NUMBER OF ITERATIONS TAKEN IN PRESSURE COMPUTATIONS (MAX)

C DELT - TIME INCREMENT

C TIME - CURRENT TIME (SIMULATION)

C TIMAX - UPPER BOUND ON SIMULATION TIME

C XNU - GREEK NU, COMPUTATION CDNSTANT

C ALPHA - COMPUTATION CONSTANT

C UTEST - USED IN CONVERGENCE TEST ON U

C VTEST - USED IN CONVERGENCE TEST ON V

C TTEST - USED IN CONVERGENCE TEST ON T

7/3

```

C   PHITST - USIN IN CONVERGENCE TEST ON PHI
C   INMODE -- MODE OF INITIALIZING RUN
C   ITNO    - ITERATION NUMBER
C   ISTOP   - TERMINATION FLAG (SET IF NOIT EXCEEDED)
C   ITOUT   - CHECK-POINT TAPE EVERY ITOUT-TH ITERATION
C   TITLE   - TITLE TO APPEAR ON PRINT-OUT
C   DTEST   - VALUE USED AS ACCEPTABLE DIVERGENCE TERM
C   TREF    - REFERENCE TEMPERATURE
C   NPI     - NUMBER OF PRESSURE ITERATIONS
C   UT      - U*T FACTOR
C   VT      - V*T FACTOR
C   PHICON  - INITIALIZATION VALUE OF PRESSURE TO DENSITY RATIO
C   LP      - LOWEST NODE VALUE FOR PRINTING
C   INC     - EVERY ** INC ** NODES PRINT
C   NPX     - NUMBER OF LAST NODE IN X DIRECTION
C   NPY     - NUMBER OF LAST NODE IN Y DIRECTION
C   ITM     - MAXIMUM NO. OF ITERATIONS IN RUN
C
C   GO TO (10,20,30),K
C   NO SLIP DIVERGENCE BOUNDARY
30  NI = NX - 3
    NJ = NY - 1
    DO 750 I = 4,NI,2
      D(I,2) = D(I,4)
      D(I,NJ) = D(I,NJ-2)
750  CONTINUE
    NJ = NY - 3
    NI = NX - 1
    DO 850 J=4,NJ,2
      D(2,J) = D(4,J)
      D(NI,J) = D(NI-2,J)
850  CONTINUE
    RETURN
20  RETURN
10  CONTINUE
C * * * * *
C   B O U N D A R Y   C O N D I T I O N S   ** NO SLIP AND LEFT IN **
C
C * * * * *
C   L E F T   A N D   R I G H T

```



```

      NJ = NY - 2
      NI = NX - 1
      DO 350 J = 3,NJ,2
      V(2,J) = - V(4,J)
      V(NI,J) = - V(NI-2,J)
      U(NI-1,J+1) = 0.
      U(3,J+1) = 0.
350    CONTINUE
C      UP AND DOWN
      NI=NX-2
      NJ=NY-1
      DO 360 I=3,NI,2
      U(I,2)=-U(I,4)
      U(I,NJ)=-U(I,NJ-2)
      V(I+1,3)=0.
360    V(I+1,NJ-2)=0.
      DO 361 I=3,NI
      T(I+1,NJ)=T(I+1,NJ-2)
      T(I+1,NJ-1)=T(I+1,NJ-2)
      T(I+1,2)=T(I+1,4)
361    T(I+1,3)=T(I+1,4)
      RETURN
      END
$IBFTC POL
      SUBROUTINE POLATE
      COMMON/MOOSE/D(53,53),R(53,53),PHI(26,26),U(53,53)
1          ,V(53,53),T(53,53),UV(27,27),U2(26,26)
2          ,V2(26,26),UVP(26,26),NOPRT(20),TITLE(12)
3          ,UT(26,26),VT(26,26)
      COMMON
1          Z      ,DELX      ,DELY      ,DELX2      ,DELY2      ,DELXY
2          ,GX      ,GY      ,NX      ,NY      ,H      ,XL
3          ,GCON      ,NOIT      ,DELT      ,TIME      ,TIMAX      ,XNU
4          ,ALPHA      ,UTEST      ,VTEST      ,TTEST      ,PHITST      ,INMODE
5          ,ISTOP      ,ITOUT      ,DTEST      ,TREF      ,NPI
6          ,PHICON      ,ITM      ,ITNO
          ,LP      , INC      ,NPX      ,NPY
C * * * * *
C
C      D E F I N I T I O N      O F      C O M M O N      T E R M S
C      D      - DIVERGENCE

```

C R - RESIDUAL IN PRESSURE COMPUTATION
 C PHI - PRESSURE
 C U - VELOCITY (X COMPONENT)
 C V - VELOCITY (Y COMPONENT)
 C T - ABOLUTE TEMPERATURE
 C UV - U*V FACTOR
 C U2 - U**2 FACTOR
 C V2 - V**2 FACTOR
 C UVP - U*V FACTOR FOR PRESSURE TEST
 C NOPRT - ITERATION NUMBER FOR PRINTING
 C Z - $2*(1/DELX^2 + 1/DELY^2)$
 C DELX - X SPACE INCREMENT
 C DELY - Y SPACE INCREMENT
 C DELX2 - DELX**2
 C DELY2 - DELY**2
 C DELXY - DELX*DELY
 C GX - GRAVITATIONAL COMPONENT IN X DIRECTION
 C GY - GRAVITATIONAL COMPONENT IN Y DIRECTION
 C NX - NUMBER OF INCREMENTS IN X DIRECTION
 C NY - NUMBER OF INCREMENTS IN Y DIRECTION
 C H - TOTAL HEIGHT OF COMPUTATION REGION (CM)
 C XL - TOTAL LENGTH OF COMPUTATION REGION (CM)
 C GCON - CONSTANT USED IN PRESSURE TEST
 C NOIT - NUMBER OF ITERATIONS TAKEN IN PRESSURE COMPUTATIONS (MAX)
 C DELT - TIME INCREMENT
 C TIME - CURRENT TIME (SIMULATION)
 C TIMAX - UPPER BOUND ON SIMULATION TIME
 C XNU - GREEK NU,COMPUTATION CONSTANT
 C ALPHA - COMPUTATION CONSTANT
 C UTEST - USED IN CONVERGENCE TEST ON U
 C VTEST - USED IN CONVERGENCE TEST ON V
 C TTEST - USED IN CONVERGENCE TEST ON T
 C PHITST - USIN IN CONVERGENCE TEST ON PHI
 C INCODE - MODE OF INITIALIZING RUN
 C ITNO - ITERATION NUMBER
 C ISTOP - TERMINATION FLAG (SET IF NOIT EXCEEDED)
 C ITOUT - CHECK-POINT TAPE EVERY ITOUT-TH ITERATION
 C TITLE - TITLE TO APPEAR ON PRINT-OUT
 C DTEST - VALUE USED AS ACCEPTABLE DIVERGENCE TERM
 C TREF - REFERENCE TEMPERATURE

```

C      NPI      - NUMBER OF PRESSURE ITERATIONS
C      UT       - U*T FACTOR
C      VT       - V*T FACTOR
C      PHICON   - INITIALIZATION VALUE OF PRESSURE TO DENSITY RATIO
C      LP       - LOWEST NODE VALUE FOR PRINTING
C      INC      - EVERY ** INC ** NODES PRINT
C      NPX      - NUMBER OF LAST NODE IN X DIRECTION
C      NPY      - NUMBER OF LAST NODE IN Y DIRECTION
C
C
C      INTERPOLATE TO FIND HALF NODE VALUES ALONG EACH INTEGRAL NODAL ROW
C      INTERNAL TO COMPUTATION REGION
      NJ = NY - 3
      NI = NX - 3
      DO 100 J = 4,NJ,2
      DO 100 I = 4,NI,2
      U(I ,J) = .5*(U(I-1,J) + U(I+1,J))
      IF(I.EQ.4) GO TO 99
      T(I-1,J) = .5*(T(I-2,J) + T(I ,J))
99      CONTINUE
      IF(J.EQ.NJ) GO TO 100
      V(I+1,J+1) = .5*(V(I,J+1) + V(I+2,J+1))
100     CONTINUE
C
C      INTERPOLATE TO FIND HALF STEP VALUES FOR THE REMAINDER OF THE
C      COMPUTATION REGION
C
      NJ = NY - 3
      NI = NX - 3
      DO 200 J = 4,NJ,2
      DO 200 I = 4,NI
      V(I,J ) = .5*(V(I,J-1) + V(I,J+1))
      IF(J.EQ.NJ) GO TO 200
      T(I,J+1) = .5*(T(I,J) + T(I,J+2))
      U(I,J+1) = .5*(U(I,J) + U(I,J+2))
200     CONTINUE
C
C      COMPUTE U**2,V**2,U*V FOR COMPUTATION REGION
C
      NJ = NY - 1

```

```

NI = NX-1
NJ2=NJ/2
NI2=NI/2
DO 300 J = 1,NJ2
DO 300 I = 1,NI2
U2(I,J) = U(2*I,2*J)**2
V2(I,J) = V(2*I,2*J)**2
UV(I,J)=U(2*I-1,2*J-1)*V(2*I-1,2*J-1)
UT(I,J)=U(2*I-1,2*J)*T(2*I-1,2*J)
VT(I,J)=V(2*I,2*J-1)*T(2*I,2*J-1)
IF(I.EQ.1) U2(I,J)=U2(I+1,J)
IF(I.EQ.NI2) U2(I,J)=U2(I-1,J)
IF(J.EQ.1) V2(I,J)=V2(I,J+1)
IF(J.EQ.NJ2) V2(I,J)=V2(I,J-1)
300 CONTINUE
RETURN
END

```